April 2021

A Generalized Method for Predictive Simulation-Based Lower Limb Prosthesis Design

Mark Price
University of Massachusetts Amherst

A GENERALIZED METHOD FOR PREDICTIVE SIMULATION-BASED LOWER LIMB PROSTHESIS DESIGN

A Dissertation Presented

by

Mark Andrew Price

Submitted to the Graduate School of the
University of Massachusetts Amherst in partial fulfillment
of the requirements for the degree of

DOCTOR OF PHILOSOPHY

February 2021

Department of Mechanical and Industrial Engineering

A GENERALIZED METHOD FOR PREDICTIVE SIMULATION-BASED LOWER LIMB PROSTHESIS DESIGN

A Dissertation Presented

by

Mark Andrew Price

Approved as to style and content by:

_____
Frank C. Sup IV, Chair

_____
Ian Grosse, Member

_____
Brian Umberger, Member

_____
Sundar Krishnamurty, Department Head
Mechanical and Industrial Engineering

DEDICATION

To everyone who kept me afloat – in the past and especially now, in the midst of a pandemic.

ACKNOWLEDGMENTS

I would like to thank Professor Frank Sup for his advisement and encouragement through my six years at the Mechatronics and Robotics Research Laboratory. I entered his laboratory with a vague desire to create technology that would help people, and through his teaching and example, I leave it with the skills, experience, and focused vision to make a material difference in the way we design assistive technology. This project would not have been possible without his guidance.

I need to thank Professor Brian Umberger for teaching me almost everything I know about human biomechanics and how to model them. More than that, he is the model of the academic I would like to become in his commitment to his students, to lifelong learning, and to humility despite broad recognition and achievement.

I would also like to thank Professor Ian Grosse for his valuable feedback and consistent involvement in my graduate career, not only by serving on my committee for this work, but also on my qualifying exam board, and my master's degree committee as well.

This work would not have been possible without the support and friendship of my labmates at the MRRL past and present – Vinh, Julio, Soumitra, Ericber, Punith, Youssef, Qiandong, and Andy. I have learned something from every single one of them. I also need to thank my colleagues in the Department of Kinesiology, especially Russell and Ryan, who both have directly helped me learn and apply knowledge I had no exposure to prior. Additionally, David Follette, Rick Winn, and Colby Norwood provided valuable labor and assistance in the fabrication of my prototype.

Finally, I need to thank all of the undergraduate assistance I had through the course of this project, formally or informally working with the lab. I'm grateful for all of their very limited time.

This work was financially supported by the National Science Foundation through the National Robotics Initiative (IIS-1526986) and by the Massachusetts Space Grant Consortium (2020 Summer Fellowship).

ABSTRACT

A Generalized Method for Predictive Simulation-Based Lower Limb Prosthesis Design

February 2021

MARK ANDREW PRICE

B.S.M.E., GEORGIA INSTITUTE OF TECHNOLOGY

M.S.M.E., UNIVERSITY OF MASSACHUSETTS, AMHERST

Directed by: Professor Frank C. Sup IV

Lower limb prostheses are designed to replace the functions and form of the missing biological anatomy. These functions are hypothesized to improve user outcome measures which are negatively affected by receiving an amputation – such as metabolic cost of transport, preferred walking speed, and perceived discomfort during walking. However, the effect of these design functions on the targeted outcome measures is highly variable, suggesting that these relationships are not fully understood. Biomechanics simulation and modeling tools are increasingly capable of analyzing the effects of a design on the resulting user gait. In this work, prothesis-aided gait is optimized in simulation to reduce both muscle effort and peak loads on the residual limb using a generalized prosthesis model. Compared to a traditional revolute powered ankle joint model, a two degree-of freedom generalized model reduced muscle activations by 50% and peak loads by 15%. Simulated prosthesis behaviors corresponding to the optimal gait patterns were translated into a two degree-of-freedom ankle-foot prosthesis design with powered bidirectional linear translation and plantarflexion. The prototype is capable of delivering up to 171 N-m of plantarflexion torque and 499 N of translation force, with 15° dorsi-/35° plantarflexion and 10 cm translation range of motion. The mass and height of the ankle-foot are 2.29 kg and 19.5 cm, respectively. The mass of the entire system including the wearable offboard system is 8.58 kg. This platform is designed to emulate the behavior of the simulated prosthesis, as well as be configurable to emulate alternate behaviors obtained from

simulations with different optimization objectives. The prototype is controlled to replicate simulated walking patterns using a high level finite state controller, mid-level stiffness controller, and low level load controller. Closed loop load control has bandwidth of 15 Hz in translation and 7.2 Hz in flexion. Load tracking during walking with a single able-bodied human subject ranges from 93 to 159 N in translation and 4.6 to 21.3 N-m in flexion. The contribution of this work is to provide a framework for predictive simulation-based prosthesis design, evidence of its practical implementation, and the experimental tools to validate future predictive simulation studies.

TABLE OF CONTENTS

LIST OF TABLES

Table **Page**

LIST OF FIGURES

Figure **Page**

CHAPTER 1

INTRODUCTION

1.1. Research Motivation

Lower limb prostheses are designed with the intent of improving user outcome measures for tasks affected by receiving an amputation. These outcome measures include metabolic cost of transport, preferred walking speed, limb loading as a risk factor for comorbidities, perceived instability, perceived discomfort, and others. The design process dictates translating these desired effects into specific functional requirements. This requires knowledge of the causal relationships between prosthesis functions and user outcomes. In practice, these causal relationships are often modeled from analysis of simplified models for gait. For example, the dynamic walking model characterizes human walking as an extrapolation from the passive dynamics of the skeletal system [1]. These analyses have highlighted reduced toe-off propulsion work as a critical factor adversely affecting outcome measures such as cost of transport and gait symmetry [1], [2]. This rationale has been used to support design decisions to focus on providing positive toe-off propulsion work [3], [4]. Additionally, it is often assumed that the prosthesis performance ideally should imitate biological motor function which was removed via amputation. The performance of prosthetic devices is often assessed in terms of kinematic and kinetic similarity to the biological joint being replaced [4]–[8], in addition to the user outcome measures. In this case, the causal relationship between a functional requirement (similarity to the amputated anatomy) and user outcomes is largely hypothesized through logical reasoning, rather than explicitly and empirically supported.

However, experimental outcomes regarding these hypothesized causal relationships are inconclusive. For example, tests using a tethered prosthesis “emulator” with off-board power [9] observed no relationship between prosthesis joint power and metabolic cost [10]. Other tests with a commercial powered ankle which provides a near-biological ankle torque and kinematic profile

(Empower, Ottobock) found no significant improvement in limb loading osteoarthritis risk factors compared with passive elastic prostheses when tested on young, active individuals [11]. However, other tests of this system do show improvement in metabolic cost [4] and osteoarthritis risk factors [12] in different test subject populations. These mixed results indicate that our understanding of the functional requirements to obtain a desired outcome among a diverse user population is not complete.

One path toward improving this understanding is to use simulations of realistic musculoskeletal models to identify the effects of specific design elements on user outcomes. A particularly promising tool is the predictive simulation of human movement, which uses optimal control strategies to calculate muscle forces in an attempt to recreate the neural process that distributes loads across the muscles [13]. Predictive simulations have generated model motions which are highly similar to experimentally recorded motions without tracking experimental data [14]–[17]. This technique has been applied to prosthesis-aided gait to investigate the effect of design and muscle control strategies on metabolic energy cost [18], [19] and joint loading [20]. By creating the framework to conduct virtual experiments, predictive simulation allows for the causal relationships between prosthesis function and user outcome to be more deeply explored than can practically be accomplished with physical prototypes. To extend the application further, the ability to estimate prosthesis design outcomes through predictive simulation invites the possibility of algorithmically optimizing the design variables. With a generalizable prosthesis model, such an optimization could serve to define the functional requirements of the prosthesis by outputting the optimal prosthesis behavior for the targeted outcome measures. This eliminates the need for simplified assumptions about causal relationships between prosthesis performance and user outcomes – this relationship is described in a complex musculoskeletal model which can be evaluated numerically.

The core motivation behind this work is that the prosthesis design process lacks a method which can directly target user outcomes to drive design decisions. Advances in computational biomechanics have introduced predictive simulation of human gait as a potential tool to accomplish this goal. In this dissertation, a design framework is presented which utilizes predictive biomechanical simulations as a prosthesis design tool for optimizing prosthesis performance for targeted user outcomes.

1.2. Research Aims and Scope

The high level goal of this work is to create a simulation and experimental validation feedback loop to enable user outcome-focused simulation-aided prosthesis design which ignores typical assumptions about the proper form and function of an artificial limb. More specifically, this can be composed into two specific aims:

1. Create a design method which takes optimal simulated generic prosthesis behaviors and translates them into an actual powered prosthesis design.
2. Create a toolset to enable the refinement of the design method based on experimental testing to validate simulated trends.

These aims support the creation of a larger design process illustrated in Figure 1.1. The overall design method is a feedback loop which progresses from optimal control simulations with a generalized model, to the implementation of simulated behaviors on hardware for experimental validation, to the refinement of the simulation constraints and objective function based on findings from the experimental validation step. The scope of the presented work is limited to creating the infrastructure required to make this larger design process possible – specifically the pipeline from simulation to experiments.

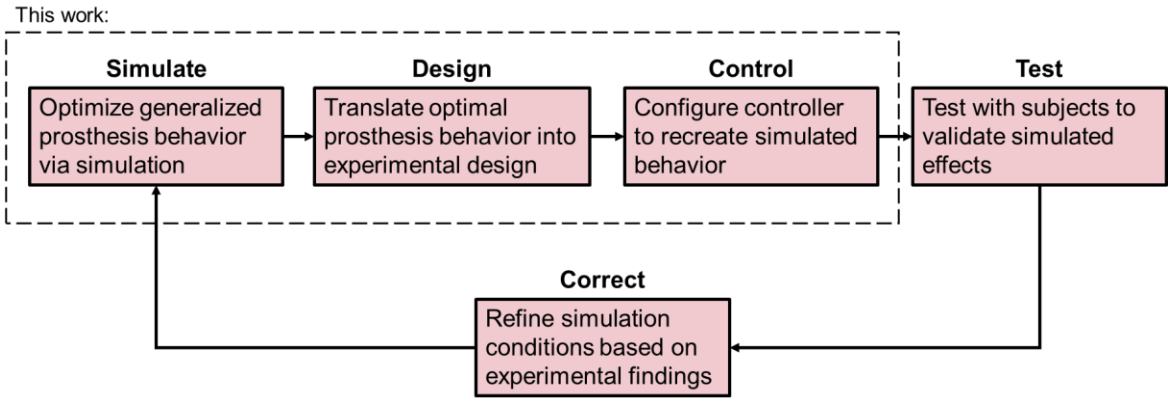

Figure 1.1. The scope of the presented work within the overall proposed design method.

1.3. Outline

This document proceeds with an analysis of current prosthesis design approaches and outlines the gaps which the presented work seeks to fill in Chapter 2. Chapter 3 follows with a simulation study which demonstrates the ability of a generalized prosthesis model to reduce selected user outcomes relative to existing design forms when applied to an optimal control framework. Chapter 4 builds upon the simulated outcomes with a prototype design capable of recreating simulated prosthesis behaviors. Chapter 5 concludes the work with the design and implementation of a control architecture capable of recreating simulated walking patterns, demonstrated with treadmill walking trials with an able-bodied human subject.

CHAPTER 2

LITERATURE REVIEW: DESIGN OPTIMIZATION IN LOWER LIMB PROSTHESES

In the previous chapter, an iterative, simulation-based design process was proposed. To motivate the need for such a design process to be created, this chapter focuses on exploring the current and developing methods being used to design prosthetic devices and analyze their performance. Gaps in the existing methods are demonstrated along with the emerging tools which may be capable of filling them.

This chapter is adapted from a review paper titled *Design Optimization in Lower Limb Prostheses: A Review*, written with second author Professor Philipp Beckerle of TU Darmstadt and third author Professor Frank Sup of the University of Massachusetts, Amherst [21]. This paper was published in IEEE Transactions on Neural Systems and Rehabilitation Engineering in August 2019.

Abstract— This review aims to develop a knowledge base and identify promising research pathways toward designing lower limb prostheses for optimal biomechanical and clinical outcomes. It is based on a literature search representing the state-of-the-art in lower limb prosthesis joint design and biomechanical analysis. Current design solutions are organized in terms of fulfilling four key functional roles – body support, propulsion, task flexibility, and loading relief. Biomechanical analyses of these designs reveal that the hypothesized outcomes are not consistently observed. We suggest that these outcomes may be improved by incorporating tools that can predict user performance metrics to optimize the device during the initial design process. We also note that the scope of the solution space of most current designs is limited by focusing on anthropomorphic design approaches that do not account for the person's altered anatomy post-amputation. The effects of prosthetic joint behavior on whole-body gait biomechanics and user experience are likewise under-explored. Two research paths to support the goal of better predicting user outcomes are proposed: experimental parameterization of designs and model-based simulations. However, while work in these areas has

introduced promising new possibilities, connecting both to improve real-world performance remains a challenge.

2.1. Introduction

Lower limb prosthesis design has evolved from creating devices that solely provide weight-bearing support to devices that perform specific behaviors to aid locomotion. The continuing improvement of prosthesis functionality has the potential to impact the quality of life of millions of people in the coming decades. Statistically, the number of persons living with limb loss in the United States is projected to number approximately 3.6 million by 2050 [22]. 65% of people living with limb loss in the US in 2005 had undergone a lower limb amputation, 61% of which removed at least the foot [22]. People who have had a lower limb amputation typically experience significantly reduced mobility and experience several impediments when completing the basic activities of daily life [23].

A major objective of prosthesis design research is to minimize both immediate and long-term detrimental effects. The evolution of prostheses driven by this research has led to quantifiable improvements in user performance metrics such as metabolic cost [4] and joint loading [24]. Researchers have investigated ways to improve a user's ability to walk on level ground [5], [25], [26], traverse inclines and declines [25], [27], [28], navigate stairs [25], [26], [29], turn while walking [30]–[32], transition between sitting and standing [33], [34], and run [35]. Efforts are ongoing by researchers to parameterize, quantify, and correlate the design factors of prostheses to desired user outcomes, thereby improving our understanding of what makes prosthetic devices effective. However, knowledge gaps between intended and actual user outcomes remain that require further exploration to more effectively address the needs of the prosthesis user [10], [36]–[38].

The objective of this paper is to act as a resource for current and prospective prosthesis designers and researchers interested in future directions to best fill these knowledge gaps. In this review, we highlight the biomechanical challenges intrinsic to lower-limb prosthesis design,

contextualize and summarize the major works to-date, identify key knowledge gaps, and highlight research paths which we expect to enable designers to meet user outcome-based functional needs. Literature for this review was obtained by investigating related papers on prosthesis design, modeling and simulation of human biomechanics with prostheses, and evaluation of prostheses with users. To this end, reference databases including IEEExplore, ScienceDirect, PubMed, and Google Scholar databases were searched and analyzed.

2.2. Biomechanical Challenges

Problems resulting from a lower limb amputation can manifest as immediate effects (i.e., asymmetrical gait compensations) and progress into long-term consequences (i.e., secondary impairments or other co-morbidities) [23], [39], [40]. This section discusses the causes of these problems and their interactions with prostheses.

2.2.1 Gait compensations and asymmetry

Lower limb amputation significantly alters the mechanics of walking from able-bodied mechanics. Muscle-tendon units interact with the skeletal system by generating, storing, dissipating, and transferring energy between segments [41]–[43], stabilizing joints [44], and enforcing compressive loading in individual bones through external tension [45]. These functions are critical for performing motor tasks, and they are removed with the amputation of a biological joint. Further, the use of a prosthesis adds an additional passive "joint" to the limb at the socket-residuum interface [46]–[49]. Methods to directly integrate the prosthesis into the residual bone exist and are becoming more common, but conventional sockets are still prevalent [50].

As a consequence, people walking with the aid of a prosthesis develop compensatory habits for the lost functionality which alters their dynamics. The resulting motion and muscle engagement changes can cause asymmetrical joint loading [51], [52]. These trends typically manifest as minimization of weight-bearing time for the prosthesis, increased work performed by the muscles on

the sound side limb, and increased muscle work at the hip of the residual limb to compensate for lost distal muscle function [23], [53]. Widely used conventional passive prostheses are designed with elastic foot segments to restore some of the energy storage and return capability that the biological muscles once provided. However, elastic energy storage and return prostheses release less than half of the mechanical energy of intact biological muscles during level walking [54]. Depending on the age and physical condition of the user, walking with a passive prosthesis typically requires more metabolic energy when compared to walking with intact biological limbs [38], [55]. The development of powered prostheses has resulted in devices capable of restoring or even exceeding power output produced by biological muscles [4], [10]. However, these devices do not necessarily reduce the metabolic cost of walking to able-bodied levels for all users, nor do they restore symmetry to the motion [10]. This suggests that lost muscle power is not the only factor in causing gait abnormalities. Powered devices also have greater distal mass relative to passive devices. Increased distal mass has been shown to contribute to reduced metabolic efficiency [56], which may mitigate some of the benefits of added power. This increased mass is similar to the biological limb mass, however – commonly between 2 and 2.5 kg for powered transtibial prostheses [4], [57], [58] compared to between 2.5 and 5 kg for the average full shank and foot [59].

The loading of the residual limb via the non-rigid socket interface can also be a significant cause for discomfort and energy losses [4], [23], [45], [60]. The socket interface introduces loads to the residual soft tissue and bone that are not experienced during walking with an intact limb [45]. Inefficient energy transfer caused by losses due to socket motion or tissue absorption may also limit desired prosthesis contributions to whole body mechanics [4]. Socket fit and alignment are also largely qualitative measures and not typically assessed when evaluating prosthesis performance. Without deterministic analyses of socket fitment, it is difficult to assess the effect of fitment on user

outcomes. However, these parameters are strongly associated with walking ability and user discomfort [23], [36], [60].

2.2.2 Secondary impairments and co-morbidities

People who have received an amputation are at risk for several secondary impairments. For example, the prevalence of knee osteoarthritis in the intact limb of unilateral lower extremity amputees has been observed to be significantly higher than experienced by able-bodied persons [23], [39], [61]. Symptomatic knee osteoarthritis has been observed to be 17 times more common in unilateral amputees than in age-matched non-amputees [61]. This painful degeneration of the intact joints further detracts from one's quality of life beyond the original amputation. Additional secondary conditions associated with lower limb loss include a reduction of bone density in the residual limb [23], muscle atrophy [23], [40], weight gain [23], chronic back pain [23], [40], [62], skin irritation [62], [63], and pressure ulcers [63]. Mitigating the risk of developing secondary impairments is an important design goal for a prosthesis to fulfill its purpose of restoring a user's quality of life.

Many of these impairments result simply from a reduced level of physical activity overall due to discomfort, pain, or difficulty walking. Loss of bone density, muscle atrophy, and weight gain post-amputation are all linked to a decline in physical activity [23]. Back pain, some skin problems, and osteoarthritis are linked to another phenomenon: loading conditions for both the residual limb and sound limb which are not experienced by able-bodied persons. Prosthesis users tend to increase loading of the sound limb to make up for lost muscle power and reduce discomfort associated with loading the socket [23]. The development of back pain, for example, has been linked to an increased anterior pelvic tilt common in people with lower limb amputation [23]. The development of osteoarthritis has been linked to increased sound knee loading after heel-strike [23], [24]. Specifically, people with unilateral lower limb loss tend to have a large peak knee external adduction moment (EAM) in the sound side limb after heel-strike [24]. Knee EAM typically has a "double hump" profile

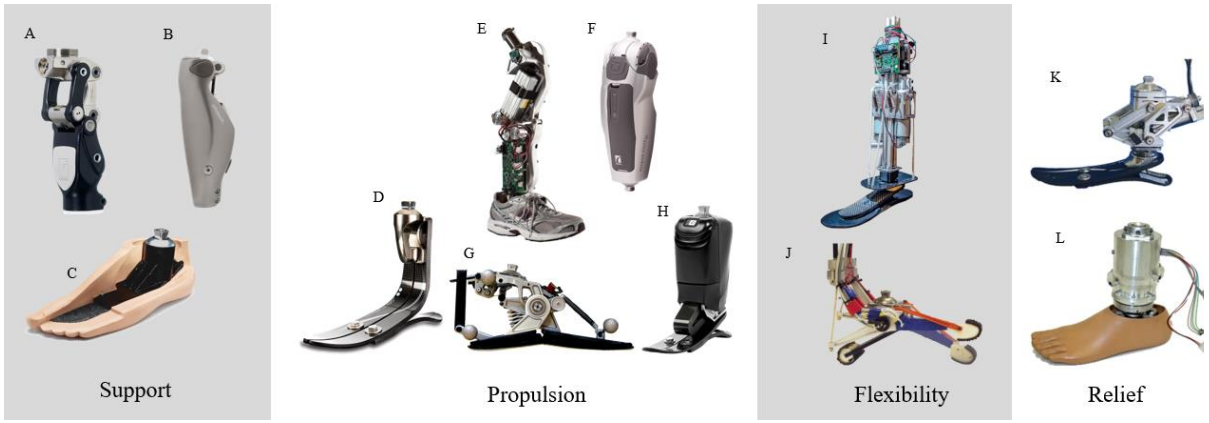

Figure 2.1. An overview of commercial and research lower limb prostheses categorized by functional emphasis. A) Total Knee® 1900, Össur [68]**: Passive polycentric knee prosthesis. B) C-Leg 4®, Ottobock** [65]**: Microprocessor-controlled hydraulically damped knee prosthesis. C) SACH, Ohio Willow Wood** [87]**: Passive ankle-foot for low-activity users with a cushioned heel and minimal energy return. D) Vari-Flex®, Össur** [86]**: Passive ankle-foot for low- to high-activity users with elastic energy storage and return. E) Vanderbilt Leg** [5], [25], [27], [35]**: Motor powered knee and ankle prosthesis which injects propulsive energy during walking. F) Power Knee®, Össur** [113]**: Motor powered knee joint prosthesis. G) CESR foot** [3], [80]**: Semi-active ankle-foot with actively controlled clutch mechanism for release of stored elastic energy at toe-off. H) Empower®, Ottobock** [4], [26], [100], [103]**: Motor powered ankle-foot prosthesis which generates positive ankle flexion work at toe-off. I) Michigan Tech 2-DoF ankle-foot** [30], [116]**: Motor powered ankle-foot with control over dorsi-/plantarflexion and inversion/eversion joint angles. J) 2-DoF ankle-foot prosthesis emulator** [114]**: Powered ankle-foot test platform with offboard motor actuation to control over dorsi-/plantarflexion and inversion/eversion joint torques. K) UMass Adaptive Alignment Prosthesis** [45], [123]**: Motor powered ankle-foot prosthesis with ankle flexion coupled with sagittal plane translation to reduce socket moment loads. L) TU Darmstadt & Blatchford shank adapter** [32]**: Motor powered parallel elastic actuator controlling shank torsion stiffness and foot alignment to reduce socket loads during turning maneuvers.**

after heel strike, the first of which is more closely associated with the development of osteoarthritis due to its higher loading rate and typically higher magnitude [64]. Poor socket fit and alignment have also been proposed to exacerbate the causes of many of these impairments, if not cause them directly [23].

A few dominant approaches have emerged to address the challenges described in this section. The next section identifies these approaches with representative examples, the hypotheses behind them, and the common metrics used to assess designs and user outcomes.

2.3. **Current Design Approaches and Methods**

The primary design goal of most current lower limb prostheses is to restore gait symmetry and effort to able-bodied levels. Targets such as reducing abnormally high loads in the joints or the residual limb, improving the ability to perform specific tasks, and increasing balance and stability are

also considered, however. The design approaches corresponding with these various desired outcomes can generally be categorized according to what the prosthesis is being designed to functionally provide: a) Support, b) Propulsion, c) Flexibility, and/or d) Relief. Examples of prostheses and research prototypes are illustrated according to these categories in Figure 2.1.

2.3.1 **Support**

Providing weight-bearing support is a fundamental function of a lower limb prosthesis. This function is performed by replacing the missing skeletal structure with a mechanical surrogate which provides static structural support. However, there are other design features which specifically serve to provide active support for balance or stability, almost all of which are commercially available. For example, active damping is commonly used in joints of both ankle and knee prostheses to stabilize the joint under load in hydraulic [65], pneumatic [66], and magnetorheological forms [67].

Prosthetic knees have also been designed to have a polycentric joint trajectory using linkages, rather than a revolute joint (Figure 2.1A) [68]. This motion more accurately mimics the range of motion of the biological knee and can be designed to allow the knee to naturally lock at full extension, offering more reliable support [69]. However, the addition of the ability to passively lock the knee during stance removes the ability of the knee to flex at heel strike, as the biological knee typically does. Semi-active devices use active components to vary the passive properties of the prosthesis, aiding the function of support when it is most needed. Microprocessor knees, the most notable examples being the introduction of the Ottobock C-Leg® and Össur Rheo Knee®, are a now common example of this approach to dynamically alter the viscous damping of the artificial knee (Figure 2.1B) [70]–[72]. The ability of microprocessor knees to adjust to task-specific behaviors such as variable stride cadences, knee joint stiffness requirements for traversing slopes or stairs, and transitioning between sitting and standing has been associated with increased balance and confidence with users [73]. A similar principle has been demonstrated for a prosthetic ankle-foot in [74], which changes the rollover shape

of the foot from a locked, shallow curve while standing to a more flexible curve while walking. This design attempts to address the task-dependent stability needs inherent in the loss of feedback and control from the foot and ankle.

Support design features are primarily dissipative in nature. Design elements which prioritize work produced at the joint tend to focus on providing propulsion.

2.3.2 **Propulsion**

The loss of "push-off" torque provided by the ankle plantarflexors during the step-to-step transition in the biological ankle has been hypothesized to be the primary factor driving asymmetrical muscle compensations, increased metabolic cost of walking, and reduced preferred speed [75], [76]. This hypothesis is based on observations of the high percentage of the mechanical work required during gait being generated at the ankle joint during gait, the magnitude of which increases with walking velocity [75]–[77]. The loss of propulsion work is also hypothesized to lead to a compensatory increase in leading limb collision work to provide the necessary forward and up acceleration to the center of mass, and thus be responsible for abnormally large joint loadings in the sound side limb [12], [24]. Under this hypothesis, mitigating the risk of developing secondary impairments and restoring gait efficiency are goals which can both be achieved by restoring ankle push-off to able-bodied levels.

Designs which provide propulsion use passive, semi-active, or fully active approaches. Fundamental to the passive and semi-active approaches is the concept of energy recycling [72], [78]. Active approaches focus on energy injection but also use energy recycling design elements to improve efficiency [79].

2.3.2.1. Energy Recycling

Designs employing an energy recycling approach attempt to recapture some of the energy that would otherwise be dissipated through friction, damping within the joints, or inelastic collision

with the ground [80], [81]. This energy is used to provide some of the positive work during the step-to-step transition that the biological ankle would normally provide, as well as generally reduce the amount of energy dissipated to the environment [80], [81]. This principle is applied primarily to passive and semi-active prostheses, but is also used in active prostheses to improve the overall energy efficiency of the design [82], [83].

Design work on passive prostheses primarily focuses on the efficient recovery of energy absorbed after heel-strike [84]. The typical approach is to incorporate elasticity into the design so that the user can store energy with their body weight, and then release it at toe-off [84]. Energy storage and return (ESAR) prostheses apply this by containing elastic heel and keel (hindfoot and forefoot) sections that each store and release energy at various stages during stance (Figure 2.1D) [85], [86]. These are prescribed as an alternative to solid ankle-cushioned heel (SACH) prosthetic feet, which offer cushioned heel-strike shock absorption with little energy recovery (Figure 2.1C) [85], [87]. The bulk of commercially available lower limb prostheses are implementations of these basic designs. Due to an aesthetic demand for anthropomorphic appearance, the geometry of these devices is limited to a similar size and shape of the biological foot. While these devices do restore some energy to the residual limb during walking, it is substantially less than is provided by the plantarflexor muscles during walking [54], [78]. However, running prosthetic feet represent specialized passive energy recycling designs exist which do not fully comply with anthropomorphic norms. These devices use high amounts of elastic displacement and a comparatively small base of support to maximize energy storage and return efficiency during running. This design style, while being impractical for heel-toe walking due to the lack of a heel, allows users to run while expending similar metabolic energy costs to able-bodied runners, and reach comparable sprint times to able-bodied runners at high levels of competition [88].

It is possible to increase the amount of energy provided during push-off using semi-active devices. Such devices control the storage and release of energy using motorized clutches and springs (Figure 2.1G) [3], [24], actuated pneumatic cylinders [89], or powered lead screws to modify the active length of a leaf-spring [90]. Commercially, semi-active devices are used to assist with propulsion by modifying the static angle of the prosthetic ankle to different set points for different scenarios [91], [92]. While passive and semi-active prostheses are capable of recycling a percentage of energy, they cannot produce net positive work over the entire gait cycle.

Active prostheses can also be designed to recycle energy through passive springs or clutches that supplement the active elements. Series and parallel elastic elements have been shown to decrease the peak power requirements of the actuator and biological joints [82], [93]. However, these benefits come with trade-offs in the form of reduced control bandwidth [94] and increased system complexity contributing to higher fault sensitivity [95]. It is common practice to use series-elastic as well as parallel elastic elements in powered prostheses to reduce demands on the actuator [5], [6], [26], [83], [96], [97]. ESAR prosthetic feet have also been used in conjunction with powered prosthetic joints [4], [5], [45]. In these cases, energy recycling is used as a supplementary feature to the primary contribution active prostheses provide: an injection of external energy.

2.3.2.2. Energy Injection

The biological ankle produces a net positive work over the gait cycle, the magnitude of which increases with walking speed [76]. The inability of passive and semi-active designs to replicate biological muscle work at the ankle joint has been hypothesized to be the cause of gait deficiencies in people walking with passive prostheses and is based on the importance of the step-to-step transition for overall energy cost of walking in dynamic walking models [1], [98]. Researchers have been motivated to inject power into the artificial joint from an external source. Most commonly used are electromechanical motors [79], but power has been also sourced using pneumatic artificial muscles

[99]. Positive net work is achieved by engaging the prosthesis actuators at the end of the stance phase, providing push-off force and torque to the residual limb. A standard approach is to produce a plantar-flexion torque about a revolute joint, and mimic the active and passive dynamics of the biological ankle [5], [6], [26], [97], [99]–[101]. However, alternatives exist which do not depend on strictly recreating the biological ankle function in the sagittal plane. For example, linkages are used to achieve polycentric rotational motion to increase efficiency and alter the passive impedance [8], [102], or to align the residual limb with ground reaction forces [45]. A device also exists which is explicitly designed to vary the amount of propulsion work above and below biological levels to test the hypothesis that reduced propulsion work is the cause for gait deficiencies in people with lower limb amputation [9]. Commercial availability of powered ankles is limited, with only one on the market (Empower® - formerly BiOM®, Ottobock [4], [103] – Figure 2.1H) and another undergoing commercialization (Walk-Run Ankle®, SpringActive, Inc. [104]). Other commercial ankles with active elements ultimately perform semi-active functions to modulate the behavior of the passive elements.

Active energy injection approaches have been developed for the knee joint as well. Most of the propulsive work in able-bodied walking is performed by the ankle, but some net positive work is also required at the knee [105]. Other activities such as running, jumping, upslope walking, and stair climbing require significant amounts of net positive knee work in able-bodied individuals [53], [106], [107]. Active knee prostheses in research have similar dominant characteristics to active ankles – flexion-extension actuation with an emphasis on emulating able-bodied biomechanics, often leveraging passive elements for efficiency purposes (Figure 2.1E) [5], [96], [108]–[112]. Polycentric linkage joints, common in passive and semi-active knees due to their natural locking properties, are not seen in these powered designs. This is likely due to the presence of linkage singularity points which cause the joint to lock - a feature in passive designs which becomes a complex control problem in active designs. The primary design focus for these examples is to actively control the knee torque and

generate net positive work. Commercially, one propulsive powered knee is currently available (Power Knee®, Össur - Figure 2.1F [113]).

2.3.3 **Flexibility**

Prostheses that are designed to provide flexibility attempt to restore the range of capabilities that the biological limb could provide, or increase robustness to variability in the environment. For example, some designs include passive or powered degrees of freedom in the inversion/eversion axis of the ankle, targeting walking stability as a design objective. It is hypothesized that controlling this additional degree of freedom can reduce side-to-side sway, improve balance confidence [114], and improve a user's ability to perform walking tasks like turning, which is accompanied by ankle inversion/eversion rotations in able-bodied individuals [30]. For example, a prosthesis has been designed with active control of the inversion/eversion of the foot by using a four-bar linkage mechanism, with a passive spring providing plantarflexion torque [115]. By actuating a prosthesis emulator with two separate toes, inversion/eversion can be controlled (Figure 2.1J) [114]. A cable-driven prototype which can steer the entire foot in the flexion axis, as well as the inversion/eversion axis, has also been developed (Figure 2.1I) [30], [116]. Passive compliance non-flexion axes are also used in commercial prostheses to assist with walking on uneven ground [117], [118].

2.3.4 **Relief**

Reaction moments and soft tissue loading between the socket and residual limb are believed to be a major cause of reported discomfort and decline in mobility over time [23], [60]. Relief from undesirable loads on the residual limb and on the body as a whole is conventionally provided at the socket-limb interface. Soft cushioned gel socket liners are used to reduce peak loads [119], but may also reduce a user's sense of stability and sensory feedback resulting in higher ground reaction forces [120]. The use of vacuum-assisted socket suspensions has also been shown to distribute pressure

away from concentration points [121]. Experimental socket designs for reducing tissue stress as well as discomfort due to tissue volume change and temperature are discussed in more detail in [49].

Socket loads may also be reduced by adding compliance and damping to the prosthesis-socket connection or the prosthetic structure, as has been done for both vertical [117], [122] and torsional loads [118] in commercial prostheses. Refining this concept, recent research has led to elastically actuated devices that modulate transverse plane torsional stiffness during gait, which allows for adaptation to the current motion patterns [31], [32]. Besides considering user requirements when designing this feature, the concept from [18] uses a parallel elastic actuator to further align foot orientation while turning during walking. Relief may also be a design goal for the prosthetic joint itself, as demonstrated by [45] (Figure 2.1K). This example has been designed to actively align ground reaction forces with the residual limb to reduce the flexion moment exerted on the residual limb by the socket, and has resulted in reduced socket moment and pressures in a pilot study with one participant [123]. Load reduction is achieved through translation of the foot segment, which does not replicate any function of the able-bodied biological ankle, but instead introduces a new axis of motion to address limb loading problems associated with the presence of a non-rigid socket-limb interface [45].

2.4. **Analysis of Current Designs**

This section looks at experimental analyses that have been performed on these devices to assess the validity of the various hypotheses informing their designs. These studies attempt to address elements of a broader research question: How do prosthesis design factors affect experimental user outcomes? The previous section detailed some specific hypotheses for answers to this question – for example, increasing propulsion work at the ankle to decrease the metabolic cost of transport and normalize gait mechanics. This section details the biomechanics analysis and experimental methods used to evaluate these hypotheses then summarizes the various results with

respect to desired user outcomes. The analysis studies detailed in this section are listed in Table 1 and are grouped by outcome measure investigated. The "gait mechanics" outcome measure refers to joint kinematics, kinetics, and power, as well as ground reaction forces. While the majority of studies consider global biomechanical measures such as gait mechanics, metabolic cost, or muscle activity, more specific information like joint contact forces or task-specific muscle contributions are less often taken into account. Despite being an important aspect of lower limb prosthetics, the user experience is rarely examined. Additionally, a large amount of the literature supporting the projects described in Section 2.4 has been published in primarily a technical context and reports mechanical device performance rather than biomechanical analysis. The analyses listed in Table 2.1 comprise a subset of the projects discussed in the previous section.

2.4.1 Experimental and Analytical Tools

Analyzing the real outcomes of a prosthesis design requires testing with human participants. Typical experiments involve the use of marker-based motion capture techniques, which allow for the calculation of joint kinematics and participant-specific model creation [105]. Motion capture testing also often includes the use of force and moment sensors embedded in the walking surface, which allow for the calculation of net forces and torques at the joints through inverse dynamics analysis [105]. Participants can also be outfitted with a respiration device which measures oxygen and carbon dioxide levels, allowing metabolic energy expenditure to be calculated [3], [4], [10]. Electromyography (EMG) electrodes may be placed above (or, in some cases, into) muscles of interest to measure their level of activity [105]. Other types of sensors may be placed inside or around the socket to measure pressure or motion between the socket and residual tissue, including the use of X-ray fluoroscopy [124]–[127].

From these experimental measures, other model- and simulation-based analyses can be performed which offer some insight into the effect of the design on a person. Induced acceleration

Table 2.1. Outcome measures of prosthesis designs

Tested outcome measure	Reference
Gait mechanics	[4], [10]–[12], [18], [24], [28], [29], [123], [134], [135], [138]–[142], [144]
Metabolic cost of transport	[4], [10], [18], [38], [136], [138], [140]
Muscle activity	[10], [18], [134]–[138]
Muscle contributions to tasks	[136], [137]
Preferred walking speed	[4]
Joint contact forces	[136]
Socket loads	[31], [123], [139], [141]
Knee external adduction moment	[11], [12], [24], [144]
Leading leg collision work	[4], [10], [138]
User experience	[10], [32], [36], [38]

analysis (IAA) is a method used to isolate the effect of individual muscles or forces on segments in the model, including segments that may not be directly connected to the source of the force [42], [43], [128]. This method is implemented by setting all forces and torques to zero for a given frame in the reconstructed kinematics and then individually re-activating each in isolation to observe the effect on the model. For example, this technique has previously been used to identify the role of individual lower limb muscles in energy generation, absorption, and transfer during cycling [43], the role of individual ankle plantarflexors to body support, forward propulsion, and swing initiation during walking [42], and the high magnitude of inter-segment energy transfer in the gait of children [129]. However, IAA remains a controversial method to some members of the biomechanics community, who argue that cannot meaningfully describe the role of muscles in a system because it does not attempt to model the adaptation of the system when a muscle force is changed [130].

The use of optimal muscle control problems is another model-based analysis method and can be applied to estimate the individual redundant muscle contributions to measured joint torques. These estimates are based on minimizing measures of total muscle effort, metabolic cost, task

performance, or other objectives, subject to kinematic constraints. The objectives related to effort measures are formulated to represent a realistic approximation of the active muscle load distribution patterns in actual locomotion tasks and have been shown to result in muscle controls which generally agree with measured EMG data [16], [131]. Various optimization techniques have been employed in numerous studies to determine individual muscle excitations for activities such as walking, jumping, and cycling [132], and also used predictively to generate theoretically optimal motions [13], [14], [16], [133]. Extracting individual muscle activations and contributions to the dynamics of remote segments allows for the identification of compensations not directly observable from the recorded kinematics and net forces. As with other simulation methods, however, model accuracy is a key factor in producing meaningful information.

These tools have been used to assess the ability of various prosthesis designs to achieve the desired results in human users. These objectives can again be broadly categorized into short-term gait restoration and long-term secondary impairment and comorbidity mitigation goals. Propulsion oriented designs have been a major focus of prosthesis analysis work. Analysis of designs which provide flexibility or relief through the prosthetic joints and structures is less common.

2.4.2 **Gait Restoration**

Gait restoration outcomes are targeted by designs across the passive-active spectrum. Metrics such as similarity to biological gait mechanics, preferred walking speed relative to able-bodied levels, reduction of muscle contributions, and reduction in the metabolic cost of walking are commonly used to evaluate the effectiveness of a prosthesis in restoring gait (Table 2.1).

Optimally, passive prostheses focusing on propulsion attempt to maximize energy recycling efficiency, in theory reducing the amount of energy required from the muscles to compensate for lost torque generation. This requires an understanding of the relationship between the design parameters and the musculoskeletal system response, which researchers have begun to address. For example,

the effect of prosthesis stiffness on gait patterns and energy storage efficiency has been analyzed using inverse dynamics and EMG data with human motion capture tests with varying prosthesis stiffness values [134]–[136]. It was found that decreasing prosthesis stiffness led to increased energy storage and return and decreased hamstring muscle activity in the residual limb. This decreased muscle activity was offset by increased muscle activity in other areas providing body support.

In a follow-up study to [134], the experimental data was used to find the individual muscle activations in a mathematical model of the musculoskeletal system by solving an optimal muscle control problem to track the measured kinematics [137]. Induced acceleration analysis was used to identify the contribution of each muscle individually, as well as the contribution of the prosthesis and gravity, to the propulsion/braking force as well as the body support force on the ground. Among other results, the prosthetic foot was found to provide an increased contribution to body support forces and decreased contribution to propulsion as stiffness decreased, despite showing an increase in total energy stored and returned as stiffness decreased [137]. Variations in individual muscle contributions to body support, propulsion/braking, trunk power, and residual leg power were also observed relative to the stiffness of the prosthesis [137]. These results suggest that optimal stiffness may vary depending on the individual compensation needs of the user. Additionally, experiments with powered devices have shown that optimal device impedance changes between different tasks (e.g., standing vs. walking) and even different phases within one task (e.g., phases of gait) [5], [25].

Current powered ankle prosthesis designs show promising results for some gait restoration metrics and mixed results for others. The Ottobock Empower® ankle has been shown to increase the preferred walking speed and decrease the metabolic cost of walking for amputees relative to their daily use ESAR prosthesis [4]. The study theorizes that this relationship is due to the increase in trailing leg push-off work observed, coupled with an observed reduction in leading leg collision work.

However, the metabolic cost of walking with the powered ankle is shown to still be higher on average than the cost of able-bodied walking at and above the participants' preferred speeds.

In contradiction to the hypothesis that metabolic cost reduction is caused by increased push-off work, researchers using a tethered prosthesis emulator with off-board power [9] observed no relationship between prosthesis joint power and metabolic cost. Additionally, they did not observe a relationship between prosthesis joint power and intact limb collision work [10]. This experiment tested amputees walking at a set speed with varying prosthesis net-power settings, rather than between powered and unpowered prostheses for slow to fast walking speeds. It was also found that the timing of prosthesis push-off from the emulator device also has a significant effect on the metabolic cost of walking [138]. The combined results from the emulator studies suggest that factors other than the magnitude of net work or work rate generated by the ankle actuator contribute to user gait performance metrics. Further complicating the problem, it has been observed that the metabolic cost of walking does not necessarily increase after transtibial amputation in exceptionally young and fit users with passive prostheses [38]. This result can be reproduced through optimal muscle control

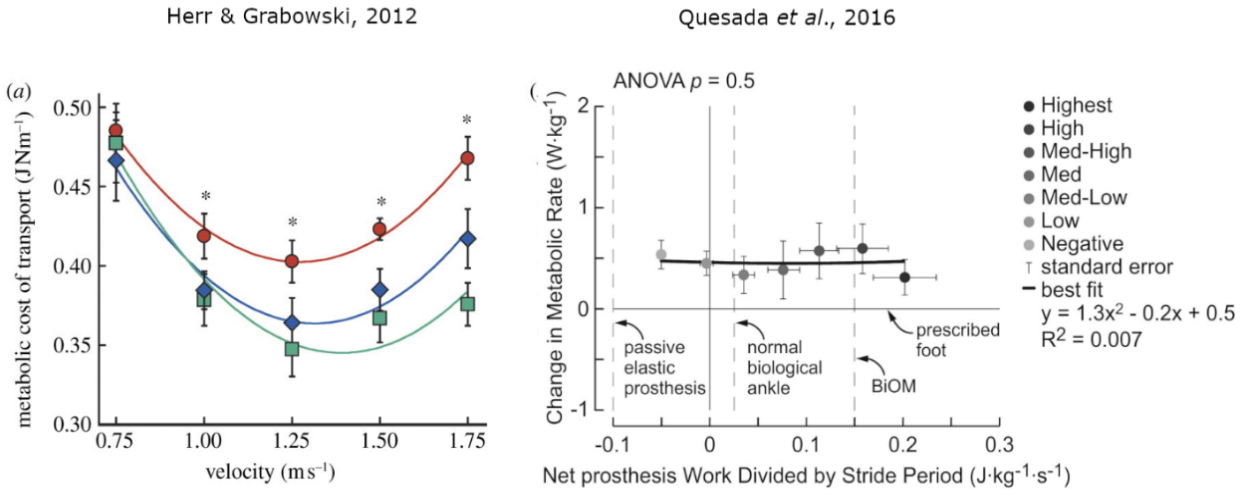

Figure 2.2. Comparison of results from [4] **and** [10]**. Note that in** [4]**, the Empower® prosthesis was compared with the daily use passive prosthesis of the subjects, whereas in** [10]**, the work output was varied for the same powered prosthesis for all trials. The results of** [4] **have been used to conclude that metabolic cost is dependent on the presence of push-off power, but this conclusion has been contested by the results of an experiment that more successfully isolated the presence of push-off power. Other factors such as normalized prototype acclimation time have not been accounted for.**

simulation [18], suggesting that user-specific factors other than the prosthesis design altogether may have a significant effect on metabolic rate as well. Metabolic rate results from [10] are compared with corresponding results from [4] in Figure 2.2.

Some analysis of prosthesis design elements which are not propulsion-focused exists as well. Literature exists which supports the ability of semi-active ankle designs, such as the commercial Össur Proprio-Foot®, to encourage able-bodied kinematics and lower socket pressures [28], [29], [139]. Semi-active knees with viscous damping have also been shown to reduce metabolic cost, as well as biological joint moments and power [140]. Stiffness effects have also been investigated for shock absorption purposes. For example, a study which investigates longitudinal compliance in prosthesis pylons observed no clinically relevant changes to the kinetics of gait for the range of commercially-available, longitudinal compliances [141], [142]. Similarly, work has been done to investigate the role of torsional compliance on the ability to perform turning tasks. Study participants have reported a reduction in perceived load and effort in performing turns while walking with an adaptive shank prosthesis capable of adjusting torsional compliance and foot alignment [32]. Increased torsional compliance in a separate adjustable torsional compliance device has also been demonstrated to reduce measured peak torsion moments when performing large angle turns without adversely affecting normal walking [31], [143]. Additionally, active alignment of ground reaction forces has been shown to reduce in-socket flexion loads and related pressures on the residual limb in a pilot study with a single participant [123]. However, the effects of these flexibility- and relief-focused approaches on broader outcome measures such as metabolic cost, preferred walking speed, walking stability, individual muscle engagement, and osteoarthritis risk factors are not well-characterized.

2.4.3 **Secondary Impairment Mitigation**

As with short-term gait restoration, the focus of many studies analyzing the ability of prosthesis designs to mitigate long-term problems is with restoring propulsion. These studies have

produced mixed results in supporting the hypothesis that near-biological levels of push-off work reduce elevated osteoarthritis risk factors like knee EAM. Results that support this hypothesis include significant correlations found between push-off work and knee EAM in a semi-active design [24], the presence of powered ankle plantarflexion and knee EAM [12], and the presence of combined powered ankle and knee toe-off assistance and knee EAM [144]. However, peak EAM values for trials with powered ankle plantarflexion in [144] were comparable to the case where no assistance was provided at all in absence of linearly increasing ankle stiffness through stance. The correlation in [12] was observed only for two of five walking speeds.

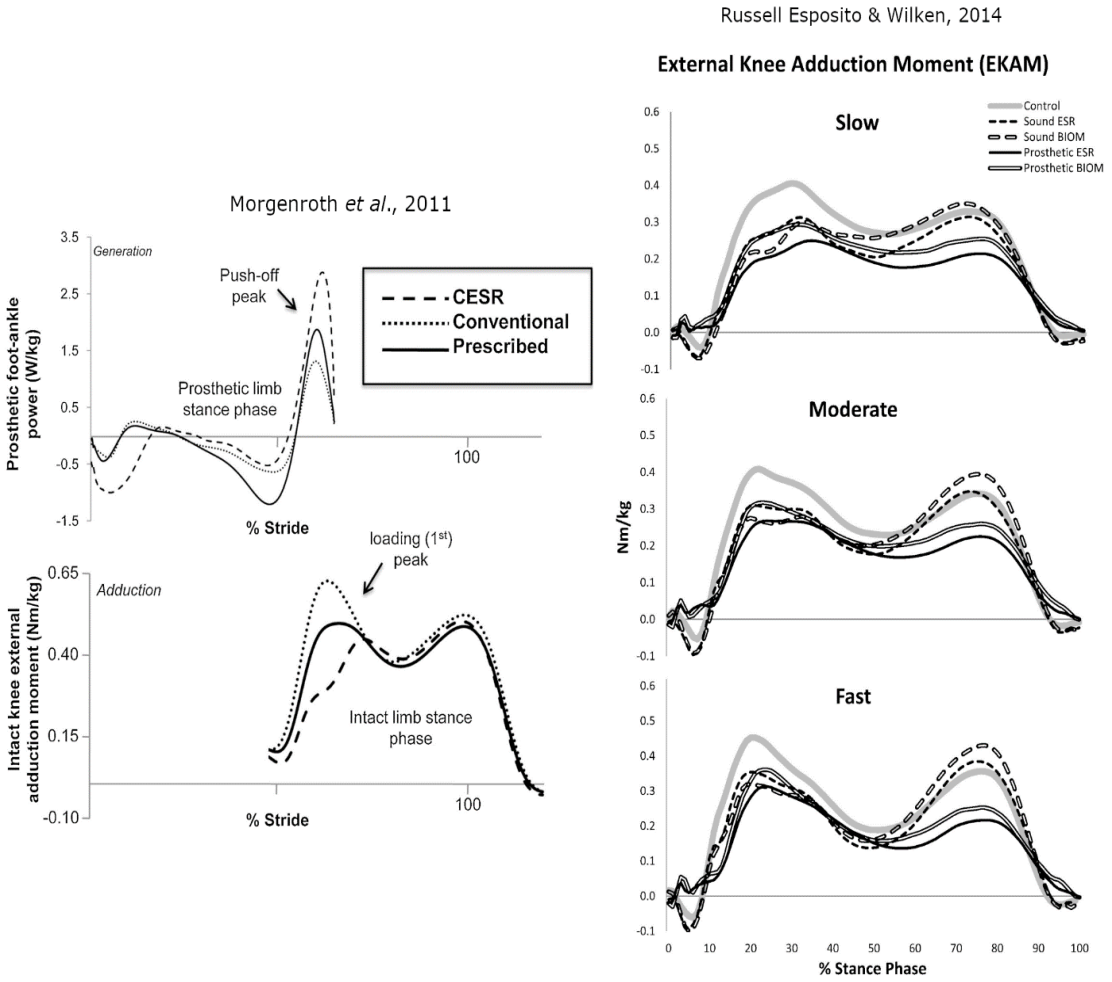

Figure 2.3. Comparison of results between two studies with different user populations. The use of additional push-off work from an Empower® ankle with young amputees not showing risk factors for knee OA did not decrease the external knee adduction moment in the sound limb in [11] **(right figure), which it did for a more typical amputee population in** [24] **using a semi-active energy recycling prosthetic foot (left figure).**

A comparison of results is shown in Figure 2.3 from two different studies with one using an energy recycling prosthesis [24] and other using a powered foot-ankle (Ottobock Empower®) [11]. While a peak EAM was observed for the energy recycling foot, no significant decrease in peak EAM or EAM impulse was observed with the use of a powered ankle-foot prosthesis compared to a passive elastic prosthesis in active young individuals within the first few years of walking with a prosthesis. This group also showed EAM values within a normal range for able-bodied persons with both prostheses, suggesting that osteoarthritis risk factors for amputees, and therefore prosthesis design priorities, change with individual health and age.

Because many comorbidities arise due to a decline in overall health and changes in lifestyle [23], another key design goal is to encourage the user to wear the prosthesis often and use it actively. This goal prioritizes outcome measures such as user satisfaction and other human factors. Some analyses of user experience measures have been performed: For example, prosthesis power was found to decrease user satisfaction with the emulator device above and below the net work setting nearest to the biological ankle [10]. In another study with young, highly athletic ESAR prosthesis users [38], ratings of perceived exertion, ease of and satisfaction with walking, and pain intensity reflected high levels of satisfaction across all metrics on average. A design method has additionally been proposed which incorporates user survey data involving ratings of perceived security, body schema integration, support, socket satisfaction, mobility, aesthetics, and general satisfaction into the design process [36]. However, a systematic review of studies that provided satisfaction questionnaires to users found that comparisons between studies could not be directly made due to a lack of standardized variables and terminology [145].

The results of these studies suggest that decreasing secondary impairment risk factors depends on more factors than increasing propulsion work. The knowledge gap, as with gait restoration objectives, is the characterization of how design factors affect the risk factors. Work to

address this gap is ongoing, and new approaches are emerging to support this effort. The next section details the work supporting these approaches and identifies opportunities for future work building on them, with the goal of developing a framework within which user outcome-based design optimization can be achieved.

2.5. Emerging Approaches and Research Challenges

2.5.1 Experimental parameterization of designs

Creating an accurate mapping between design parameters and clinical outcomes is a significant research challenge. Efforts have been made to isolate individual design parameters and experimentally determine their effects on users' biomechanics and experiences. This type of analysis has been performed for passive prosthesis stiffness [134], [137], [146], as well as for parameters of active propulsion designs such as net work and push-off timing [10], [138]. However, there are many other parameters and relevant user outcomes for which a considerable research potential remains. Examples include prosthesis size/geometry, nonlinear stiffness response, damping ratio, actuator power density and distal mass distribution, range of motion, deflection or actuation in additional degrees of freedom, and time-variant or actively controlled mechanical properties. User outcome measures include socket loading, user stability, metabolic cost, preferred speed of walking, peak knee adduction moment, and user needs and experience (e.g., satisfaction with a device).

It is possible that some design parameters are more crucial for specific user outcome measures. Identification of population-specific responses to design parameters is also an important research area, as there is a significant amount of variability currently being introduced by comparing young versus old, traumatic versus dysvascular amputation, and months versus years of walking on a prosthesis. Well-modeled relationships between design parameters and outcomes would enable the design process to prioritize specific outcomes differently and arrive at different solutions accordingly.

Experimental approaches also have substantial challenges. Quantifying the parametric effects on the biomechanics of the user requires a significant effort to be made to isolate the parameters being investigated. Variables such as the user's age, weight, time post-amputation, activity level, and preferred walking speed are difficult to control for due to a typically limited number of volunteer participants. Acclimation to a new prototype design is also difficult to control for between studies due to individually varying comfort levels and familiarity with different prostheses. Additionally, it is difficult to determine when a participant has acclimated to a device due to a lack of defined metrics or thresholds. Consistency between subjects is further complicated by the qualitative nature of prosthesis alignment and socket fit assessments and the varying availability of professional prosthesis fitting and installation staff. Aside from the logistical challenges, the existing work illustrates that the biomechanical response to a single parameter variation can be highly complex and coupled to other factors that are not measured [10], [137], [138], [146]. For example, increasing push-off work for a powered ankle may increase metabolic rate in one user while decreasing it in another [10].

2.5.2 **Model-based simulation**

Model-based biomechanics simulations are increasingly being used to analyze the performance of prosthetic designs on the overall musculoskeletal system. Models of gait based on simple passive dynamic walker models have been used to motivate ankle propulsion work as a critical function of below knee prostheses [1], [2], [147]–[149]. In these models, the stance leg is assumed to act as the rigid rod of an inverted pendulum, with a powered transition period taking place between steps required to accelerate the center of mass forward and upward onto another inverted pendulum trajectory. Other simple gait models include additional degrees of freedom in the leg to more closely resemble human gait mechanics, such as the spring-loaded inverted pendulum (SLIP) [150], [151], telescoping leg [152], [153], and muscle-actuated knee joint models [153], [154].

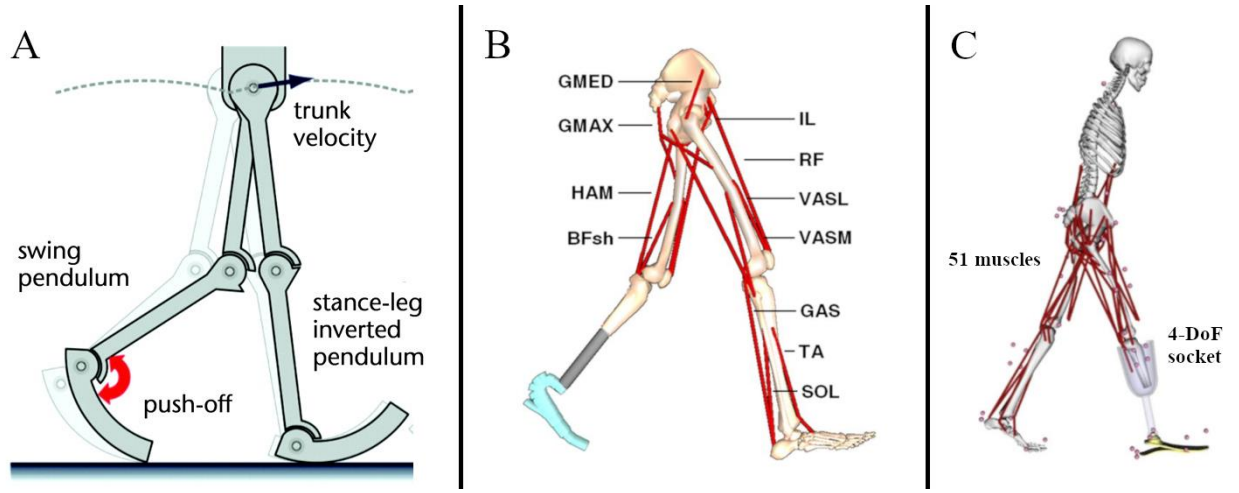

Figure 2.4. A) Human walking model based on simple dynamic walking mechanics [1] **compared with B) a model incorporating realistic muscle behaviors and a rigid socket connection developed in SIMM (Motion Analysis Corp.), and C) a model incorporating realistic muscle behaviors and socket motion using OpenSim** [48]**. In the dynamic walking model, the mechanics of walking are modeled as a series of inverted pendulum trajectories with a double-stance step-to-step transition period. In the musculoskeletal models, muscles are modeled with physiological activation dynamics and attachment points, rendered here as red lines.**

Recently, more elaborate musculoskeletal models have become prevalent in simulating human locomotion, including physiologically accurate muscle dynamics and insertion points [48], [137]. A dynamic walking model is shown in Figure 2.4A, and more complex human musculoskeletal models are shown in Figures 2.4B and 2.4C. This increased level of detail is due, in part, to the increasing availability of commercial modeling and simulation software such as AnyBody (AnyBody Technology A/S), Visual3D (C-Motion, Inc.), and SIMM (Motion Analysis), as well as open source software such as such as OpenSim [155]–[157]. These platforms facilitate modeling and simulation work by integrating customizable musculoskeletal models and analysis tools. Furthermore, as modeling and simulation become more prevalent as analysis tools, they are increasingly being integrated into the design process.

Researchers have begun to use model-based simulation to optimize designs of assistive devices for simulated user outcomes. For example, gait simulations based on tracking experimental kinematics were used to optimize passive ESAR foot parameters for minimal metabolic cost and knee contact force with a simulated annealing algorithm in [136]. Other projects have used simulation to

identify ways in which prosthetic devices may diverge from the biological anatomy to improve performance. The actuation trajectory of the powered ankle in [45] was designed by simulating the gait of a user by tracking able-bodied gait kinematics for the biological joints of the model and measuring the calculated moment through the socket-limb connection. It was found that allowing ankle motion in a non-anatomical translation arc reduced simulated socket-limb interaction moments [45]. Similarly, a parameter search to design an asymmetric transfemoral prosthesis was performed in [158], in which the artificial knee center of rotation and the mass distribution of the prosthesis limb segments were altered to enforce symmetrical passive walking dynamics in forward simulations. It was found that symmetry in the passive walking dynamics could be restored by designing the prosthesis parameters to be asymmetrical with the sound limb, with different limb segment lengths, mass distributions, and knee axes of rotation [158].

With the exception of the last example, which removes active control from the problem entirely, these examples make use of human data to provide a realistic reference for simulations to track when solving for actuator or muscle controls. However, this limits the scope of the design problems which can be solved and forces the designer to make the assumption that the resulting motion will be the same as some previously recorded motion with a different prosthesis or an able-bodied person. Research in predictive simulations of human gait, alternatively, solves the optimal control problem for objectives in which the resulting motion is not (or is loosely) prescribed in an attempt to simulate the way a person “would” perform a task, considering the new dynamics of the human walking with the device. With accurate and efficient predictive simulations of human gait, virtual experiments could be conducted with hypothetical prosthesis designs. This could eliminate the physical requirement of a working prototype to estimate its effect on gait or be used with simulators to perform human-in-the-loop experiments even before a prototype is built [159]–[161].

Predictive simulations of human walking have been able to capture many of the characteristic features of human gait primarily through optimization of muscle activations for minimum effort [13]. This approach is based on the hypothesis that humans naturally pursue the most energetically efficient means of locomotion [14], based on data which show that preferred walking and running patterns approximately minimize metabolic energy cost [162]–[164]. Minimization objectives for this approach include summed muscle activations raised to a power [13], calculations of metabolic cost based on muscle models [14]–[16], summed muscular mechanical energy expenditure [17], and summed muscle stresses [133].

This approach has also been applied to gait with a powered prosthesis, in which prosthesis energy cost and metabolic energy cost are used as competing objectives in the minimization [19]. The results of this study suggest that an ideal powered prosthesis could reduce the metabolic cost of walking below able-bodied levels. The same group later simulated multiple ankle flexion controllers as implemented in specific research prostheses and found that they do not improve the metabolic cost as much as the unrestricted optimal control result, suggesting that control design may factor into the modest metabolic efficiency gains seen in existing prototypes [165]. In [18], predictive gait simulations were used with a passive prosthesis model to determine that metabolic cost may not necessarily increase after limb loss if intact muscle strength is maintained.

However, it is still unknown whether simulation conditions which yield accurate estimates of able-bodied gait may require modification to accurately simulate and address issues specific to walking with a prosthesis. For example, predictive simulations using a passive prosthesis model have included minimization of joint moment asymmetry as an objective [20]. This approach highlights an attribute of gait specific to people with amputations and finds that simulated joint moment asymmetry can be substantially reduced at the expense of muscle effort while maintaining similar kinematics. Additionally, accurately reproducing the features of able-bodied gait is still a major

challenge, indicating that perhaps additional objectives or conditions for simulating walking with a prosthesis are necessary as well – for example, physical discomfort or perceived instability. Defining the objective function in the context of prosthesis design could also function as part of the design process by indicating the relative priority of functional design criteria.

However, a major component of this work is being able to identify when results reflect an artifact of the model or simulation method rather than a real physiological trend. Gait patterns due to personal biomechanics and socket fit show strong inter-individual variations, which predictive simulation cannot compute without personalized models. Additionally, simulations with prototype prostheses require assumptions to be made about the mass distribution or other mechanical properties of the design which may not match the final device [166]. It is, however, a significant challenge to establish model and simulation fidelity sufficient to draw generalized conclusions and make design decisions.

One approach toward improving simulation accuracy focuses on increasing the quality and level of detail of the models themselves. For example, a key attribute of the coupled system human-prosthetic system is the mechanics of the socket-residuum interface, due to the potentially large effect it might have on gait mechanics and muscle control decisions. This attribute is often represented as a rigid connection [18]–[20], [54], [136].

Efforts to measure and model socket-residual limb behavior are ongoing. One approach has been to indirectly calculate the kinematics of the socket relative to the underlying bone from marker-based motion capture data based on assumptions about joint constraints imposed on the system [48]. This method attempts to calculate socket motion non-invasively and without the harmful side effects of repeated X-ray exposure, but is limited in that possibly non-physiological constraints on the socket joint must be imposed to calculate a unique solution. This work has not yet resulted in the construction of a mechanical model of the socket. Other approaches attempt to model the tissue

mechanics directly by fitting parameters to match recorded data. For example, a two-dimensional socket-limb model with elastic and friction parameters was developed and optimized to agree with experimental pressure and kinematic data obtained from previously published experiments in [13]. Other researchers have attempted to model the tissue mechanics of the residual limb using a finite element approach, optimizing the material properties to match force response measurements recorded from indenter devices used on a user's residual limb [117]–[119].

All of these methods face challenges in modeling for a highly variable set of conditions per individual, including tissue mass, limb length, and suspension type, some of which also exhibit strongly nonlinear behavior. They also face challenges in the limited amount of data available for socket forces and kinematics across a wide population.

Another major challenge with simulation-based approaches is resource feasibility. As model realism increases so does model complexity in the form of more degrees of freedom, more muscles, more complex measures of values such as metabolic cost, and more complex or denser contact models – including soft tissue models such as the socket-residuum interface. The trade-off between model complexity and computational cost is a key concern and is especially significant in computationally expensive operations like predictive simulation, of which the cost of each iteration scales with model complexity, number of constraints, and granularity of time resolution. Predictive able-bodied gait simulation studies often use one standard deviation for each coordinate of experimental walking kinematics and ground reaction forces as a simulation accuracy benchmark [15], [20], [133]. However, regardless of complexity, computational models are subject to uncertainty in fundamental parameters such as body segment lengths and inertial properties [167]–[169]. Efforts have been made to identify the sensitivity of simulation results to model parameters [167], [168], which could allow for more efficient models tuned for specific simulation tasks.

Improvements in computing power and algorithm efficiency have made predictive simulation a more practical tool [170], but pushing the boundary of this trade-off to allow more efficient simulations with a high degree of accuracy, as well as identifying the level of accuracy required to obtain practically useful results, remains an important direction for future work. This is especially true for potential future applications in which simulations occur in real-time or in embedded systems (e.g., control and adaptation).

Currently, no method exists for a prosthesis design to be generated or optimized using predictive simulations of its effect on human mobility tasks and outcome measures. To do so and test the resulting prototype on human users would provide valuable insight into the validity of the method as well as potential mechanisms for prosthetic influence on user outcomes. Such experiments could also provide data to assess and modify predictive simulation methods. Development of realistic multi-objective predictive simulations could also help to identify the causes for gait abnormalities by reproducing them with modifications to the optimization objectives.

2.6. **Conclusions**

Research work in lower limb prostheses has focused heavily on restoring propulsive work to the affected limb. The inconsistency of results and broader analysis of biomechanical effects illustrate the degree to which a more detailed understanding of the causal relationships between design factors and outcome measures is needed. Traditional gait restoration metrics such as metabolic cost and kinematic similarity to able-bodied gait are not sufficient to fully capture the efficacy of a prosthesis in enabling optimal gait patterns. Limb loading, socket fit, walking stability, and individual muscle compensations are all likely contributors to discomfort, excessive effort, and user dissatisfaction in general. The characterization of how prosthesis design factors affect the outcome measures remains the primary knowledge gap in targeting design objectives. Efforts are ongoing to experimentally evaluate these relationships by isolating design parameters and observing user outcomes. Many of

these efforts have focused on global biomechanical measures such as metabolic cost or gait mechanics, but measures of user experience or more specific biomechanical information such as task-specific muscle contributions are also important aspects to the design problem. It is possible that many of these performance measures may be better improved by de-emphasizing anthropomorphism in prosthesis design because the biomechanical and sensory system of a person with a lower limb prosthesis is distinct from that of an able-bodied person. However, the limits to which deviation from anthropomorphic norms are functionally useful or acceptable to the user are unknown and likely vary by user and application. Modeling and simulation efforts offer the potential to conduct virtual experiments, but establishing accuracy and trustworthiness of the resulting solutions remains a significant challenge, and simulation results cannot replace experimental measures and user feedback.

A range of research opportunities to advance the ability to design for optimal user outcomes exists between two suggested research paths: experimental parameterization of designs and model-based simulations. Progress in both paths could improve the accuracy of a broad scope of predicted user outcomes using prosthesis design models, which may allow these outcomes to be factored early into the design process. Opportunities for work in these paths exist across domains including engineering design, biomechanics simulation and modeling, experimental biomechanics, user experience surveys, and engineering analysis. The advancement and synthesis of these fields may create the framework to optimize lower limb prostheses for desired user outcomes.

With respect to the work presented in this thesis, optimal control simulations provide a unique toolset to explore unconventional and unrestricted design ideas and their theoretical effects on selected user outcomes. The lack of existing approaches which fully exploit the flexibility of this approach is what motivates the simulation approach discussed in the following chapter, in which the

behavior of a generalized prosthesis model is optimized to simultaneously improve two user outcomes – reducing both muscle effort and peak socket loads on the residual limb.

CHAPTER 3

DYNAMIC OPTIMIZATION OF GAIT WITH A GENERALIZED LOWER-LIMB PROSTHESIS MODEL

Potential avenues to explore the prosthesis design space outside of the traditional process via simulation studies were identified in Chapter 2. This chapter defines the scope and goals of a specific simulation study designed to result in the identification of prosthesis behaviors which improve selected user outcomes.

This chapter is adapted from a conference paper titled *Dyanamic Optimization of Gait with a Generalized Lower-Limb Prosthesis Model*, written with second author Brian Umberger of the University of Michigan and third author Professor Frank Sup of the University of Massachusetts, Amherst [171]. This paper was presented at the International Conference of Rehabilitation Robotics in Toronto, July 2019. In this chapter, we simulate walking with a below-knee prosthesis capable of outputting loads and displacements freely in the sagittal plane.

Abstract — Predictive simulation of gait is a promising tool for robotic lower limb prosthesis design, but has been limited in its application to models of existing design types. We propose a modeling approach to find optimal prosthesis dynamics in gait simulations without constraining the prosthesis to follow kinematics allowed by a specific joint mechanism. To accomplish this, we render a transtibial prosthetic device as the composition of its resultant forces and moments as they act upon the prosthetic foot and socket and allow 3 degree-of-freedom planar motion. The model is implemented into a human musculoskeletal model and used to solve dynamic optimizations of muscle and prosthesis controls to minimize muscle effort and loading on the residual limb during walking. The emphasis on muscle effort vs. limb loading is varied in the minimization objective and the resulting optimal prosthesis dynamics are compared. We found that muscle effort and socket loading measures were reduced for our prosthesis model compared to a revolute joint prosthesis model. We interpret large displacements in the linear axes to transfer energy to the plantarflexion

action before toe-off and reduce loading at the socket-limb interface. Our results suggest this approach could assist in the design of non-biomimetic prostheses but requires experimental validation to assess our modeling assumptions, as well as progress toward increased fidelity of predictive simulation approaches more generally.

3.1. Introduction

Advances in robotic lower-limb prostheses have demonstrated the potential to improve their users' locomotor performance [79]. Improvements such as decreased metabolic cost of transport [4], increased preferred walking speed [4], decreased muscle contributions to positive work performed on the center of mass [3], decreased external knee adduction moment in the intact limb [24], decreased pressures on the residual limb [123], and increased kinematic symmetry [123] have been observed with the use of powered robotic prostheses in comparison to passive prostheses. However, despite the ability of current designs to closely mimic the dynamics of the missing anatomy, these metrics have not been fully restored to able-bodied levels [3], [4], [10]. The performance gap has motivated recent research attempting to uncover the underlying biomechanical factors and design parameters that determine the effect of a prosthesis on user outcomes.

One result of this ongoing work is an increased focus on computational simulation of human biomechanics to estimate user response to a prosthesis. Optimal control simulations of human walking can be obtained by minimizing performance criteria, such as the metabolic energy expenditure or summed muscle activations of a human musculoskeletal model [13], [14]. This approach enables researchers to conduct virtual experiments with hypothetical designs and analyze the effects of changing design parameters on gait. For example, gait simulation studies have analyzed the effect of powered prosthesis work rate on metabolic energy expenditure and suggest that an ideal powered ankle prosthesis could reduce the metabolic cost of transport in transtibial amputees below able-bodied levels [19], [172]. In addition to effort measures, other minimization objectives have been

considered. For example, it was observed that joint loading asymmetry in amputees could be reduced at the cost of increased metabolic expenditure in simulation [20].

However, current research is limited to the optimization of gait with existing prosthesis design forms, constrained to follow the dynamics allowed by the mechanism model. This has left an opportunity to research the full design space to better understand optimal prosthesis dynamics. For example, assumptions of a revolute ankle joint may result in sub-optimal prosthesis dynamics due to constraining the behavior from adapting to changes in the overall human dynamical system introduced by the addition of a non-rigid socket-limb interface. Our present work proposes to search the prosthetic design space without constraints of a preconceived design solution by directly optimizing prosthesis dynamics as they interact with the connecting limb segments, irrespective of the mechanism required to generate those dynamics. This modeling approach is illustrated in Fig. 1.

The objective of this work is to demonstrate that a generalized (mechanism-agnostic) prosthesis model can be developed to simulate the gait of a prosthesis user based on optimal control methods. The approach can be used to address how prosthetic devices could behave differently from anatomical joints when motion constraints in the sagittal plane are removed. Further, it could be used to study how human-prosthesis dynamics change when priority is placed on different optimization objectives (i.e., socket loading, joint loading, metabolic energy, prosthetic performance).

The chapter is organized in five sections starting with this introduction and followed by Section 3.2 which describes the modeling and simulation methodology used to generate planar prosthesis dynamics, as well as the specific parameters being investigated in this study. Section 3.3 presents the optimal control solutions, Section 3.4 discusses notable results, and we provide conclusions and describe future work in Section 3.5.

3.2. **Methods**

This study consists of a series of dynamic optimizations of human walking. Optimal control problems were formulated to generate a full stride of gait at a prescribed walking speed with the generalized prosthesis model incorporated into the musculoskeletal model. This section describes the specifics of the model implementation and the form of optimal control problem being solved.

3.2.1 **Human-Prosthesis Musculoskeletal Model**

The human-prosthesis model is shown in Figure 3.1. The model was created with the OpenSim open-source musculoskeletal modeling and simulation platform [155]. The human-prosthesis model is a 12 segment, two-dimensional musculoskeletal model with 15 degrees-of-freedom (DOF) in the

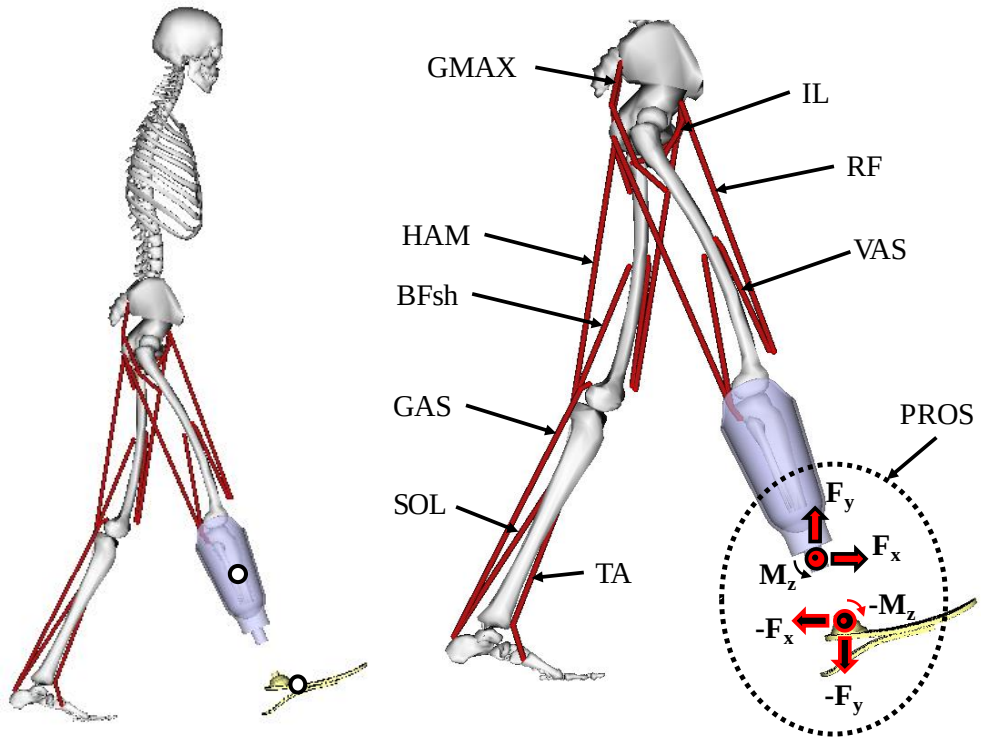

Figure 3.1. OpenSim rendering of the human-prosthesis model used for this study. Locations of the joint axes for the socket joint and prosthetic foot bending are indicated in the full-body illustration. Both legs have identical sets of 6 muscles: Gluteus maximus (GMAX), iliopsoas (IL), hamstrings (HAM), rectus femoris (RF), biceps femoris short head (BFsh), and vasti (VAS). The sound side limb has three additional muscles which cross the biological ankle: Gastrocnemius (GAS), soleus (SOL), and tibialis anterior (TA). The prosthesis model (PROS) has three model actuators which react against both the socket and the prosthetic foot.

sagittal plane. The biological joints are actuated using 15 Hill-type muscle models based on a computational implementation developed in [173].

The model includes a right-side unilateral transtibial amputation and prosthesis socket. This socket is connected to the residual tibia with a 2-DOF joint (flexion and axial translation, or "pistoning"). Each of these coordinates is subject to a passive elastic force relationship, consisting of a linear spring-damper with stiffness values (flexion: 600 Nm/rad, pistoning: 35,000 N/m) corresponding to peak socket displacement values relative to subject mass taken from data in [48]. We included this joint in the model due to the potential for motion at the socket to influence the optimal planar dynamics of the prosthesis.

A passive prosthetic foot is modeled as two rigid segments connected by a pin joint. Foot flexion is approximated with lumped stiffness and damping parameters acting at the pin joint (450 Nm/rad). This simplification of the continuous flexion of a foot prosthesis is included for computational efficiency, as commonly seen in the literature [18], [20], [165]. Foot-ground contact is modeled using Hunt-Crossley contact mechanics between the ground plane and contact spheres on the bottom of the feet [156].

The prosthetic ankle joint is represented as a 3-DOF planar connection between the socket and the prosthetic foot. This generalized prosthesis model is described as "mechanism-agnostic" because it does not include any model segments, but instead contains a virtual ideal force or moment actuator aligned with each DOF. These actuators are governed by:

$$F_x(t) = k_x u_x(t) \tag{3.1}$$

$$F_y(t) = k_y u_y(t) \tag{3.2}$$

$$M_z(t) = k_z u_z(t) \tag{3.3}$$

$$-1 \leq u(t) \leq 1. \tag{3.4}$$

where k is a scalar gain applied to the control signal $u(t)$ to define the saturation limit for the output force or moment in the corresponding coordinate frame. In this frame, the x-axis is the anterior-posterior axis of the foot, the y-axis is the inferior-superior axis, and the z-axis is the flexion axis of the ankle. The control signals act as inputs to the model actuators and are included in the controls vector along with the muscle excitations. These outputs act on both the prosthesis socket and the prosthetic foot connector in opposite directions. This simulates the net resultant forces exerted on the adjacent segments by an undefined prosthetic joint, allowing the simulation to optimize prosthesis output dynamics irrespective of mechanism constraints. This model was also implemented with the two linear translation coordinates locked, and is referred to as a revolute ankle prosthesis model in the simulation experiments.

3.2.2 **Objective Cost Functions**

Solutions for gait were found by minimizing a weighted sum of performance objectives. The overall objective function includes terms for muscle effort, socket-residuum loads, net positive work injected into the system by the prosthesis, and tracking of able-bodied walking kinematics. Each of these terms is normalized against the value obtained from a gait solution which tracked able-bodied joint kinematics using the revolute prosthesis model, with the exception of the net work objective, which was normalized against the approximate net positive work generated at the biological ankle during level walking near 1.3 m/s (approx. 8 J for our 76 kg model [174]).

The minimum effort term is described by

$$F_{\text{effort}} = \frac{1}{N_m t_f} \sum_i \left[\int_0^{t_f} A_i(t)^3 \, dt \right] \tag{3.5}$$

where N_m is the number of muscles in the model, $A_i(t)$ is the activation of muscle i as a function of time t, and t_f is the time in seconds to complete one full gait cycle. We use a muscle activation approach for this objective as in [13], [133]. We include this term to minimize the muscle fatigue of the user.

The socket loading term is described by

$$F_{\text{loading}} = \frac{1}{2t_f}\int_0^{t_f}\left[M_{\text{flex}}(t)^{10} + F_{\text{pist}}(t)^{10}\right]dt \tag{3.6}$$

where $M_{\text{flex}}(t)$ and $F_{\text{pist}}(t)$ are the flexion moment and pistoning force exerted on the residual limb by the socket at time t, respectively. We include this term to minimize discomfort or pain caused by high load magnitudes at the socket – an additional factor in walking with a prosthesis which may not be accounted for with energy optimality criteria. This objective is constructed to approximate a min-max function with high exponents while maintaining differentiability [175].

The able-bodied tracking objective is described by

$$F_{\text{track}} = \frac{1}{N_q t_f}\sum_j\left[\int_0^{t_f}\left[\frac{q_j(t)-q_j^*(t)}{\sigma_j(t)}\right]^2 dt\right] \tag{3.7}$$

where N_q is the number of tracked coordinates in the model, $q_j(t)$ is the value of coordinate j at time t, $q_j^*(t)$ is the value of tracked reference coordinate j at time t, $\sigma_j(t)$ is the between-subjects standard deviation of coordinate j at time t, and t_f is the time in seconds to complete one full gait cycle. Reference coordinates and standard deviations were used from [176], and include hip, knee, and ankle kinematics as well as ground reaction forces. Ankle flexion was not tracked on the prosthesis side due to the non-anatomical mechanics of the model joint. We include this term to influence the solution toward average, non-pathological gait-like behaviors, weighted two orders of magnitude smaller than F_{effort} to prevent tracking from dominating the optimal control solution [177]. An objective function that more accurately represents the motor control strategies sought by prosthesis users should not require this term, and instead would contain additional terms for control objectives not considered here (e.g., joint loading, stability, smoothness of motion).

The prosthesis work minimization objective is described by

$$F_{\text{work}} = \frac{1}{t_f}\sum_k\int_0^{t_f}\left[\tau_k(t)\dot{\theta_k}(t)\right]^2 dt \tag{3.8}$$

where τ_k is the kinetic output of virtual actuator k at time t (either force or moment) and $\dot{\theta_k}$ is the velocity (linear or angular) of the corresponding kinematic coordinate at time t. We include this term to penalize an unrealistically high energy output from the prosthesis that results in marginal improvements in the other objectives. It is weighted three orders of magnitude smaller than F_{effort} to ensure that its effect on the biomechanics in the solution is minimal, similar to the optimal human cost condition in [19].

The entire objective function is described by

$$F = F_{\text{effort}} + \alpha F_{\text{loading}} + \epsilon_1 \text{F}_{\text{track}} + \epsilon_2 F_{\text{work}} \tag{3.9}$$

where $\epsilon_1 = 10^{-2}$ and$\epsilon_2 = 10^{-3}$. We parametrically vary socket loading weighting α on a logarithmic scale from ϵ_2 to 10 to assess the effect of increasing or decreasing loading minimization on the output prosthesis dynamics. This range is designed to simulate minimal consideration for socket loading on one extreme to socket loading being the dominant objective by one order of magnitude on the other.

3.2.3 **Optimization Structure and Constraints**

We minimize these objectives using a direct collocation approach [13], [178], using MATLAB to interface with OpenSim and run the open-source IPOPT [179] solver, as in [170]. We render a full gait cycle with 51 nodes. Constraints exist at each node to satisfy the system dynamical equations. Additional constraints enforce periodicity of the resulting motion as well as the average walking velocity. The net power generated by the summed prosthesis actuators was constrained to be less than 300W at each node, and the planar range of motion was constrained to ±5cm (linear) and ±60° (flexion).

To simulate variability present in the biomechanics of actual human subjects, an array of simulations with modified simulation parameters was run for each objective function condition. Three walking speeds were enforced: 1.1, 1.3 (nominal), and 1.5 m/s. Additionally, three socket stiffness

multipliers were used in the model: 0.75, 1 (nominal), and 1.5. This combination of parameters results in 9 different simulations run for each objective function condition, for a total of 45 solutions. An identical set of simulations was run using the revolute prosthesis model. 1-way ANOVA was used to assess the effect of the simulation variables on the objective values.

The tracking solution used to normalize the objective values was supplied as the initial guess for the generalized prosthesis model at nominal conditions and α = 0.1. The resulting simulation was then used as the initial guess for all remaining conditions. Some simulations did not converge to gait-like locomotion (i.e. hopping on one leg, unable to satisfy system dynamics constraints) and were omitted from the results. 38 solutions were used for the generalized prosthesis model, and 37 solutions were used for the revolute model.

3.3. **Results**

The normalized objective values for muscle effort and socket loading are shown for all three conditions in Figure 3.2. The peak socket loading objective was more sensitive to the objective weights when using the revolute ankle prosthesis model compared to the generalized prosthesis model, with mean values ranging from 4% to approximately 1200% of the normalized baseline compared to a range of 4% to 49%. Mean muscle effort ranged from 22% to 40% of baseline for the revolute model, and from 17% and 28% of baseline for the generalized prosthesis model. Averaging all solutions, the generalized model reduced the socket loading objective from the revolute model by 91% ($p=0.02$), and reduced the muscle effort objective by 43% ($p=0.002$). Actual peak socket load magnitudes were reduced from the revolute model by 15% on average. Peak socket loading is strongly increased by reduced socket stiffness ($p<0.001$), and muscle effort is increased by increased walking speed ($p=0.003$). The effects of socket stiffness on muscle effort and walking speed on socket loading were not statistically significant ($p=0.1$ and $p=0.25$, respectively).

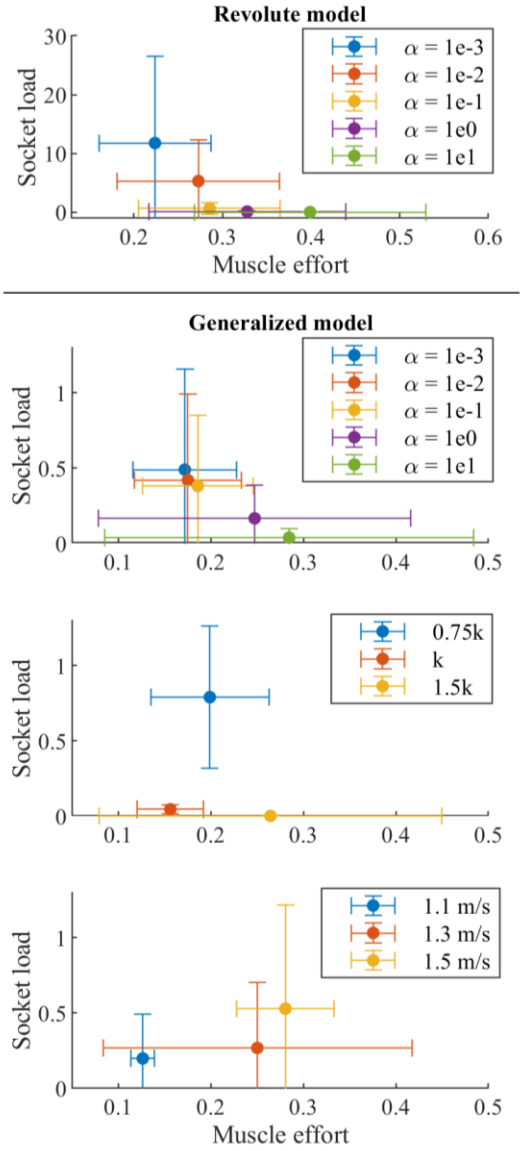

Figure 3.2. Objective values for solution arrays with five socket loading weight conditions (n=38 generalized, n=37 revolute). Error bars indicate +/- 1 SD.

Gait mechanics for the biological joints are shown in Figure 3.3. Peak hip flexion remains consistent with able-bodied patterns, but peak extension does not cross past the neutral position, reducing the hip range of motion by approximately 10°. Knee flexion is reduced during swing by approximately half. Peak ankle plantarflexion is observed at heel-strike instead of at toe-off, accompanying a spike in braking force and vertical ground reaction force at heel strike and a reduction in the second peak of the vertical ground reaction force.

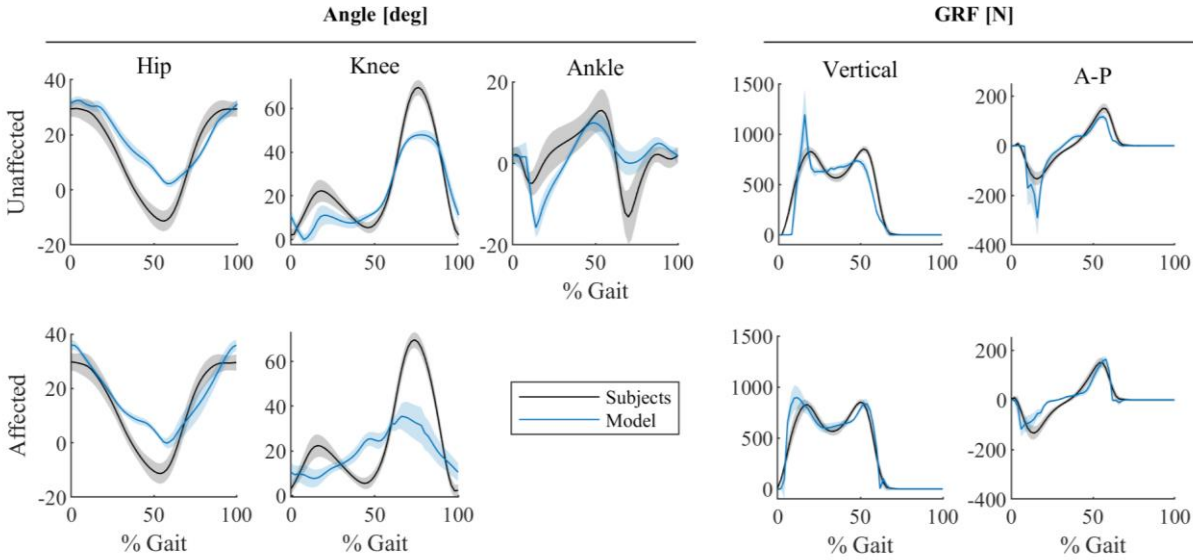

Figure 3.3. Biological joint kinematics from able bodied subjects (n=8) and simulation solutions (n=38). Shaded envelopes indicate +/- 1 SD. Prosthetic ankle joint is omitted due to 3-dof behavior in the sagittal plane. Positive angle values refer to flexion and negative refer to extension. Dorsiflexion and plantarflexion are positive and negative respectively for the ankle. Anterior and superior are positive for the GRFs. The gait cycle begins at heel-strike for each limb.

Work loops and powers for each prosthesis degree of freedom are shown in Figure 3.4. The linear displacements range across approximately 10cm in both axes (corresponding with the simulation bounds). The prosthesis aligns the socket anterior to the foot connector as stance progresses and returns to a neutral position during swing for all objective conditions. The vertical distance between the foot and the socket decreases rapidly before toe-off as the joint plantarflexes. The magnitude of the peak vertical force decreases as α increases. Flexion ranges across approximately 80° and reaches the bound of 60° of dorsiflexion near heel-strike. The flexion axis exhibits a burst of power generation shortly before toe-off as with the biological ankle. This is accompanied by a simultaneous burst of negative power in the y-axis nearly equal in magnitude. These peaks are reduced as the socket loading weighting increases in the objective function. Peak power magnitudes at toe-off are reduced by 29% in the y-axis and 36% in flexion from $\alpha = 1$ to $\alpha =$

10. A smaller positive power burst is seen in the x-axis as the socket displaces posterior from its forward position at toe-off.

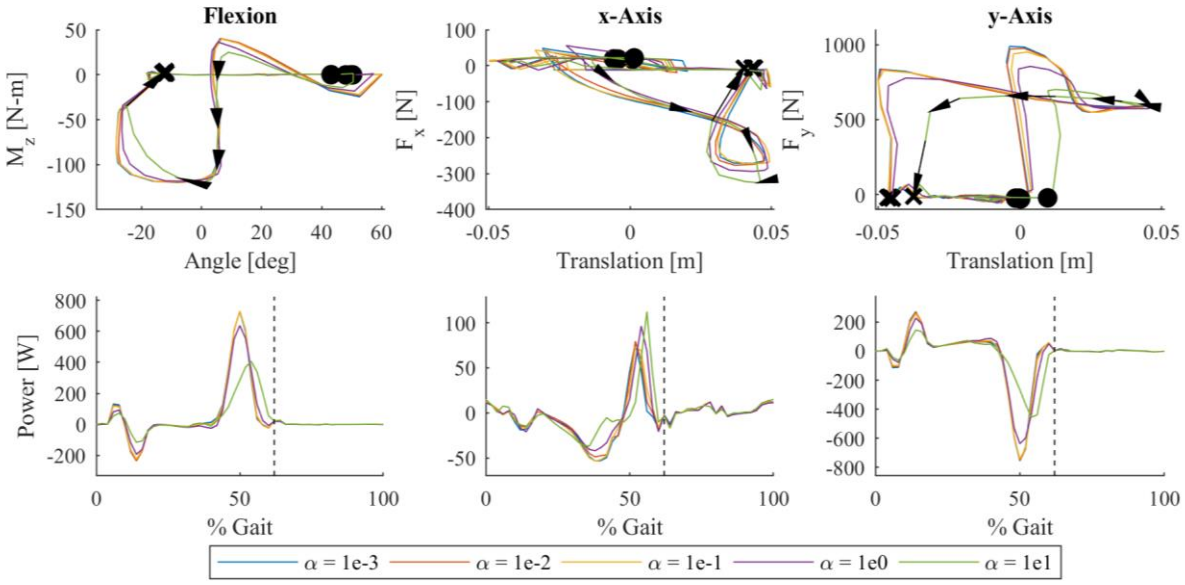

Figure 3.4. Mean work loops and prosthesis actuator powers for each actuated coordinate of the prosthesis model for each objective condition. Positive flexion indicates dorsiflexion, positive x-displacement anterior displacement of the socket, and positive y-displacement indicates superior displacement of the socket. A black circle marks heel-strike and a black 'x' marks toe-off of the affected limb for each work loop. A dashed line marks toe-off in the power plots.

The net mechanical work performed by the prosthesis over one stride for each objective condition is illustrated in Figure 3.5. The optimized prosthesis dynamics output approximately 20 J of positive net work, and about 40 J of energy is absorbed by the vertical displacement axis and transferred to the flexion axis, which exhibits about 60 J of positive net work across conditions. Net work at the x-axis is between -1 and -5 J across conditions. No visible trend is observable between objective conditions in the net work over the stride despite trends in the peak powers.

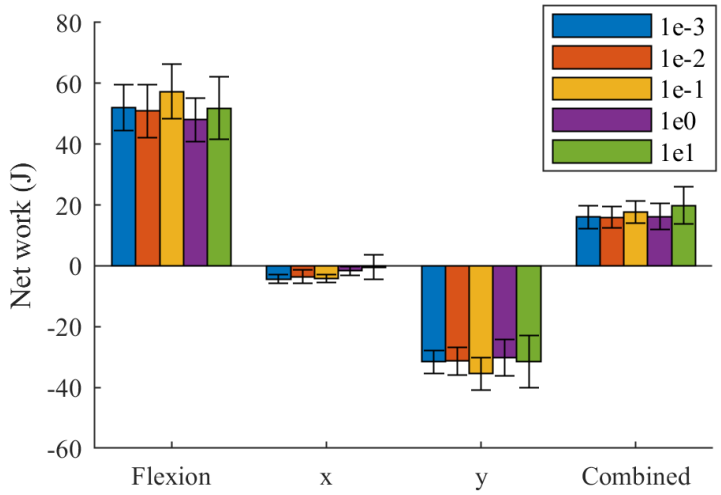

Figure 3.5. Prosthesis model net mechanical work over one stride for solution arrays with five socket load objective function weightings. Error bars indicate +/- 1 SD.

3.4. **Discussion**

In this study, we have presented optimal control solutions for gait and generalized prosthesis dynamics for multiple performance criteria. We found that a prosthesis model which is not anatomically constrained allowed for significant reduction in both the socket loading and muscle effort criteria over a flexion-only prosthesis model. However, the model biomechanics deviated from able-bodied gait patterns in ways which suggest that our minimization objective drives solutions toward an abnormal amount of asymmetry. Despite this, useful trends are observable in the prosthesis dynamics, including the presence of motion patterns in the translation axes to reduce socket loading, as well as apparent power coupling between flexion and vertical translation to reduce actuator demands.

3.4.1 **Muscle effort vs. socket loading minimization**

The objective function values of the solutions trend toward a Pareto-like distribution, as expected. Large amounts of variance are present in the objective values due to the perturbation of the speed and socket stiffness conditions. As observed experimentally, increasing walking speed is

associated with increasing metabolic cost [163]. Reducing socket stiffness by 25% of nominal increased peak socket loads by a factor of 17 for the generalized model. While our socket model is simplistic, this result supports the idea that a poor socket fit is a major factor contributing to discomfort in walking with a prosthesis.

3.4.2 Deviation of joint mechanics from able-bodied

In comparing the joint mechanics, major deviations from able-bodied biomechanics are present in the simulated gait. The lack of plantarflexion before toe-off and large amount of plantarflexion induced by heel-strike in the biological ankle joint is likely a result of muscle activity being heavily penalized in comparison to prosthesis activity, which drives asymmetry. The large peak ground reaction forces at heel strike of the unaffected limb compared to the relatively smooth ground reaction forces on the prosthesis side further indicate this loading asymmetry. Shallow knee flexions during swing can be similarly explained: The solution is driven to minimize the muscle activations required to achieve ground clearance, regardless of how unstable this gait pattern might be in unideal conditions. However, the amount of knee flexion of either limb while in swing should have little effect on the prosthesis dynamics during stance. We do not expect the simulated biomechanics to closely match able-bodied biomechanics due to the non-anatomical nature of the prosthesis model. However, the loading asymmetry of these biomechanics highlights that more realistic optimal control objectives for gait with the aid of a prosthesis likely require additional terms to account for factors such as stability, movement smoothness, or joint loading.

3.4.3 Functional analysis of prosthesis dynamics

The prosthesis energetics and work loops suggest specific roles for each coordinate axis through the gait cycle. The x-axis absorbs a small amount of net work over the gait cycle but exhibits a large translation magnitude. This serves to align the socket pylon toward the toe of the foot as stance progresses, suggesting that the primary role of this motion is in reducing the flexion moment on the

socket. The substantial positive work at the flexion axis suggests that net positive ankle flexion work remains an important factor in reducing muscle effort, as suggested by other simulation studies [19], [172]. The negative net work accompanied by large deflections in the y-axis suggests that this motion serves to reduce peak pistoning loads at the socket. The near inverse power curves of flexion and the y-axis suggest that these coordinates are coupled. Energy transfer between them may be an efficient way to reduce the required work output of the ankle flexion actuator. The work loops also reveal a behavior pattern in which the device alternates between periods of high and low stiffness with sharp transitions between the two, suggesting a finite-state impedance control approach may be practical.

3.4.4 **Study limitations**

The presented work has some key limitations. First, optimizing prosthesis dynamics for gait alone may leave the resulting design poorly adapted to other tasks. Similarly, the variability included in this study does not fully encapsulate the variability shown between actual subjects, ignoring variables such as subject mass, height, and residual limb length. A robust approach may require the simulation of multiple tasks and a wider range of model variability. Additionally, as with any simulation-based approach, this work is heavily dependent on model and simulation accuracy for useful results. Our use of a single initial guess risks converging to local minima, and accounts for the lack of successful convergence of some conditions. Our simulation is constrained to motion in the sagittal plane and includes a simple approximation of socket mechanics, and these limitations may prevent the simulations from capturing important factors in the optimal biomechanics of walking with a prosthesis. Additionally, uncertainty toward the correct objective function is a knowledge gap persistent in the predictive simulation of gait which further work is needed to address. As our understanding of optimality criteria best representative of walking with a prosthesis improves, confidence in predictive simulation outputs should also improve. Experimental work with prototype

designs capable of recreating simulated prosthesis dynamics would additionally provide feedback to refine the simulation assumptions and improve the accuracy of the results.

3.5. Conclusion

The presented prosthesis simulation approach optimizes prosthesis behavior in search of specified outcomes designed into the objective function without being constrained to the behavior of a specific joint mechanism. By solving optimal control problems for the human-prosthesis system, the effect of changes to the prosthesis dynamics on the biomechanics of the user are considered. The primary contribution of this work is the introduction of a tool for generating prosthesis design targets which are not based on assumptions of what a prosthetic joint should look like. The results of this study support the idea that optimal prosthesis performance may not align with biomimetic norms when the full system dynamics are considered.

Future work for this project will focus on designing and prototyping a robotic prosthesis test platform for experimental evaluation of simulated prosthesis dynamics on human subjects. Additionally, work remains to refine the predictive simulation objective function and socket-residuum model to increase the fidelity of gait simulations for persons with lower limb amputations.

CHAPTER 4

NON-ANTHROPOMORPHIC PROSTHESIS DESIGN GENERATED FROM SIMULATED GAIT OPTIMIZATION

The simulated prosthesis behavior provides guidelines for the design of new prototypes. However, simulation studies such as conducted in the previous chapter require equivalent experiments with human participants in order to validate their findings. In this chapter, the simulation method of the previous chapter is applied to generate design requirements for a prototype test platform capable of recreating a wide range of simulated prosthesis behaviors for experimental validation. These specifications are used to design the mechatronic system for the prosthesis test platform.

This chapter is partially adapted from a conference paper titled *Non-anthropomorphic Prosthesis Design Generated from Simulated Gait Optimization*, written with second author Professor Frank Sup of the University of Massachusetts, Amherst. This paper was accepted to the IEEE RAS/EMBS International Conference on Biomedical Robotics & Biomechatronics in New York City, November 2020. The sections detailing the concept development, load sensor design, structural analysis, actuator performance testing, and discussion sections dealing with the above were added for this document due to the conference publication being submitted as a work-in-progress.

Abstract— Simulations of walking biomechanics offer a tool for optimizing prosthesis performance while including estimates of the effects of the prosthesis on the rest of the body. We have previously used this technique to optimize the output behaviors of a generalized prosthesis model in the sagittal plane. In this paper, we present the design of a prototype prosthesis testbed for validating generalized prosthesis model predictive simulation results with experimental feedback. Design specifications are generated from simulated prosthesis dynamics and comparison with existing powered prostheses. A complete mechatronic system design based on these specifications is

presented. The design consists of two sub-systems: the ankle-foot prosthesis and a wearable off-board actuation and control system. The overall system is designed to function as a validation tool for prosthesis simulation experiments generally, and to provide experimental feedback to the simulation-based prosthesis design loop.

4.1. Introduction

People with lower-limb loss experience reduced mobility and an elevated risk for developing secondary health conditions or disabilities. With currently available passive prosthesis technology, lower-limb loss commonly results in higher energy costs for locomotion [55], chronic back pain [23], knee osteoarthritis [23], [39], [61], muscle atrophy [23], skin irritation [63], and pressure ulcers at the site in contact with the prosthesis socket [63]. More complex and powered devices have been shown to reduce some of these effects [4], [12], but user outcomes are inconsistent and usually do not improve to able-bodied levels. The persistence of these adverse effects necessitates the development of new prosthesis designs capable of mitigating them. To meet this design challenge, researchers may need to take advantage of new design tools.

Biomechanical simulations have shown promise as a tool to understand better the optimal behavior of a prosthesis and how the wearer might interact with the device. These simulations estimate whole-body effects for a specific prosthesis and control approach, potentially providing more information about the user outcomes of the device than an analysis based on previously collected experimental data with a different design. Simulating hypothetical designs with musculoskeletal models enables the designer to conduct virtual experiments and rapidly refine the design targets before developing a physical prototype. For example, Fey *et al*. optimized the stiffness of an energy storage and return (ESR) foot model to minimize simulated metabolic cost and knee contact loads during walking [136]. Handford and Srinivasan simulated a powered ankle-foot prosthesis, which decreased the computed metabolic cost of transport below that of an able-bodied person when

optimized for maximum energy output and minimum weight and allowing for asymmetric joint kinematics [19]. Beyond optimizing known designs, biomechanics simulations can be used to optimize unconstrained device behaviors. The previous chapter demonstrates how simulations can be constructed which remove assumptions about the mechanical construction of the prosthesis, thereby generating performance targets for new designs of an unspecified form.

However, simulated outcomes can be misleading and require experimental validation. Work addressing the gap between simulation and experimental performance has been conducted in [165] by simulating the controller performance of devices for which experimental data exists, including the commercial Empower ankle-foot prosthesis [180], passive SACH foot [181], and an ankle-foot prosthesis emulator [9]. However, the device behaviors generated from the methods used in Chapter 2 are highly unconventional and have no experimental counterpart. In this paper, we present the design of an experimental prototype for the validation of generalized prosthesis optimization studies, using simulation outputs to generate design specifications.

4.2. Selecting Design Metrics

Mechatronic design targets were interpreted from dynamic optimizations of human walking with a generalized prosthesis model. This section describes the model and optimization method, the resulting simulated prosthesis behaviors, and the translation of those behaviors into design specifications.

4.2.1 Dynamic Optimization of Gait

The human-prosthesis musculoskeletal model was adapted from the model used in the previous chapter and is shown in Figure 4.1. It has 12 body segments, 14 degrees-of-freedom (DOF), and 15 Hill-type muscle models [173]. The residual tibia is connected to the prosthesis socket with a 2-DOF viscoelastic joint to simulate a soft tissue interface. The prosthetic foot is modeled to flex about

a pin joint simulating the elasticity of an ESR foot. Specific details about this model are discussed in Chapter 3.

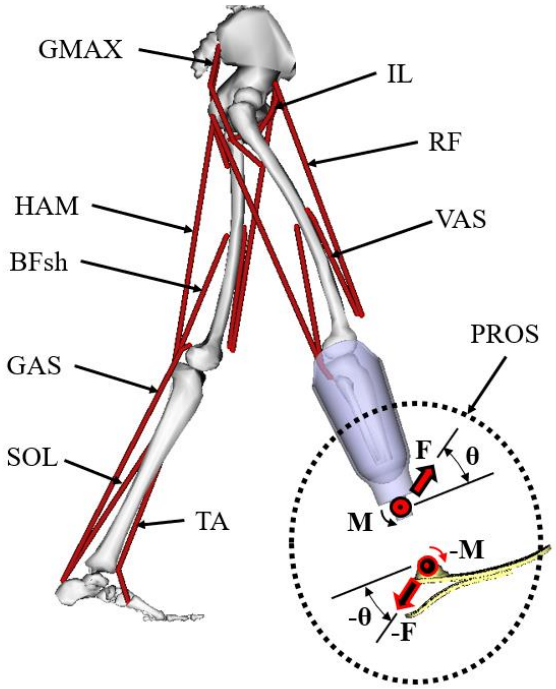

Figure 4.1. OpenSim rendering of the human-prosthesis model used for the simulation portion of this study. Locations of the joint axes for the socket joint and prosthetic foot bending are indicated in the full-body illustration. Both legs have identical sets of 6 muscles: Gluteus maximus (GMAX), iliopsoas (IL), hamstrings (HAM), rectus femoris (RF), biceps femoris short head (BFsh), and vasti (VAS). The sound side limb has three additional muscles which cross the biological ankle: Gastrocnemius (GAS), soleus (SOL), and tibialis anterior (TA). The prosthesis model (PROS) has two model actuators which react against both the socket and the prosthetic foot.

While the previous prosthesis model was free to move in the sagittal plane, the model used for this study was constrained to have one linear translation axis and one rotation axis (plantar-/dorsiflexion). It was observed in Chapter 2 that planar translation appeared to primarily reduce socket loading by absorbing shock and realigning ground reaction forces to reduce the socket flexion moment arm, while powered plantarflexion served to reduce muscle effort. Because the vertical and horizontal translation components both act primarily on the same objective, we hypothesized that coupling these degrees of freedom would retain most of the muscle effort and socket loading reduction observed for free planar motion while greatly simplifying the mechanical design of the device.

The objective function was constructed as a combination of muscle effort, socket loading, able-bodied gait kinematics tracking, and net prosthesis work minimization. Muscle effort and socket loading are the primary minimization objectives, while the tracking and prosthesis work objectives are used to influence the simulation toward standard gait-like behaviors. Muscle effort is calculated by summing cubed muscle activations cubed across the duration of the gait cycle, and socket loading is calculated by summing socket flexion and pistoning loads raised to the 10th power to approximate a minmax operation. This function is described by

$$F = F_{\text{effort}} + \alpha F_{\text{loading}} + \epsilon_1 \mathrm{F}_{\text{track}} + \epsilon_2 F_{\text{work}} \tag{4.1}$$

where $\alpha = 10^{-1}$ $\epsilon_1 = 10^{-2}$ and $\epsilon_2 = 10^{-3}$. The definition of these terms and their scalar weight assignments are discussed in more detail in Chapter 3.

Dynamics for a full gait cycle were simulated using a direct collocation approach [13], [182] with 51 nodes, with constraints enforcing the system dynamics on the model states at each node. The periodicity of the motion was enforced by requiring the start and end states to be identical. Additional constraints set the average walking velocity, limited the total prosthesis power output to 300W at each node, and limited the prosthesis range of motion to ±5cm of translation and ±60° of ankle flexion. Objectives were minimized by using MATLAB to interface with OpenSim and run the IPOPT interior-point solver [183].

A set of translation angles (represented by θ in Figure 4.1) were tested in simulation to find the optimal linear coupling, ranging from horizontal to vertical at 30° increments above and below the horizontal axis, then further refined to 10° increments around the angle with the lowest objective function value. For this second phase of the angle optimization, a set of three walking speeds and three socket stiffness values were simulated for a total of 9 simulations per translation angle. Solutions were obtained from two different initial guesses to reduce the likelihood of converging to local minima, of which the lowest objective value was chosen for each condition.

4.2.2 **Simulation Results and Design Specifications**

The minimum objective function value was found for a translation angle of 10° above horizontal. The highest objective cost was found for the vertical translation angle, which increased the muscle effort value by nearly 10 times the 10° translation angle model. In comparison with the 3-DOF prosthesis model used in Chapter 2 with the same objective function weights, the muscle effort objective value and summed peak socket loads for the 2-DOF design are 15.9±24.6% and 9.2±25.3% smaller, respectively (mean ± 1SD). Relative to the revolute prosthesis simulated in Chapter 2, this is a 45.2% decrease in muscle effort and a 13.0% decrease in summed peak socket loads, on average. Note that the socket load metric reported in this paper is the sum of the actual peak loads rather than the 10^{th} power minmax approximation.

In these simulations, the 2-DOF design outperformed the 3-DOF design, though the change is smaller than the variance in the output. This suggests that the 3-DOF solution may have been vulnerable to converging to local minima. Regardless, the 2-DOF simulation is a marked improvement over a simulated revolute design, and so the simulation results were converted into design requirements for a prototype matching the simulated 2-DOF behaviors.

The kinematics and kinetics for the selected prosthesis model are illustrated in Figure 4.2. The translation axis utilizes the full allowed range of motion of 10 cm. The average rotational motion ranges from approximately 15° dorsiflexion to 30° plantarflexion. Peak plantarflexion moment sustained during stance is 120 N-m. The peak translation force of 260 N occurs shortly after heel-strike. In addition to the peak loads, loads above 50 N-m and 100 N are maintained for nearly the entire stance phase, indicating that these values should be within the continuous operation regions of their respective actuators. After removing outlier spikes and backdriven motion, maximum velocity is approximately 3.0 rad/s (172°/s) and 0.8 m/s for flexion and translation, respectively. The motion can be described as an anterior translation of the residual shank shortly after heel-strike which is held

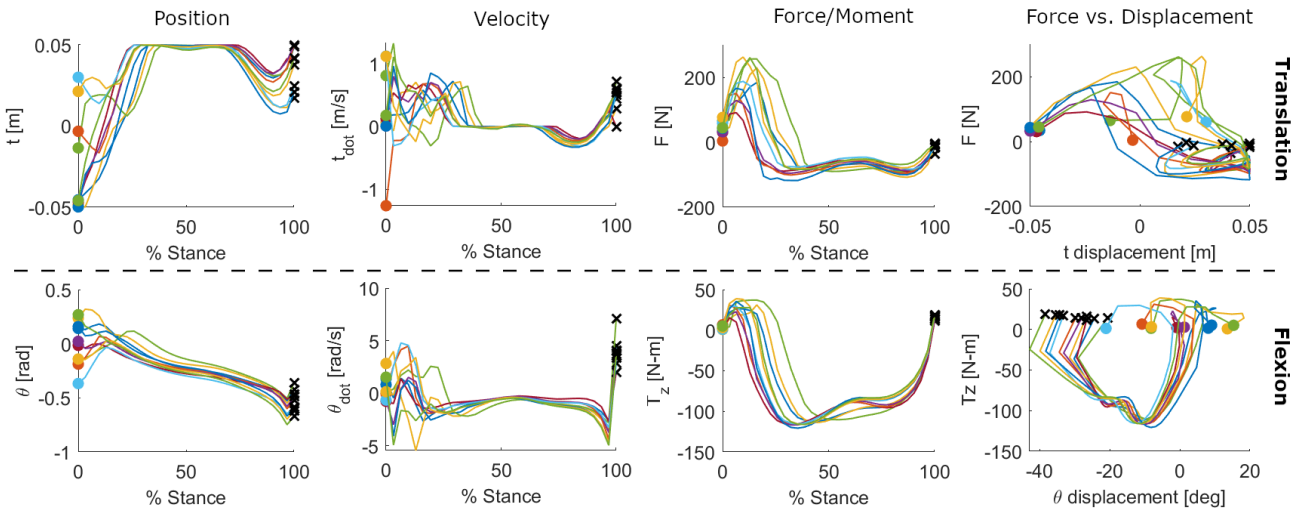

Figure 4.2. Simulated prosthesis kinematics and kinetics for the stance phase in both degrees of freedom. Each trajectory corresponds with a simulation condition. Individual trajectories are shown instead of mean/SD to more clearly show how behaviors differ over time. A circle marks heel-strike and a black 'x' marks toe-off. Positive translation corresponds with anterior and upward translation of the residual limb with respect to the artificial foot. Positive flexion corresponds with ankle dorsiflexion.

constant for most of the stance phase. Plantarflexion moments of a magnitude typically associated with toe-off are maintained throughout stance, with an approximately linear elastic behavior after about 25% stance. Despite a clear trend in linear translation displacements, no consistent elastic behavior is observed in the force vs. displacement curves for this coordinate.

These results provide the minimum actuation requirements for a prototype design. Structural and size specifications may be derived by examining existing devices. Table 4.1 contains the build height and mass of other powered ankle prostheses. For the prototype to provide a useful comparison to similar devices, the height is limited to 20 cm, and the mass is limited to 2.5 kg. [184] [45] [185] [58] [114] [186] [187] [6]

4.3. Mechatronic Design

4.3.1 System Definition

The top-level system is designed around the intended application for the device: to be used as a validation tool and laboratory test-bed for general prosthesis model simulation studies such as

Table 4.1. Size and Mass of Powered Ankle Prostheses

Device	Mass [kg]	Build Height [cm]
Ottobock Empower® [184]	**1.9**	**25-30**
UMass 4-Bar Ankle-Foot [45]	**1.9**	**18**
p^2 Ankle [185]	**1.0**	**12**
Vanderbilt Ankle [58]	**2.3**	**21**
2-DOF Emulator [114]*****	**0.72**	**8**
3-DOF Emulator [186]*** †**	**1.2**	**-**
Mich. Tech 2-DOF [187]*** †**	**1.1**	**-**
AMP-Foot 3 [6]	**~3**	**26**

*** Does not include off-board motors, cables, or electronics**
† Build height information not in cited reference

the one conducted in the previous section. While a single simulation solution may be simplified by coupling degrees of freedom without significant alteration to the device behavior – similar to [45] – changes to the model or optimization construction may result in highly variable device behaviors. An experimental device designed to validate the generalized prosthesis optimization method needs to be able to reproduce the simulation outputs closely; hence the prototype is designed with independent translation and flexion degrees of freedom.

Because the proposed prototype system requires two actuators instead of one, along with additional supporting electronics and higher power source requirements, it is unlikely that the size and weight requirements can be met with the full system embedded in the prosthesis. Other multi-DOF wearable robots have successfully employed off-board cable-driven actuation and control systems to make the wearable device as light and compact as possible [114], [186], [187]. The planar 2-DOF prosthesis is designed with cable-driven actuation, though in order to facilitate convenient over-ground testing, the off-board system is designed to fit into a backpack worn by the user.

4.3.2 **Concept Development**

Concepts for the prosthesis mechanism and corresponding remote actuator were developed independently for each degree-of-freedom. The main design priorities for these actuator-mechanism assemblies were their ability to reproduce the simulation motion, minimizing prosthesis mass, and minimizing mechanism complexity. Early concepts involving linkage mechanisms were ruled out due to the size of the linkage required to reproduce the both the translation and rotation ranges of motion indicated by the simulations, as well as the variability in the output loads depending on linkage angle. Design concepts focus on representing each mechanism as either a simple revolute or prismatic joint, and the variables primarily reduce to: Uni- or bi-directional operation, the method of converting motor rotation into cable tension, and the method of converting cable tension to either linear or rotational motion at the end effector.

These variables reduce the design concepts into permutations of a few key options listed in Table 4.2. Illustrations of these concepts are shown in Figure 4.3.

Table 4.2. Prosthesis Concept Design Variables

Actuator mechanism	Controllable directions	Translation mechanism	Flexion mechanism
Linear actuator	**1**	**Cable to pulley**	**Cable to lever**
Powered winch	**2**	**Rack/pinion**	**Cable to pulley to lever**
		Lead screw	

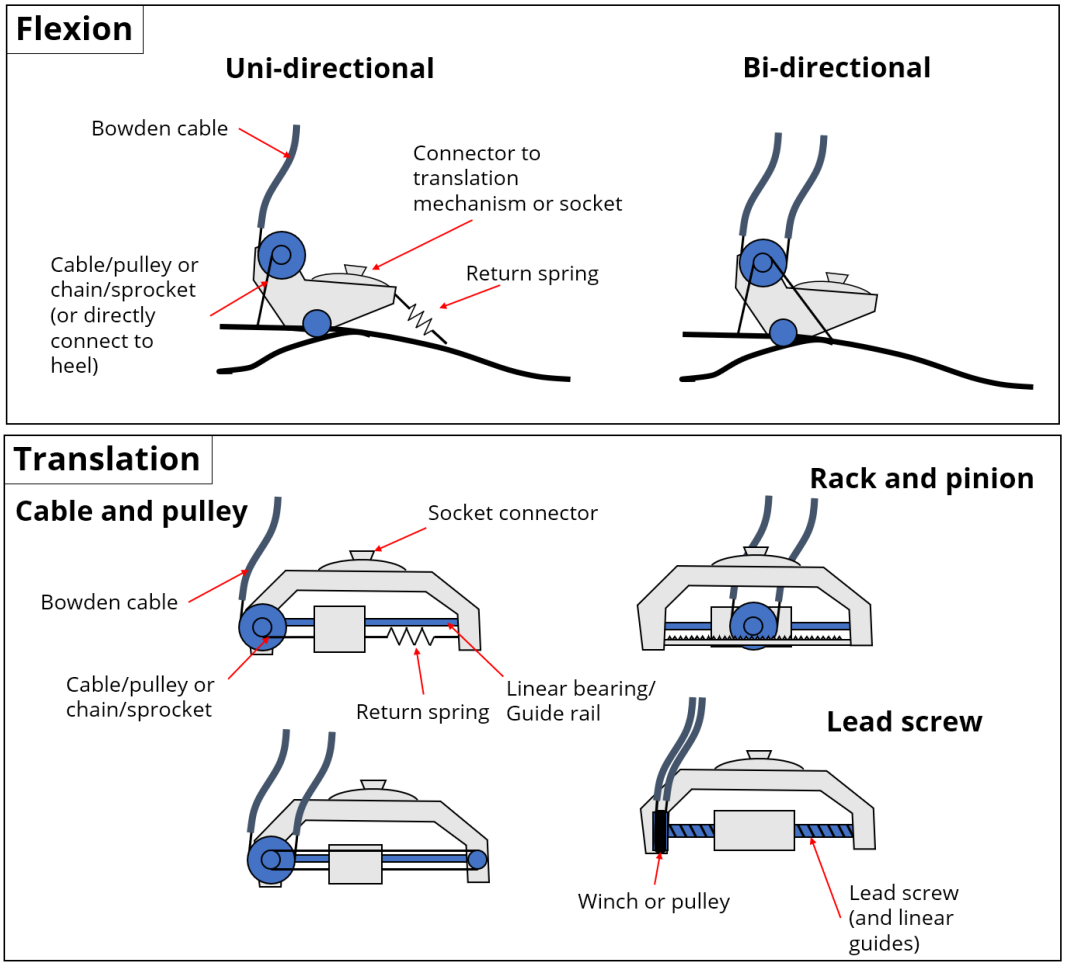

Figure 4.3. Ankle-foot mechanism concepts for both actuated degrees-of-freedom.

The final design concept was determined based on the functional requirements implied by the simulation results. A uni-directional actuator was chosen for the flexion axis because nearly all of the simulated output torque is in the plantarflexion direction. A bi-directional actuator was chosen for the translation axis because forces in both directions of similar magnitude were simulated. Additionally, this axis of motion has no anatomical analogue, so its behavior may differ significantly for different simulation conditions. Bi-directional control allows for greater flexibility in how the translation motion may be used, despite the added complexity and friction brought by the addition of another Bowden cable.

It was determined that plantarflexion torques of the appropriate magnitude could be generated without the aid of a pulley system located on the prosthesis if the load magnification could be added to the transmission ratio on the actuator side of the transmission chain. Moving load from the distal segment to a more proximal one results in less effort required by the muscles, so the final flexion mechanism concept involves the cable connecting directly to a lever at the rear of the prosthetic foot, and a ballscrew linear actuator mechanism in the backpack to achieve the required transmission ratio at high efficiency.

Because the cable motion is already linear, the pulley mechanism to redirect this motion along the translation axis was chosen. Other concepts transform linear cable motion to rotational motion and then back to linear motion, resulting in added complexity, mass, and energy losses. A powered winch was chosen as the actuator concept, because the high efficiency of a ballscrew mechanism comes at the cost of a significantly more complex design and added mass, and the translation load magnitudes do not require the aggressive gear reduction required by the plantarflexion loads, as discussed in more detail in Section 4.3.4.

4.3.3 **Ankle-foot Design**

These combined mechanism concepts comprise a modular overall prosthesis system design. The combined mechanism in comparison with the simulation range of motion is illustrated in Figure 4.4, and the completed mechanical assembly of the ankle-foot prototype is shown in Figure 4.5. The translation component consists of a sliding stage on linear bearings. Pulleys at the front and back direct the Bowden cables in toward the sliding stage from the actuator unit above, providing active bi-directional control. A frame is constructed around and above the sliding stage to support the socket-pylon attachment point above. The frame allows 10 cm of linear translation. The translation angle can be adjusted up to ±8° at the pyramid connector at each end of the mating pylon, and angled connectors may also be used for more pronounced angles.

The flexion component consists of a fixed-axis revolute joint mounted below the sliding stage. Plantarflexion moment is generated via upwards cable tension on a lever extending from the rear of an artificial foot. A parallel elastic element comprised of elastic bands provides dorsiflexion. The artificial foot and lever are additively manufactured as one piece, allowing the series elastic behavior of the plantarflexion actuator to be designed alongside the rollover elasticity of the foot. The Bowden cable attachment point is cantilevered 15 cm behind the flexion axis to avoid self-collision through the full range of translation motion. Rubber stops are located at the rear to limit plantarflexion to 25° (or 35° if desired translation angle is horizontal). Dorsiflexion is limited to 15° by the length of the linear actuator and is adjustable up to 38° is less plantarflexion is required. The flexion assembly connects to the translation assembly with a pyramid connector bolt pattern, allowing it to be used as a 1-DOF revolute powered ankle-foot.

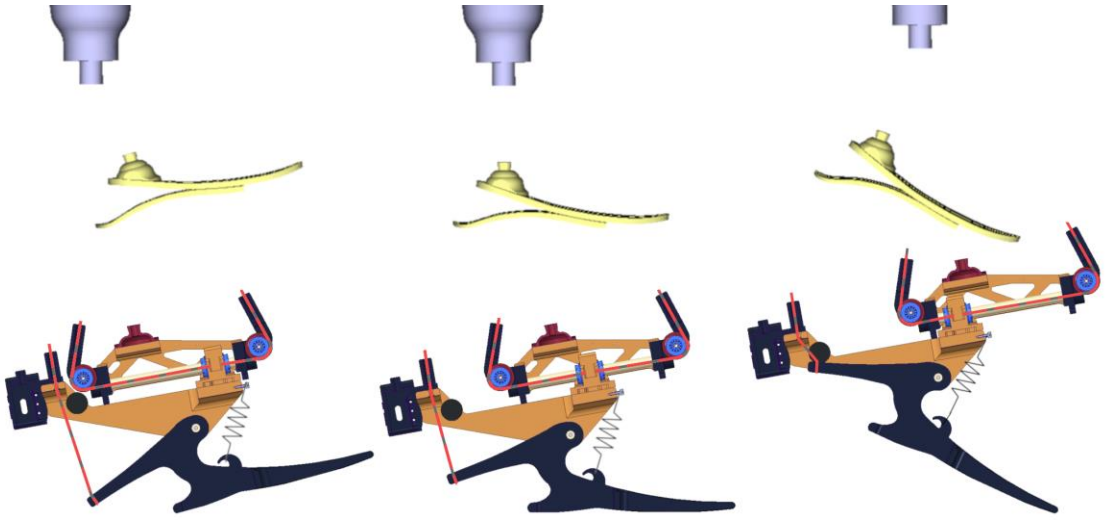

Figure 4.4. Ankle-foot prosthesis mechanism range of motion compared with corresponding simulation coordinates. Red dashed lines represent Bowden cable connections. A passive elastic component is used to dorsiflex the artificial ankle. From left to right: -5cm translation/15° dorsiflexion, neutral position, +5cm translation/25° plantarflexion.

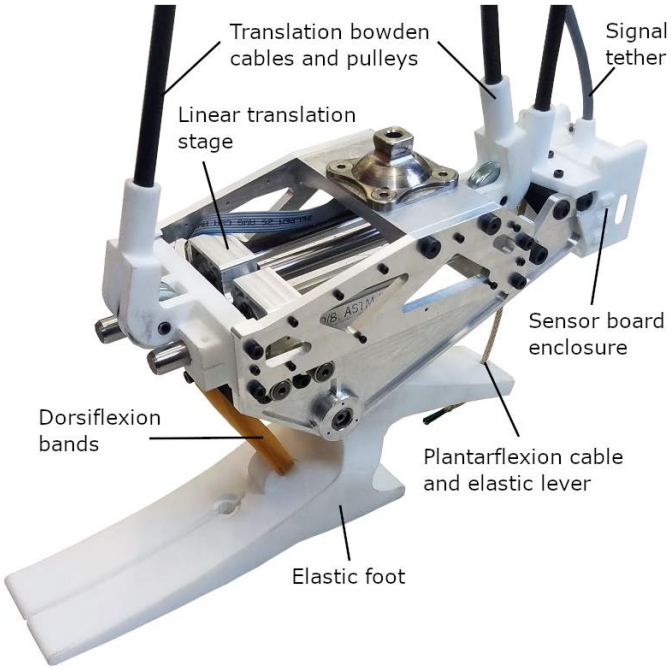

Figure 4.5. The ankle-foot prosthesis assembly is cable-actuated in both the translation and flexion degrees of freedom. Cable force is transmitted directly to an integrated lever on the artificial foot to plantarflex the joint. Cables are routed through pulleys and connected to both sides of a linear stage to transmit force in both directions. A standard pyramid connector is used to connect the prototype to the user.

The structural frame for both components was CNC machined from aluminum 6061. Some parts were 3D-printed from sintered nylon powder (Formiga P110) or carbon-fiber-reinforced nylon filament (Markforged Mark 2) to reduce weight and combine parts in locations away from critical loads. Sintered nylon is used for parts where a lower stiffness is required (artificial foot, flexure clamps), and carbon fiber-reinforced nylon is used for sections of the structural frame.

The structure is designed to safely accommodate a 100 kg person walking up to 1.5 m/s. Finite element static load analyses were performed on solid models of the structural components using Creo Simulate (PTC Inc., Boston). Peak simulated vertical ground reaction force and plantarflexion moment loads were scaled up by a factor of 33% in estimation of the loads exerted by a 100 kg person (the model mass is about 75 kg). Additionally, torques up to 50 N-m about the anterior-posterior axis were added to a combined force-moment loading condition to account for the possibility of side loads.

Material was added or removed from key structural parts until a yield safety factor of 2 was achieved (von Mises stress < 138 MPa). Parts with non-critical load paths were designed to with the same safety factor using sintered nylon material properties (von Mises stress < 25 MPa).

Flexural stiffness was estimated for the rear lever and forefoot of the nylon foot using settings for calculating large deflections – linearly increasing the load from 0 to maximum in 5 stages and propagating load histories through each deformation step. The foot dimensions were manually modified until the lever stiffness was between 25 and 35 N-m/deg, and the foot stiffness was between 10 and 15 N-m/deg with no material yielding. Examples of static structural and flexural analysis results are shown in Figure 4.6.

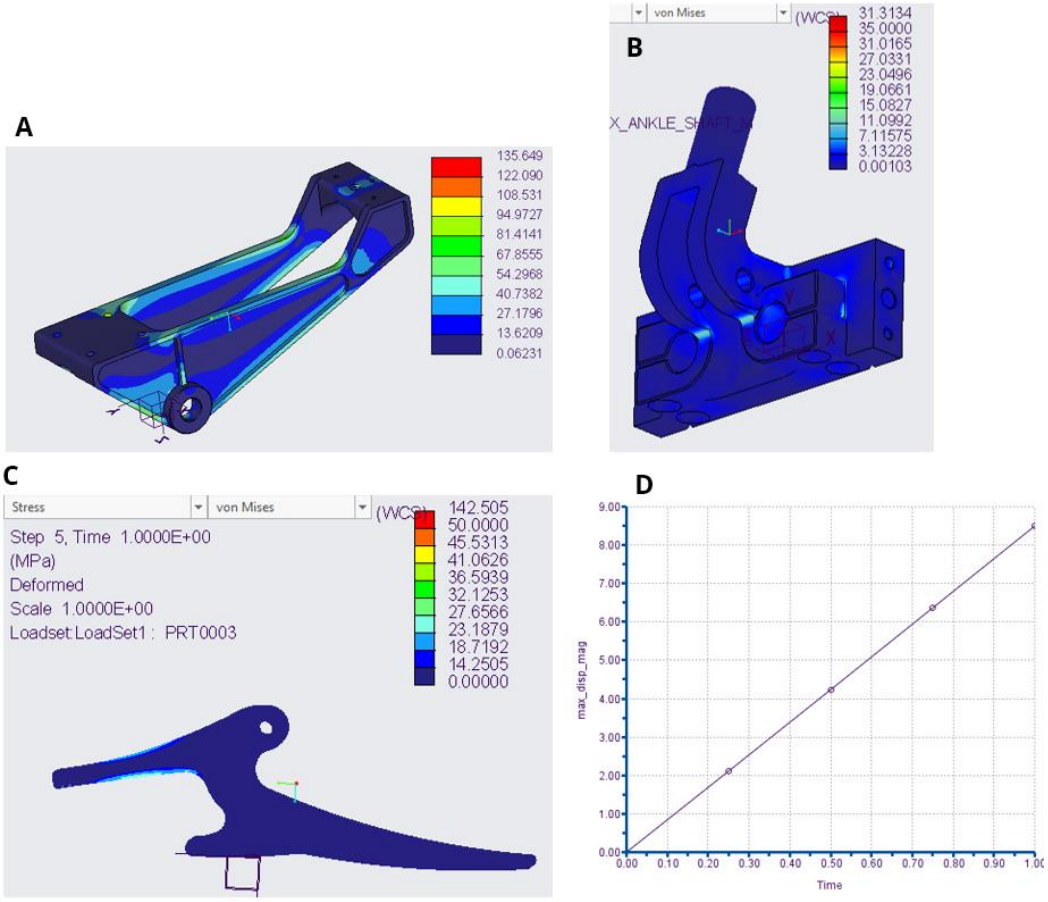

Figure 4.6. Finite element structural analyses and flexural stiffness tuning. All stress units are MPA. (A) Tuned material cutout size and depth in a CNC machined aluminum part, (B) Structural piece with low loading stress designed as a sintered nylon part with attached flexure clamp and pulley mount features, (C) Large deformation simulation of leaf spring lever of the artificial foot and (D) a linear deflection response as load is linearly increased with time.

Ankle flexion angle is measured with a 1024 count miniature magnetic rotary encoder (RM08, RLS) mounted on the flexion axis shaft. The translational position is measured with an incremental magnetic encoder with a 20 μm resolution linear magnetic scale (RLC2IC, RLS). A 3-axis accelerometer (ADXL335, Analog Devices) is mounted to a custom circuit board at the rear of the prosthesis for the detection of heel-strike during walking. A PIC microcontroller (dsPIC33FJ64MC202, Microchip) located on the custom board processes the sensor data and routes it to the wearable off-board system for logging and controller feedback via signal cable tether.

4.3.4 **Wearable Off-board System Design**

The off-board system consists of two motorized actuator assemblies and a RaspberryPIC GoPack, a custom embedded system [188]. The GoPack is the central signal and control hub for the entire system. It takes sensor data from the prosthesis and motors as inputs and sends motor commands as outputs. Each actuator exerts forces on the prosthesis via Bowden cables. The elasticity of the load transmission chain is used to estimate loads at each degree of freedom by measuring prosthesis displacements and comparing it to the motor displacements. The design of this load sensing method are discussed in more detail in the next subsection.

The GoPack is comprised of a 16-bit PIC microcontroller (dsPIC33FJ64MC204, Microchip) mounted to a custom circuit board, which communicates with an attached Raspberry Pi 3 running MATLAB Simulink. Power is supplied from two 4-cell lithium polymer batteries, which is routed through the custom board and reduced to 5V and 3.3V to supply power to the sensors and integrated circuits. Low-level signal processing and sampling is performed by the PIC microcontroller, and high-level processing, data logging, and control is performed in Simulink on the Raspberry Pi microcomputer. Both motor supply circuits are routed through a relay that is opened or closed by a handheld emergency stop switch.

Both actuators are powered by 200W brushless DC motors (EC-4pole 30 + MR encoder, Maxon) using Maxon motor drivers (ESCON 50/5, Maxon). Transmission ratios have been calculated using the motor torque and speed parameters provided by the manufacturer [189], assuming a 40V power supply and a 15A current limit dictated by the motor drivers. Meeting both torque and velocity requirements requires a different reduction ration in each degree of freedom, with plantarflexion requiring a more substantial reduction to meet the load demands. To achieve a large reduction with high efficiency, the plantarflexion actuator consists of a linear actuator assembly using a miniature ball screw (MRT 8X2.5, Nook) rated at 95% efficiency under typical friction conditions. Additional reduction of 2.5:1 is provided by a timing belt and pulley assembly. Assuming a Bowden cable transmission efficiency of 80%, the total transmission efficiency is estimated to be 76%. Therefore, the estimated maximum plantarflexion moment and velocity are 286 N-m (95 N-m continuous) and 1.53 rad/s, respectively. Maximum velocity under maximum load is estimated to be 1.36 rad/s, for a peak output power of 389 W.

The linear translation actuator consists of a bi-directional winch assembly. A 23:1 planetary gearhead (GP 32 HP, Maxon) is mounted to the motor and coupled to the winch shaft. The winch drum is 3D printed from sintered nylon powder, and the winch structure is machined aluminum 6061. Idlers mounted to torsion springs apply tension to both cables to prevent slack from forming and causing uncontrolled motion. The gearhead efficiency is reported as 75%, and using the same Bowden cable efficiency, the total efficiency of the assembly is estimated to be 60%, resulting in a maximum translation force and velocity of 476 N (159 N continuous) and 0.73 m/s, respectively. Maximum velocity under maximum load is estimated to be 0.65 m/s for a peak output power of 309.4 W.

The full off-board system is designed to mount to acrylic panels that fit inside a backpack with padded sides, measuring 44.5 x 30.5 x 15.2 cm (Hardshell Camera Backpack, Endurax). This assembly is illustrated in Figure 4.7.

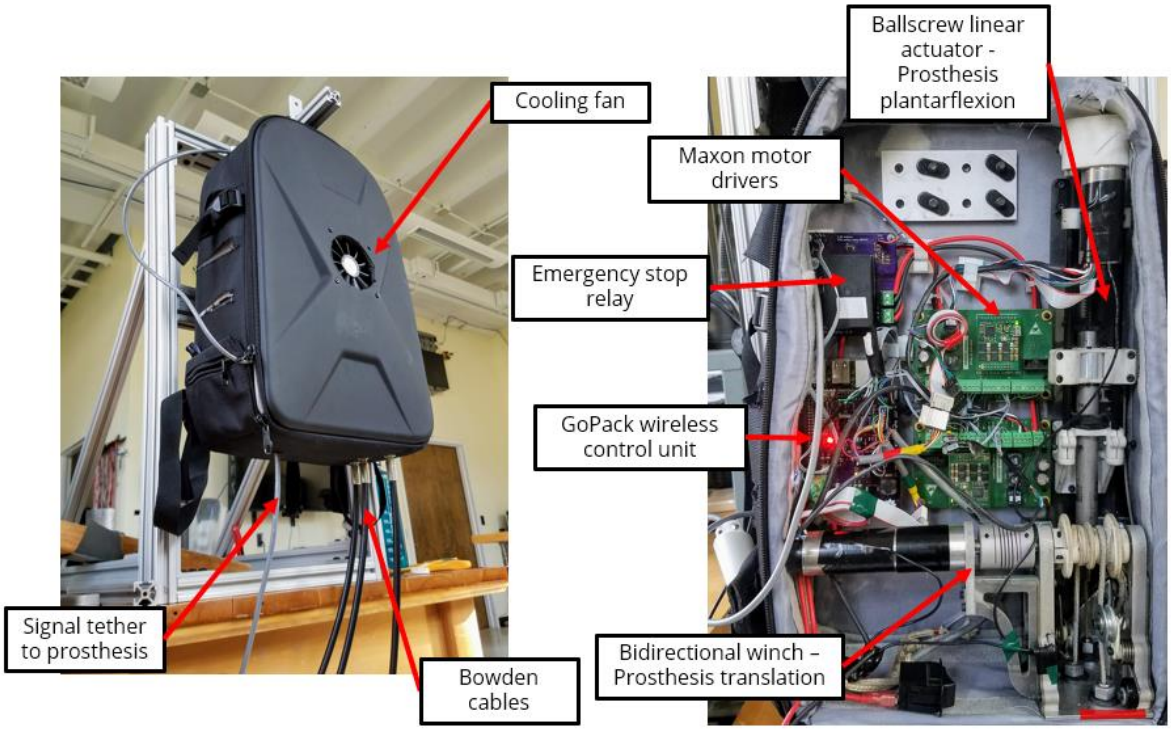

Figure 4.7. The off-board control and actuation system is designed to fit into a backpack, with Bowden cables exiting from the bottom. The actuator systems can be controlled via WiFi, making the entire wearable system self-contained and wireless.

4.3.5 **Load Sensor Design**

In order to reduce the number of components and the mass of the device, translation force and plantarflexion torque are estimated by modeling the elasticity of the system and measuring the deflection of the end effector relative to the motor position as opposed to implementing traditional strain gauge load cells. This elasticity is designed into the flexion transmission chain as a leaf spring lever at the rear of the prosthetic foot. Force sensing in the translation axis is primarily for introducing additional compliance to its behavior rather than seeking specific force targets, due to the indication of the simulation results that translation is primarily used to position the residual limb advantageously rather than generate substantial positive work. Therefore, no additional series elastic component has been introduced to the translation kinematic chain. The vectran cable itself does stretch under load, however, allowing for some estimation of cable tension.

The elasticity of the series spring built into the prosthetic foot has been characterized from tensile tests conducted with an Instron testing machine. Futher tests were conducted with the assembled system using static weights in both actuated degrees-of-freedom. A linear stiffness was approximated from the resulting load-displacement curve using a least-squares fit for both axes. However, because of the large magnitude of unloading hysteresis present in the translation axis measurement resulting in a poor linear fit, the linear regression for the whole dataset was discarded in favor of a linear approximation of only the loading response. The results from these tests are illustrated in Figure 4.8.

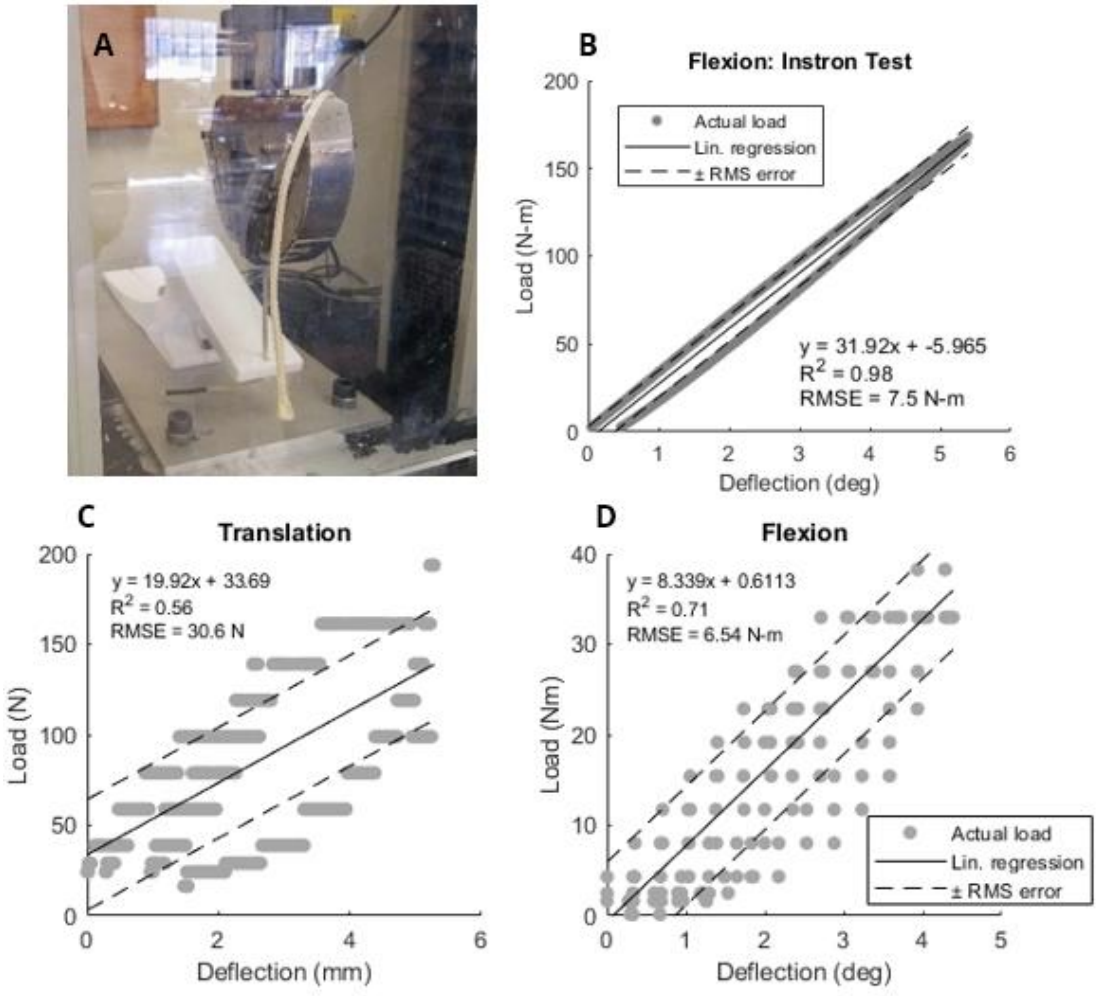

Figure 4.8. (A) The Instron test machine setup to measure series elasticity in the foot prosthesis leaf spring lever. (B) Load/deflection curves from that test. (C) Load deflection curves for the overall plantarflexion transmission system, and (D) the overall translation transmission system.

This method of load sensing is based on transforming cable tension into the load being measured. For the translation axis, output force and cable tension are the same value. However, plantarflexion torque and cable tension have a nonlinear relationship based on the angle of incidence between the cable and the flexion moment arm. This relationship is dependent on the ankle flexion angle, and is defined by

$$\tau = TL\sin(\beta) \tag{4.2}$$

$$\beta = 110° + \alpha + \theta \tag{4.3}$$

$$\alpha = \sin^{-1}\left(\frac{x - L\cos\theta}{\sqrt{(x - L\cos\theta)^2 + (y - L\sin\theta)^2}}\right) \tag{4.4}$$

where τ is the output torque, T is the cable tension, L is the distance of the tip of the foot lever arm from the flexion axis of rotation, θ is the ankle flexion angle, and x and y are the horizontal and vertical distance of the Bowden cable exit point to the flexion axis of rotation, respectively. The geometry of this relation and the effect of ankle flexion angle on torque are illustrated in Figure 4.9.

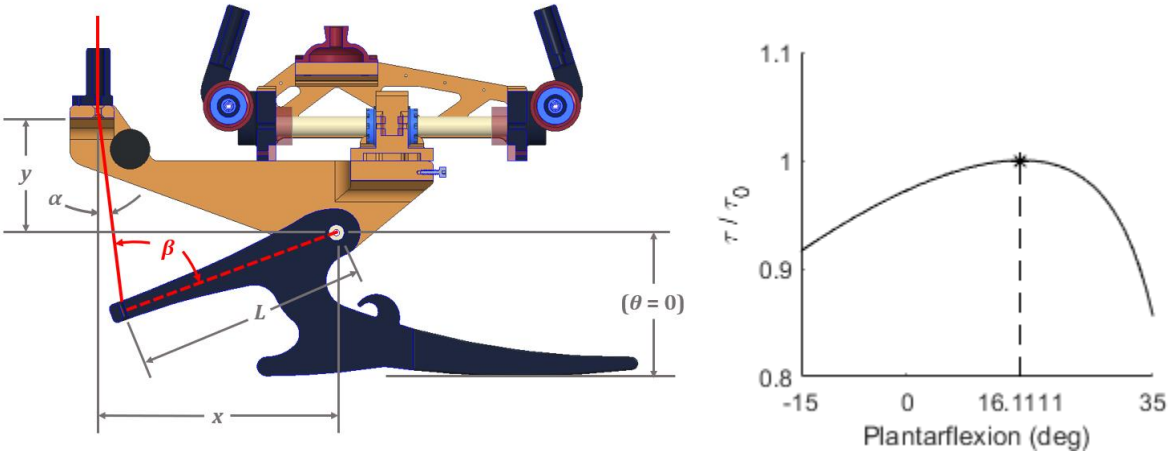

Figure 4.9. Left: Plantarflexion torque angle of incidence geometry variables. Right: Plantarflexion torque percentage of ideal torque as a function of ankle plantarflexion angle.

4.4. Evaluation

The dimensions and mass of the final assembly were measured to confirm that they fall within specifications. Benchtop tests were also conducted to assess force/torque measurement accuracy

and maximum actuator load, speed, and power. Maximum actuator tests were performed to compare against the designed specifications and assess the accuracy of the transmission efficiency calculations.

4.4.1 Evaluation methods

The prototype dimensions and mass were measured with a tape measure and laboratory scale (Tor-Rey Electronics), respectively.

Load measurement accuracy was characterized as root mean squared (RMS) error between applied and measured loads by applying known forces to each prosthesis motion axis using free-hanging weights. Weights were sequentially added and removed to record the presence of any loading-unloading hysteresis. The prosthetic foot was bolted to the benchtop and weights were hung from the front of the linear translation stage at its maximum forward translation to measure ankle plantarflexion torque. The prosthesis was cantilevered horizontally from the benchtop with its translation axis aligned vertically, and weights were hung from the base of the sliding linear stage to measure translation force. This test was performed with both the anterior and posterior side of the device facing up to accurately measure bidirectional force. For each test, the motors under load were controlled to maintain a fixed position and the prosthesis was allowed to deflect.

Peak load, speed, and power were determined by attaching the prosthesis to a compliant load and generating a step input beyond the maximum capability of the actuator. The calibrated on-board load sensors and prosthesis encoders were used to record load and velocity values for these tests, respectively. The system was powered by a laboratory power supply providing 40V – about 83% of the nominal voltage rating of the motors. Each degree of freedom was tested individually. For the plantarflexion test, the prosthesis frame was attached to the benchtop through an extension spring, and the foot was bolted rigidly to the table. For the translation test, the device was cantilevered over the edge of the benchtop and the linear stage was anchored via extension spring to the floor. The

degree of freedom not in use was controlled to maintain a fixed position for each test. Photographs of the benchtop experiment conditions are shown in Figure 4.10.

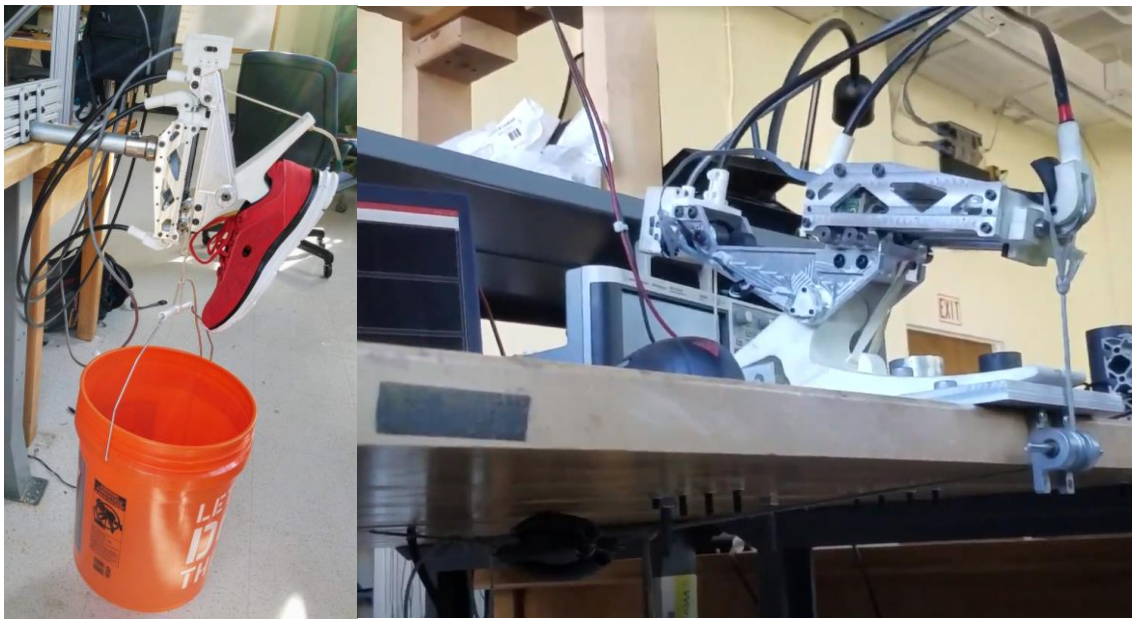

Figure 4.10. Sensing and actuation benchtop experiments for load sensing evaluation (left) and maximum actuator characteristics (right). The prosthesis configurations for tests on the translation axis (left), and the flexion axis (right) are also shown.

4.4.2 **Evaluation results**

The overall height of the ankle-foot prototype is 19.5 cm, and the overall mass is 2.29 kg. The off-board assembly, including cables, has a mass of 6.29 kg and a combined weight of 8.58 kg with the ankle-foot.

RMS error for translation force and plantarflexion torque were 49.5 N and 6.8 N-m, respectively. Static loads were limited to approximately 230 N and 50 N-m primarily due to physical size limitations of the testing setup. Hysteresis is observable in both measurements and is the main contributing factor to load measurement error. Measured vs. actual load comparisons are illustrated in Figure 4.11.

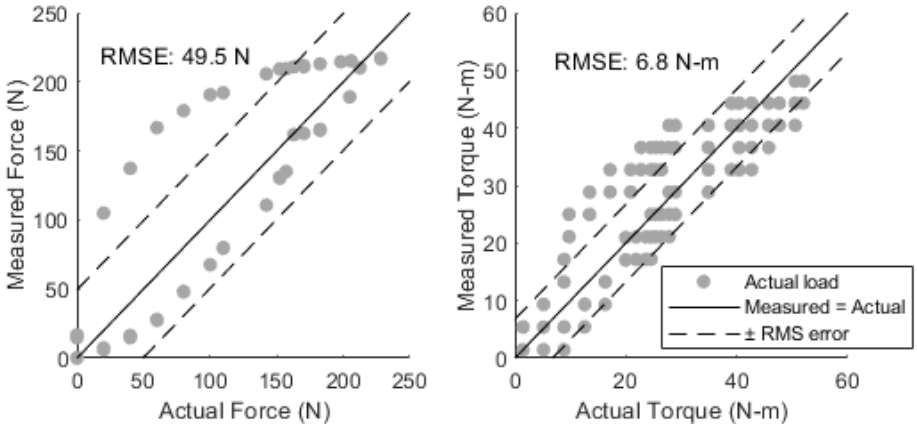

Figure 4.11. Measured vs. actual load comparison for (A) translation force and (B) plantarflexion torque.

Peak translation force and plantarflexion torque were 499 ± 3 N and 171 ± 6 N-m (mean ± S.D.), respectively. Peak prosthesis translation and flexion velocity under maximum load were 0.544 ± 0.026 m/s and 0.958 ± 0.204 rad/s, respectively. Peak translation and plantarflexion power were 267 ± 15 W and 113 ± 20 W, respectively. The response curves over time for these measures are illustrated in Figure 4.12. The device specifications are presented in comparison to the design targets in Table 4.3.

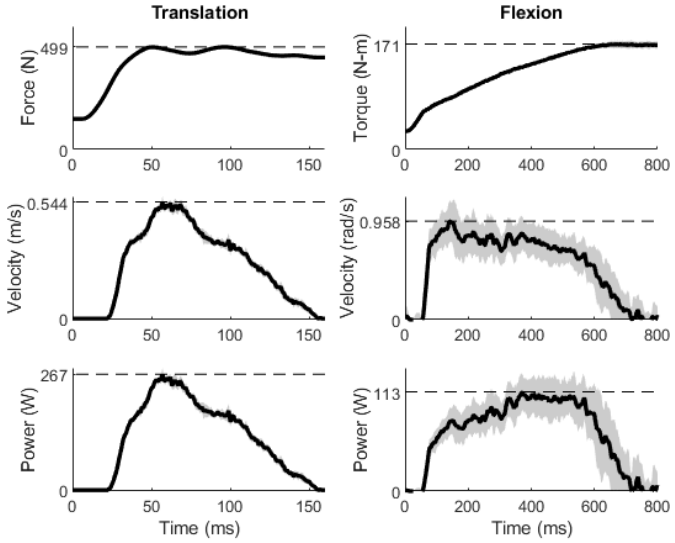

Figure 4.12. Experimentally determined maximum actuator characteristics.

Table 4.3. Prosthesis Design Specifications

Specification	Target value	Actual value
Mass (kg)	<2.5	2.29
Build height (cm)	<20	19.5
Flexion range of motion (rad)	0.26 dorsi. to 0.52 plantar.	0.26 dorsi. to 0.61 plantar.
Translation range of motion (m)	-0.05 to +0.05	-0.05 to +0.05
Maximum plantarflexion torque (N-m)	120	171
Maximum translation force (N)	260	499
Continuous plantarflexion torque (N-m)	50	57
Continuous translation force (N)	100	166
Maximum flexion velocity (rad/s)	3.00	0.96
Maximum translation velocity (m/s)	0.80	0.54

***Green shading indicates the target was successfully met.**

4.5. Discussion

4.4.3 Sensor performance

RMS errors for the load sensors are similar to the linear fit RMS errors associated with the calibration data, indicating that any further improvement in the sensing accuracy would require a change in the sensing method or improvements to the mechanical system. Hysteresis is introduced into the measurement both from the elastic behavior of the vectran cable and the friction between the cables and their conduits. Hysteresis should in theory be more exaggerated for measurements of static loads, because the measurement depends on the cable sliding against the conduit interior in order to register a deflection, and testing with static loads allows the cable to come to rest and for static friction to take hold. Additionally, according to the belt friction equation, friction force will increase exponentially with the cumulative bending angle of the cable conduit, making the load measurement uncertainty dependent on the amount of bending in the cables.

Despite these sources of error, the translation cable transmission has a relatively linear stiffness when being loaded, with almost all of the error occurring during unloading. This indicates that it may be a reliable force measurement for “rising edge” type measurements such as the step response test used to measure the maximum actuator capabilities. In less predictable circumstances, the force measurement should be treated as a qualitative indicator. The additional linear series elasticity designed into the plantarflexion cable transmission contributes to make the measurement much more reliable for quantitative measurements, especially as load magnitudes increase to the full range expected during walking (i.e. over 100 N-m).

For more accurate load measurement, it is recommended to investigate a strain gauge based solution in future design iterations. It may be possible to strategically mount strain gauges directly to the prosthesis structure which can isolate material strain in response to the desired loads. Any sensing method which requires cable stretch or motion through the conduits in order to detect deflection will be subject to uncontrollable nonlinearities due to friction.

4.4.4 **Actuator performance**

Translation actuator performance was in line with the design estimations. Maximum translation force exceeded the predicted value by 23 N, or 4.8% of the estimated maximum. This deviation is within the error tolerance of the force sensor. Velocity under load was 16% lower than the design estimate. Peak power was 14% lower than the design estimate, indicating that the actual transmission efficiency is approximately 52%.

However, plantarflexion actuator performance indicates far lower transmission efficiency than estimated, with peak torque reduced from the estimated value by 40% and peak velocity under load reduced by 30%. Peak power was reduced by 71%, indicating an actual transmission efficiency of approximately 22%. These values indicate significantly more friction losses than originally anticipated. This may be due to the complexity of the linear actuator design leaving many potential sites for energy

losses – e.g. misalignment of the guide rails, sliding contact between the moving output cylinder with the structural frame, bending of the structural frame under load causing misalignment. The efficiency of the ballscrew mechanism itself may be 95%, but the overall mechanism underperforms the estimated 75% efficiency of the planetary gearhead used with the winch actuator unless a highly rigid structure machined to tight tolerances is created to support it. Given the added mass and volume such a structure would require, it is recommended to use a winch design for both actuators in future iterations, adding to the existing winch structure to accommodate a second actuator for relatively little increase in mass and required space.

Estimation errors of actuator performance notwithstanding, some compromises between the specifications and the prosthesis as designed have been made. While the chosen motors can perform most of the simulated behaviors, the output load was given preference over speed in cases where both specifications could not be met. One reason this was done was to prevent thermal damage to the motors in situations where high loads are persistent. The other reason is that simulated prosthesis velocities sometimes far exceeded typical joint velocities during walking, and excessively fast actuation of the prosthesis could be surprising or cause instability for the user, even if such speeds are theoretically optimal in a simulation environment.

These problems could be avoided with limits on the controller outputs and selecting more powerful motors. However, increasing the motor power would increase the mass of the system, impacting its wearability. A fully wearable system is more practical for overground testing, which allows for a greater range of tasks to be more easily tested than an experimental setup confined to a treadmill. This flexibility is desired for this design due to the open-ended nature of the possible simulations the device was designed to imitate. The Maxon EC-4pole motors were chosen for their size and mass preserving the wearability of the system as well as their performance characteristics, achieving most of the simulation demands.

4.4.5 **Overall system evaluation**

A functional 2-DoF ankle-foot prosthesis with wearable off-board actuation and wireless control has been successfully designed and built. The size and range of motion specifications derived from optimal control simulations have been met. The powered system is capable of exerting the loads required to replicate simulated walking behaviors. Actuation speed under full load is below the maximum speeds indicated by simulations, which may require a revised analysis of the optimal prosthesis behavior with the real actuation limits accounted for. Increased actuator performance may be possible with increased supply voltage or replacement of the linear actuator with a winch mechanism. Further increased actuator power may also be possible with more powerful motors at the cost of increased mass borne by the user, which may offset any potential user outcome improvements and necessitate a ground-mounted off-board system.

The prototype may be further optimized, but the current iteration is capable of undergoing preliminary tests recreating simulated walking behaviors.

4.6. **Conclusion**

A wearable prosthesis test-bed for validation of non-anthropomorphic prosthesis simulations has been created. This work represents the first step in a simulation-to-experiment workflow and is designed to provide a critical step in a larger process of iteratively refining gait and prosthesis simulations to produce more predictive biomechanics and more effective prosthesis behaviors. With the prototype capabilities established, the final step to creating a functional test platform is the design and implementation of the control system.

CHAPTER 5

EMULATING SIMULATED OPTIMAL GAIT PATTERNS WITH A NON-ANTHROPOMORPHIC PROSTHESIS TEST PLATFORM

5.1. Introduction

Robotic prostheses cannot (yet) read their users' minds. They require external controllers to process information, make decisions about what is happening, and tell the hardware what to do. All three of these requirements come with their own challenges, but addressing the last is perhaps the most fundamental. What should a prosthesis do?

As discussed in previous chapters, many past approaches suggest an answer: A transtibial prosthesis should replicate the primary function of the ankle during straight-ahead walking, and provide push-off assistance just before toe-off during each stride [5], [6], [26], [97], [99]–[101]. However, closely mimicking the behavior of the biological ankle has not resulted in capturing all of the benefits of the biological ankle [3], [4], [10].

One reason for this may be inflexibility or delays in the control methods used, such as the popular event detection-based finite state machine scheme [5], [190], [191], which can struggle to adapt quickly to changing speed or activity type (i.e. walking to stair climbing, turning, start-stop). Some groups have begun to focus on new techniques to smoothly transition between control modes and predict user intent through use of virtual constraints which are enforced by modeling gait progression as a continuous phase variable [192], attaching inertial sensors to other limb segments for greater robustness in detecting gait events [193], and machine learning techniques with wearable sensors [194]. However, while these methods do improve control performance and accuracy, they cannot alone account for the mechanical changes in the biomechanical system.

Accounting for mechanical system changes introduced by fitting an artificial limb to the residual tissue requires rethinking the control targets altogether. Similar to experiments with

modifying passive prosthesis stiffness to observe the effects on walking human subjects, Collins et al. have designed a series of powered prosthesis emulators which control the magnitude of specific performance parameters: work rate [9], inversion-eversion torque magnitude [114], and center of pressure progression through stance [186]. These devices enable experiments where specific prosthesis contributions can be controlled across a range to investigate the effects on measures such as metabolic cost. However, this approach requires some estimates and assumptions as to which contributions will have a strong effect on the outcome measures.

Identification of these contributions may be assisted by using optimal control simulations of gait to generate theoretically optimal prosthesis behaviors. In this scenario, the control target of the prosthesis is neither biomimetic behavior nor parametric variation of that behavior, but emulation of simulated behavior. This control approach is based in the philosophy that a change in the biomechanical system necessitates new limb mechanics, and as such, limb control targets should be derived by optimizing the limb behavior for the task of interest, not by trying to replicate the behavior of the intact limb. However, it is important not to simply recreate the simulated prosthesis motions, which will not be robust to any variation from the simulated body mechanics, and potentially be unsafe to wear. Instead, similar to other prosthesis controllers referenced above, the controller must be responsive to interaction forces and torques as well, ideally emulating the simulated kinetic-kinematic relationship while in contact with the ground. In this chapter, I present the design of such a control approach, implemented and tested on the non-anthropomorphic prosthesis test platform described in the previous chapter.

5.2. **Control Objectives: Adapting Simulated Gait Behavior**

Predictive walking simulations were performed on the model shown in the previous chapter, updated to reflect the actual mass and maximum actuator capabilities of the prototype. The objective of these simulations was to determine the optimal prosthesis behaviors with fewer unknowns and

assumptions made about the device geometry and capabilities. The simulated forces, torques, and trajectories were used to design a control strategy for the prototype and assign control parameters to mimic the simulated behavior.

5.2.1 Simulation Methodology

As in Chapter IV, a musculoskeletal model of a transtibial amputee was implemented in OpenSim. This model has the same number of body segments and muscles, and retains the 2-DoF viscoelastic socket joint. However, the generalized prosthesis model was reconfigured to reflect the inertial properties of each independent segment of the prototype device. The placeholder foot prosthesis was replaced with a model of the custom nylon prototype foot consisting of 3 segments – 2 segments with a torsion spring connection representing the main body of the foot as before, and an additional segment for the back lever and cable anchor point, also connected to the first segment with a torsion spring. The stiffness values for these two elastic connections match the elasticity information determined in the previous chapter.

To reflect the cable-actuated nature of the prototype, the ideal torque actuator was replaced with a linear contractile element fixed along the route of the cable from the prosthesis frame to the foot lever segment. As with the prototype, dorsiflexion torque is provided by a passive elastic element connecting the foot to the front of the prosthesis frame. Because the translation force acts directly along the axis of motion in the prototype, the ideal force actuator along the linear translation axis remains unchanged. A comparison of the two models is shown in Figure 5.1.

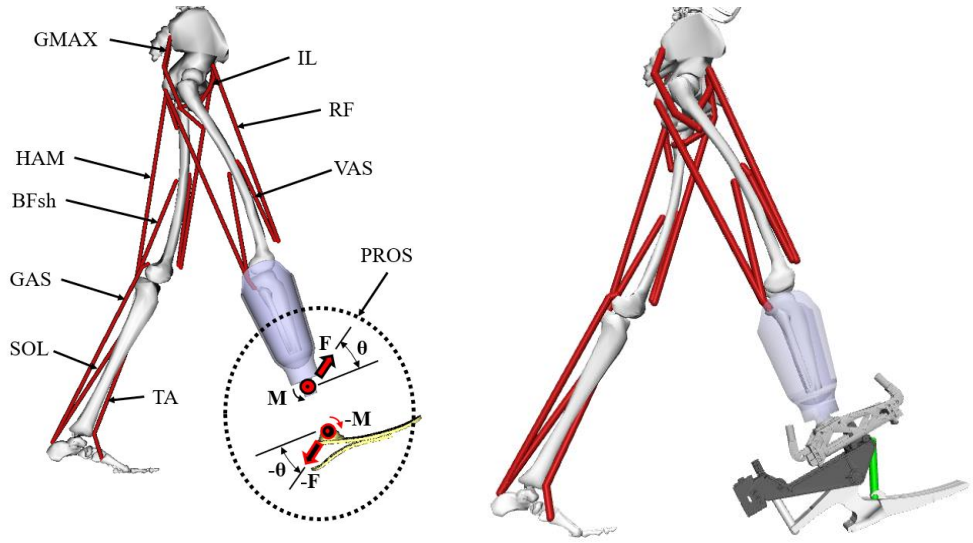

Figure 5.1. Comparison of the 2-DoF generalized prosthesis model and the 2-DoF prototype model as implemented in OpenSim. Torques acting about the flexion axis are exerted as forces along the lines of action of the actuation cable and elastic bands. The artificial foot model includes the modeled compliance of both the main foot section and the rear lever. Each moving segment of the prototype has been modeled with its actual inertia.

Optimal control simulations were performed using the same methodology as in Chapters 3 and 4. The objective function retains the same terms as before with the addition of a "smoothness" term, added to counteract the tendency of this model to briefly leave the ground in mid-stance. This term is defined as:

$$F_{\text{smooth}} = \frac{1}{t_f}\int_0^{t_f}\left[\frac{d^3CoM_x}{dt^3}\right]^2 dt + \frac{1}{t_f}\int_0^{t_f}\left[\frac{d^3CoM_y}{dt^3}\right]^2 dt \tag{5.1}$$

where t_f is the time in seconds to complete one full gait cycle, and $\frac{d^3CoM_x}{dt^3}$ and $\frac{d^3CoM_y}{dt^3}$ are the third derivatives of the model center of mass position in the horizontal and vertical axes, respectively. The objective function becomes

$$F = F_{\text{effort}} + \alpha F_{\text{loading}} + \epsilon_1 \mathrm{F}_{\text{track}} + \epsilon_2 F_{\text{work}} + \epsilon_3 F_{\text{smooth}} \tag{5.2}$$

where $\alpha = 10^{-1}$, $\epsilon_1 = 10^{-2}$, $\epsilon_2 = 10^{-3}$, and $\epsilon_3 = 10^{-6}$.

This objective was minimized using the IPOPT solver with OpenSim interfacing through MATLAB to calculate the model states and derivatives in accordance with the direct collocation

method. The array of walking speed and socket stiffness values was increased to include an additional walking speed of 0.9 m/s, to accommodate the fact that prosthesis users tend toward slower walking speeds than their able-bodied counterparts (average approx. 1.4 m/s). The full set of simulation conditions is:

Walking speed = [0.9, 1.1, 1.3, 1.5] m/s

Socket stiffness = [75%, 100%, 150%] nominal.

5.2.2 **Interpreting Control Targets from Simulated Behavior**

Simulated prosthesis motion, force/torque, and power output, are shown in Figure 5.2. As before, the translation axis tends toward saturating the range of motion. The addition of coordinate limit forces to replace strict bounds on the range of motion during optimization resulted in force saturation at the position bounds as well. However, ankle flexion behavior remains relatively the same as in previous simulations, with peak torque near 100 N-m and peak power below 200 W.

Force-displacement work loops and velocity-force motor performance curves are shown in Figure 5.3. The simulated prosthesis behavior remains largely inside the continuous operation parameters of the selected actuators, with most exceptions in the translation axis occurring in opposition to the range of motion limit forces. Distinct modes of behavior can be observed between the two higher and lower walking speeds.

The simulated results provide both load and kinematic targets for a controller to match. In order to replicate the simulated device mechanics, the controller must target the relationship between load and position, rather than either value in isolation. This can be accomplished by designing an impedance controller, which aims to simulate the response of a passive mechanical system with configurable parameters, most commonly in the form of a linear spring-damper connection between

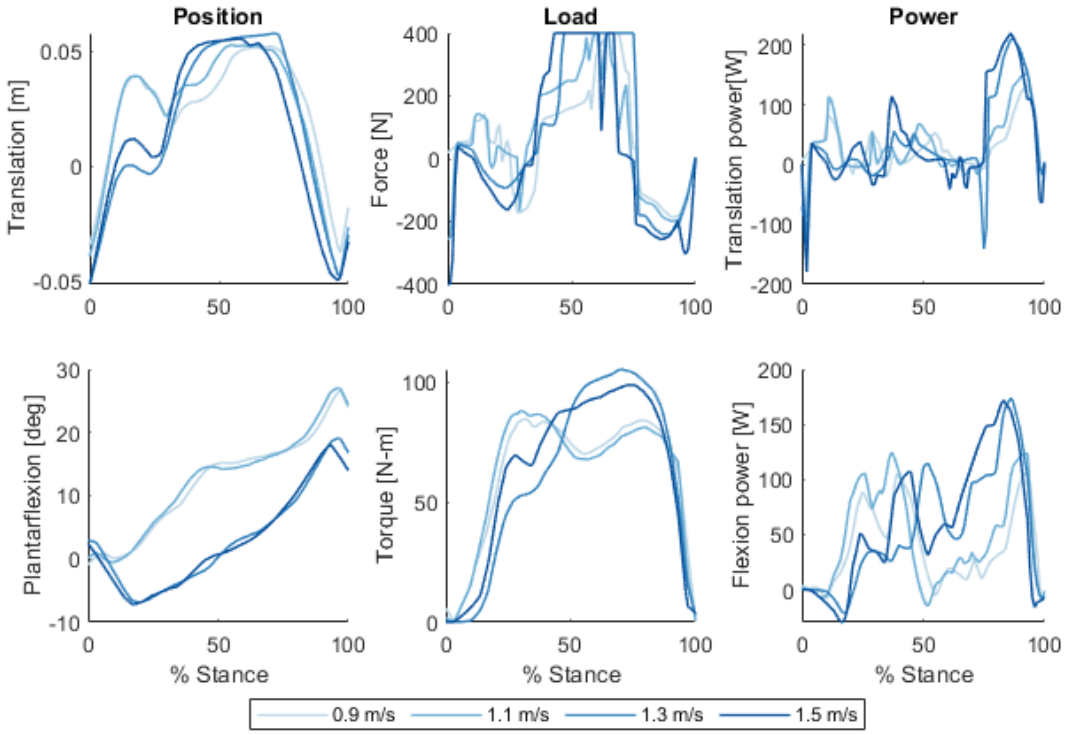

Figure 5.2. Simulation results for the updated prosthesis model averaged between walking speeds for the stance phase. Positive values correspond with anterior translation of the residual limb and plantarflexion of the artificial ankle.

the joints of a device or between the end-effector of a device and the environment [195]. However, the load-displacement relationships in the simulation results indicate a non-linear stiffness and a positive net-work. Both of these deviations from the ideal linear passive spring-damper relationship can be accounted for by controlling the set-point position of the virtual spring. This results a form of force-sensitive position control, which can be made to match desired kinetic and kinematic behaviors simultaneously. This form of control also provides robustness to user variation from the simulated motion, in that the device will not force close trajectory tracking when interaction forces are high, and is governed by consistent mechanical rules not defined by contact or lack of contact with external forces.

The virtual stiffness and set-point trajectory for an ideal impedance controller were optimized using the *fmincon* function in Matlab to match the simulated force profiles as closely as possible. This

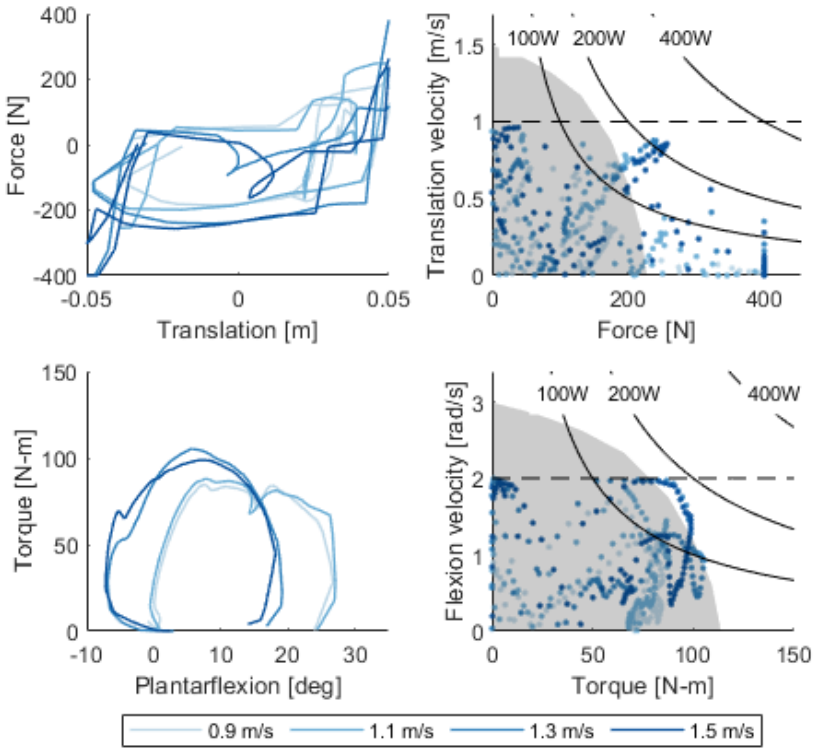

Figure 5.3. Simulated actuator dynamics. Left: The force/position relationship through stance for each speed. Right: Actuator output load and velocity at each time point in the simulation overlaid with the continuous region of each motor scaled by the designed transmission ratio.

was accomplished by separating stance into multiple phases with the position setpoint moving in a linear trajectory roughly approximating the simulated prosthesis kinematics during each phase. Trajectories were optimized for each simulated walking speed, with the reference trajectory averaged across socket stiffness conditions. The optimization parameters and their optimized values are provided in Tables 5.1 and 5.2. Controller targets with respect to the simulated behavior are shown in Figure 5.4.

This impedance control scheme fits into a broader control architecture which enables the device to activate, deactivate, and adjust the walking behavior to the user's gait. It also requires the

design of a lower level force/torque controller to accurately match the simulated impedance. The design of this broader architecture is discussed in the next section.

Table 5.1. Optimized Impedance Control Parameters - Plantarflexion

Walking speed (m/s)	0.9	1.1	1.3*	1.5*
K1 (N-m/deg)	2.68	5.03	1.90	3.67
Setpoint 1 (deg)	3.21	2.78	1.08	-0.28
K2 (N-m/deg)	6.67	8.49	11.40	9.08
Setpoint 2 - Start (deg)	0.95	5.42	-4.28	-1.05
Setpoint 2 – End (deg)	17.74	19.47	24.17	25.28
K3 (N-m/deg)	5.59	4.15	5.35	5.52
Setpoint 3 – Start (deg)	23.75	30.00	27.31	21.42
Setpoint 3 – End (deg)	36.47	40.00	17.14	13.78
K4 (N-m/deg)	11.90	15.00	-	-
Setpoint 4 – Start (deg)	30.00	28.54	-	-
Setpoint 4 – End (deg)	23.97	24.63	-	-
Phase 2 Stance %	9.36	14.50	19.50	19.27
Phase 3 Stance %	27.50	30.60	93.50	94.50
Phase 4 Stance %	96.14	96.50	-	-

*** The upper two walking speeds did not require a 4th phase of stance to accurately fit the torque profile**

Table 5.2. Optimized Impedance Control Parameters - Translation

Walking speed (m/s)	0.9	1.1	1.3*	1.5*
K1 (N/m)	2000	2000	2000	2000
Setpoint 1 (m)	-0.05	-0.05	-0.05	-0.05
K2 (N/m)	8000	8000	10000	10000
Setpoint 2 - Start (m)	0	0	0	0
Setpoint 2 – End (m)	0.35	0.35	0.22	0.25
K3 (N/m)	6000	10000	10000	12000
Setpoint 3 – Start (m)	0.04	0.04	0.04	0.04
Setpoint 3 – End (m)	-0.1	-0.1	-0.1	-0.08
Phase 2 Stance %	5	5	27	27
Phase 3 Stance %	75	75	75	68

*** Position setpoint saturates at +0.05/-0.08 m. Values which exceed these bounds were optimized to control the speed with which the position reference reaches saturation.**

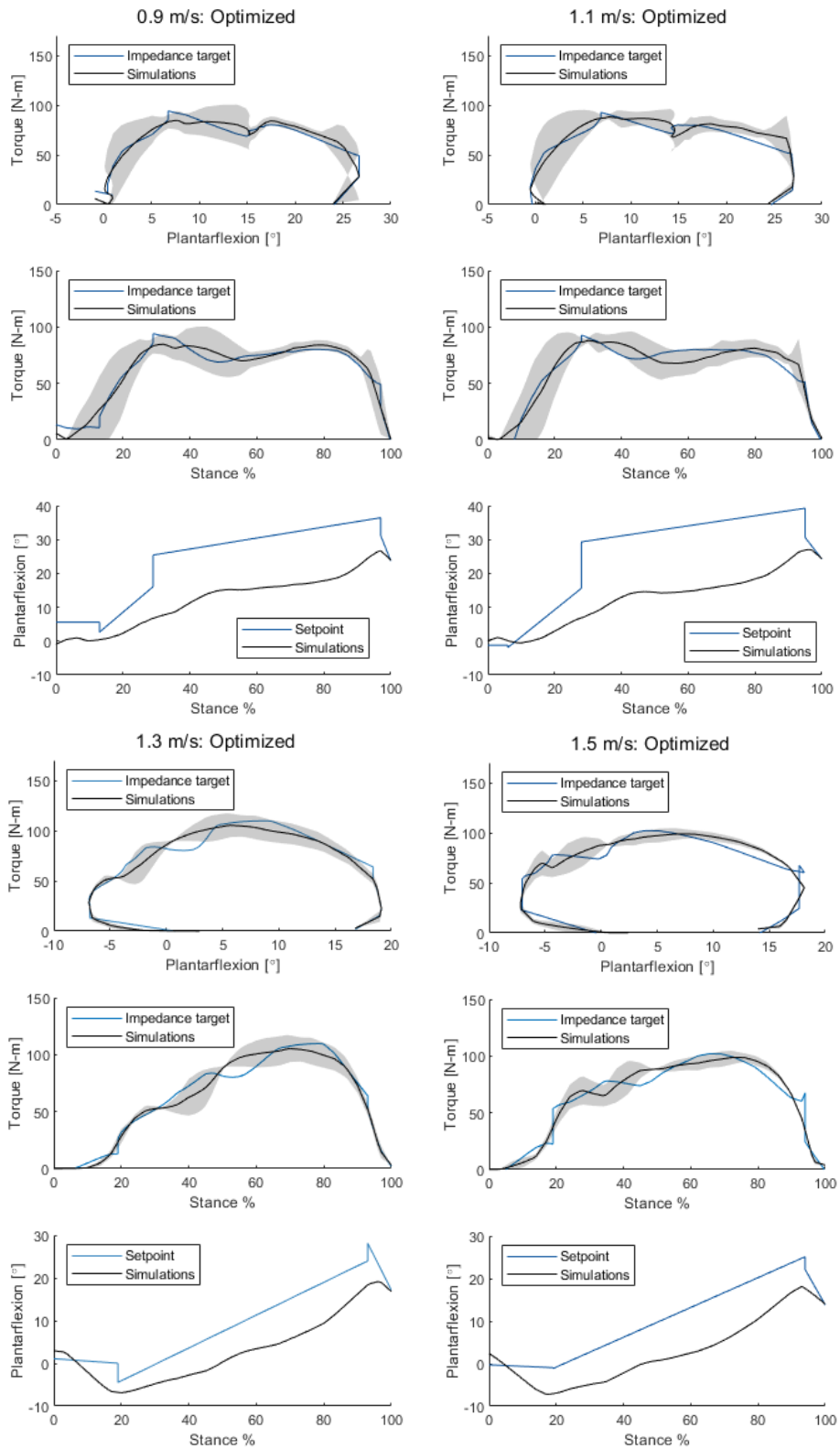

Figure 5.4. Optimized impedance control targets. Stiffness and setpoint trajectories are modified to match the

5.3. **Controller Design**

The prosthesis controllers are designed in a hierarchical structure. At the top level, walking events are detected using the onboard sensors and used to identify the phases of progression through the gait cycle as they happen. This information is used to switch between mid-level controller states assigned to the corresponding gait phases. These individual controller states are designed to replicate the simulated prosthesis interaction force and motion for each gait phase by emulating the simulated joint mechanical impedance. The impedance controller operates by commanding an output force or torque determined by the mechanism deflection from a virtual setpoint in imitation of a spring-damper system. The virtual setpoint and impedance properties are designed to produce behavior which matches the simulated behavior. The desired force and torque are output using a low-level force/torque PD controller. This control architecture is illustrated in Figure 5.5.

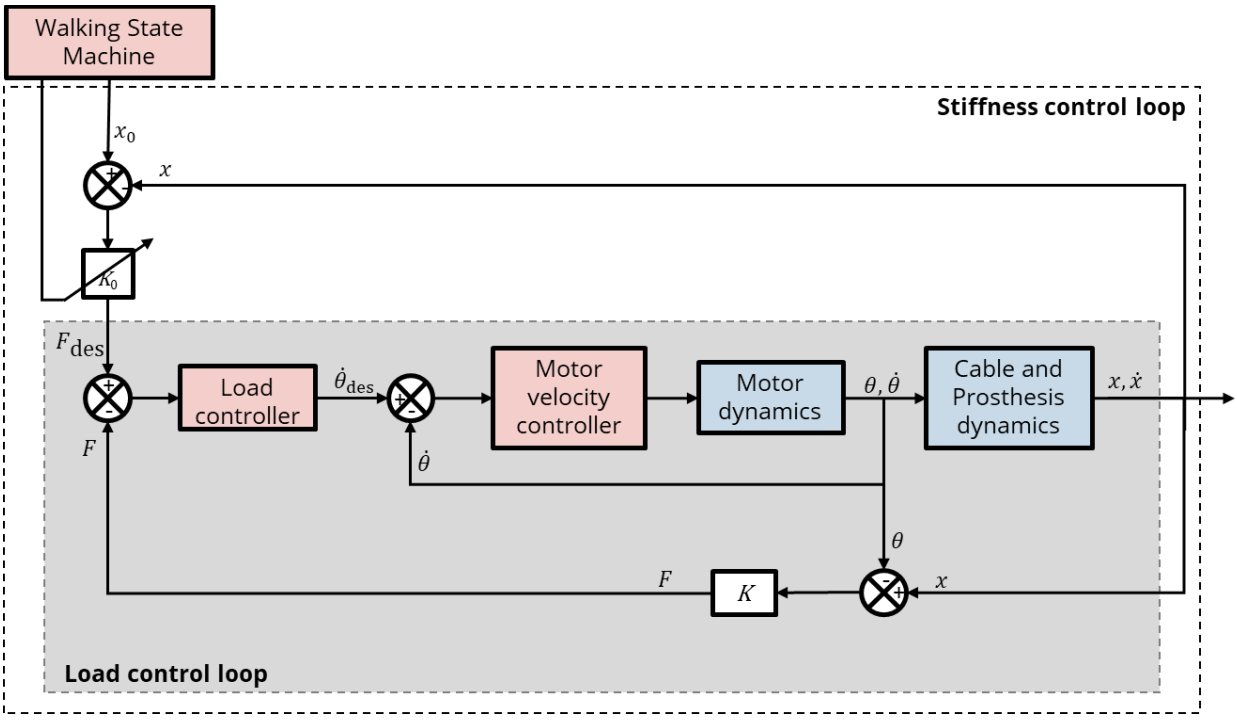

Figure 5.5. Overall prosthesis control architecture.

5.3.1 **Top-level: Walking controller**

The walking gait cycle for one leg can be broadly separated into two phases: stance phase and swing phase. Because the prosthesis is not in contact with the ground during swing phase, its influence on the rest of the wearer's biomechanics is far smaller than during stance phase. The walking controller thus takes the form of a finite state machine where the simulated prosthesis interaction with the ground is closely emulated during stance phase, and is controlled to avoid dragging on the ground and to reset for the beginning of stance during the swing phase.

The onboard sensors allow for gait events to be detected in two ways: 1) rapid changes in prosthesis acceleration, and 2) interaction force and torque exceeding or falling below certain thresholds. For this application, the largest spike in prosthesis jerk (time derivative of acceleration) occurs at heel-strike, or the very beginning of stance. Plantarflexion torque reaches its maximum during late stance, and then falls to near-zero after toe-off at the beginning of swing. This falling edge of the torque measurement is used to mark the end of the stance phase. Stance phase duration is calculated from the time difference between heel-strike and toe-off events. This duration is used to estimate the progression through stance for the subsequent step. The stance duraction calculation repeats for each step, adjusting the speed of the progression through the impedance trajectories for the current step based on the observed duration of the previous step. Active control of the device is signaled to begin by the heel-strike event, and the impedance control targets are dictated by the estimated progression through stance. This finite state machine logic is implemented via Stateflow in Simulink and is illustrated in Figure 5.6.

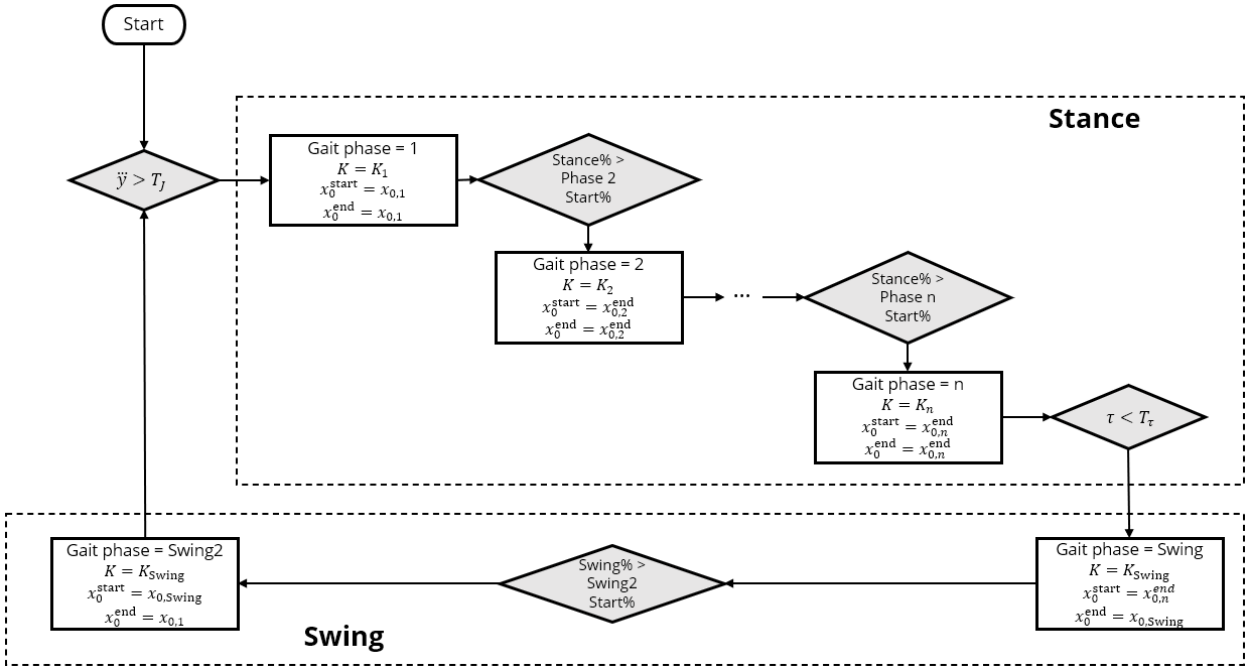

Figure 5.6. Walking controller finite state machine. Vertical jerk and plantarflexion torque thresholds are used to detect the transition between stance and swing phases. Subphase transitions occur based on estimated progression through stance or swing.

Impedance control parameters are also adjusted based on the estimation of walking speed to match the corresponding simulation behavior. For this system, walking speed can be estimated from either the stride time (if the average stride length of the wearer is known), or by integrating the forward acceleration as measured by the inertial sensor. However, this latter method will not function on a treadmill, where average forward velocity is zero.

5.3.2 **Mid-level: Stiffness controller**

The stiffness controller is designed to make the prototype behave with the dynamics of a linear spring system in each degree of freedom. Output force and torque are commanded based on the following control law:

$$F = K(x - x_0) \tag{5.3}$$

where F is the commanded load, K is the linear stiffness of the virtual spring, x is the measured prosthesis position for the corresponding axis, and x_0 is the virtual setpoint. Inertial terms are not included, making each actuator response resemble that of a massless spring with a tunable stiffness

connecting the moving parts of the prototype. This configuration allows the natural inertial properties of the device to govern its dynamic response.

A damping term was originally included to control the overall mechanical impedance rather than only the virtual stiffness. Damping was eventually not included due to the natural damping of the physical system proving large enough for oscillations to not be a concern for stiffnesses up to the actual stiffness of the cable transmission.

5.3.3 **Low-level: Load and position controllers**

The force and torque commanded by the impedance controller is output by the low-level load controller. This controller is designed with a PD architecture and outputs a commanded motor velocity. This architecture has been shown to have smoother and higher bandwidth performance for series-elastic actuators than direct motor current or voltage control [196]. Closed loop velocity control is implemented internally by the Maxon ESCON 50/5 motor drivers. Torque control is linearized by applying the cable tension to torque correction factor derived in Chapter 4. Desired torque is converted into desired cable tension, which is used as the controller input, and which has a more linear relationship with motor velocity. A block diagram for this controller is illustrated as the "Load control loop" in Figure 5.5.

The PD control architecture is based on wearable cable-actuator robotics work in [197], where force or torque is provided as proportional feedback, but motor velocity is used as derivative feedback rather than the time derivative of the load measurement. This control technique has demonstrated superior performance with cable-driven SEAs due to the lower noise in the motor velocity signal obtained from encoder feedback compared to an analog load signal. Additionally, as with using motor velocity control over current control, motor velocity feedback is preferred because the dynamics of SEA load are dominated by deflection of the series elastic component, which is in turn controlled by

motor position. This control scheme takes advantage of the smoother response allowed by designing a compliant mechanism.

Low-level position control is also accomplished using a PD controller architecture. This controller is not implemented during stance but is used to provide dorsiflexion when in the swing phase due to the torque sensing method being unable to sense net dorsiflexion torque. This controller is also used when the prosthesis needs to rigidly hold a set position, such as during benchtop testing or when being calibrated. When in use as a prosthesis, moving the impedance controller setpoint is preferred when a position needs to be commanded, because the resulting behavior more under the control of the wearer, making it safer and more comfortable.

5.4. **Evaluation Methods**

Benchtop tests were conducted to characterize device performance in force/torque measurement accuracy, force/torque step response time, frequency bandwidth, and peak load, speed, and power. Higher level control performance was assessed by performing treadmill walking trials with one able-bodied subject using a boot adapter. Results reflect the mean values ± 1 standard deviation unless otherwise specified.

5.4.1 **Benchtop evaluation**

To perform force and torque step response tests, the prosthesis frame and foot was rigidly fixed to the benchtop (Figure 5.7). Desired plantarflexion torque was commanded as a square wave with a 5 second period from 0 to 100 N-m. Desired translation force was commanded with the same load profile from -300 to 300 N. 10 trials were performed for each degree of freedom for this and the following benchtop tests.

Bandwidth tests were performed with the device fixed in the same configuration. Desired force and torque were commanded as a logarithmic chirp from 0.1 to 30 Hz over 20 seconds. Plantarflexion torque oscillated between 20 and 70 N-m, and translation force oscillated between -

200 and 200 N. The measured and desired torque were converted into the frequency domain using a fast Fourier transform, and the magnitude ratio and phase difference across the frequency range were used to create a Bode plot. The bandwidth was determined using -3dB as the magnitude cutoff and 45° as the phase margin cutoff.

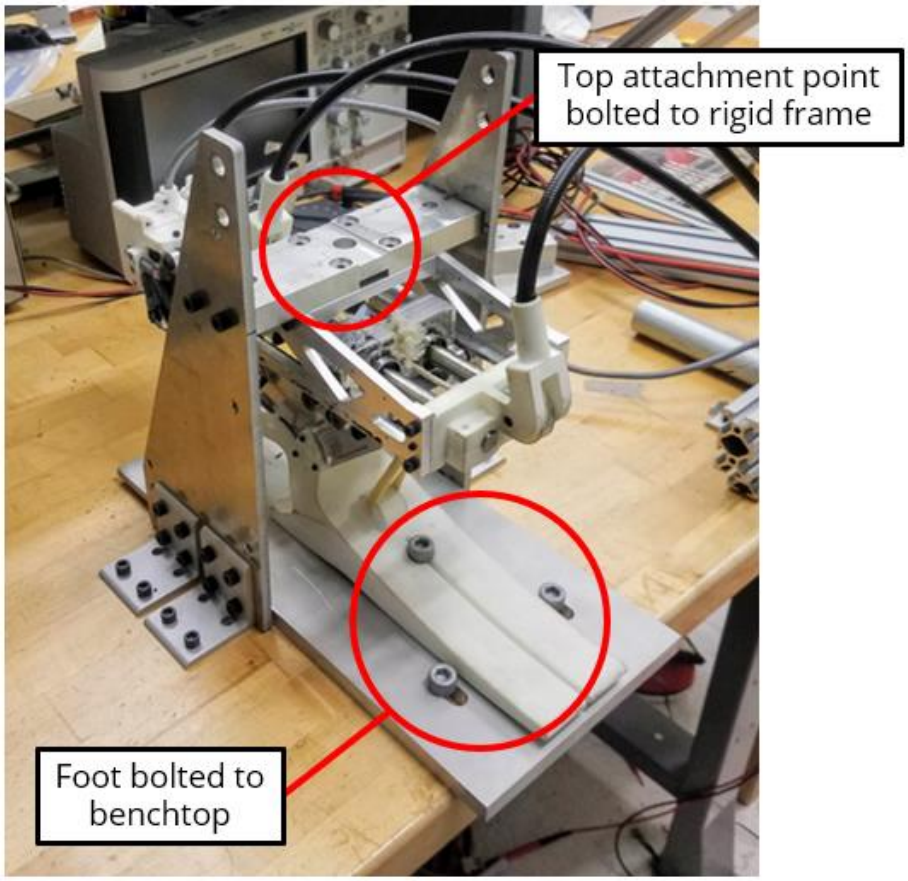

Figure 5.7. Benchtop testing setup for closed-loop force and torque control. A rigid metal frame constrained both degrees-of-freedom by fixing both the artificial foot and the top attachment point of the device to the benchtop.

5.4.2 **Walking evaluation**

The walking performance of the device was evaluated by conducting treadmill walking trials at each of the four simulated speeds (0.9, 1.1, 1.3, and 1.5 m/s) to showcase the separate control modalities. One able-bodied user (75.1 kg, 1.91 m tall, 29 years, male) wore the prosthesis using a set of adapter boots designed to immobilize the anatomical ankle and safely transmit the device loads

through to the body. Kinematics and loads were measured for each degree of freedom during walking and compared with the target load/position relationships. Similarity to the simulated behavior being emulated was measured as RMS error between measured and target mechanical impedance. The experimental setup for the walking evaluation trials is shown in Figure 5.8.

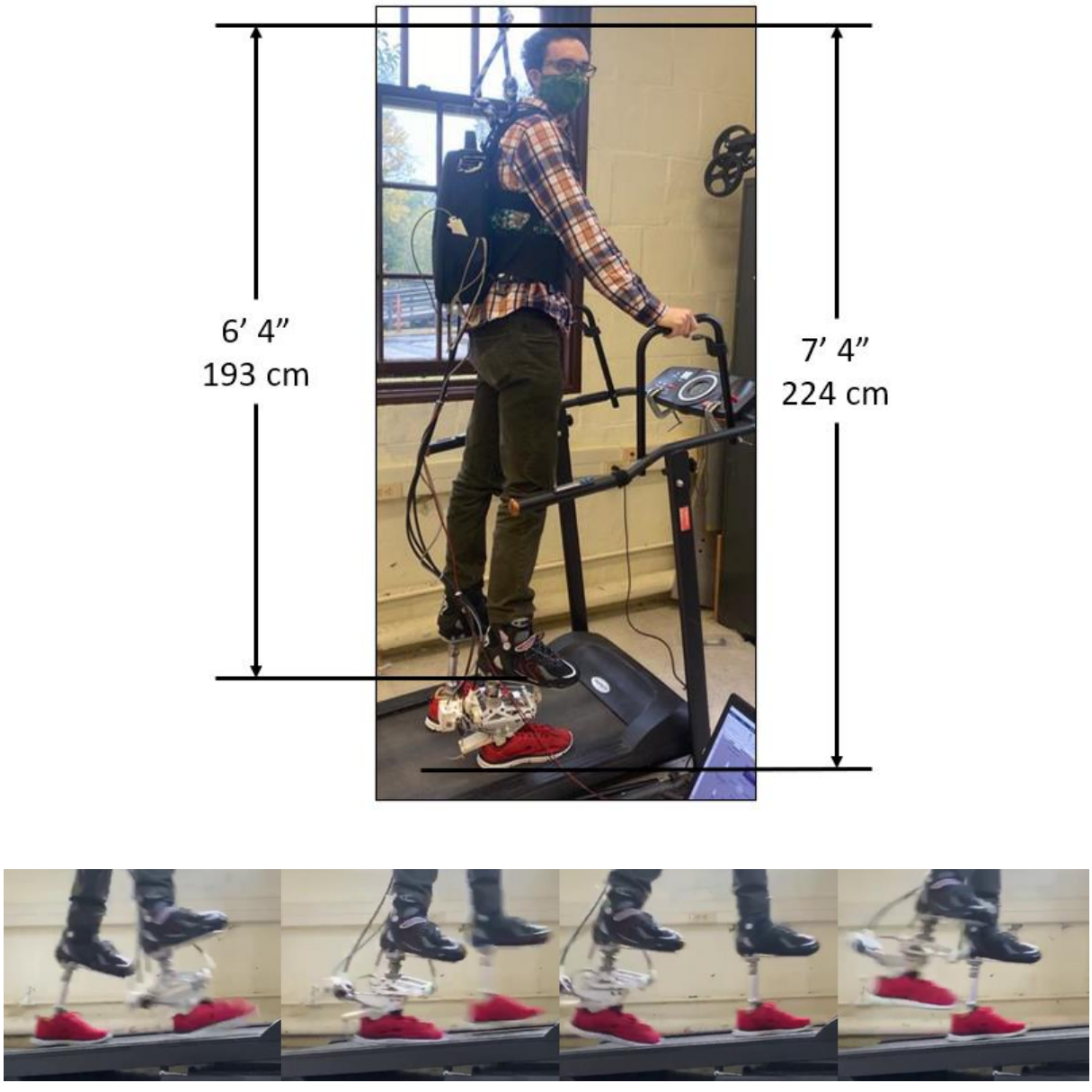

Figure 5.8. Top: Able-bodied subject preparing to walk on a treadmill wearing boot adapters. The treadmill was set for walking at the four simulated speeds. Additional handrails were added to the treadmill to accommodate the added height of the adapters. The subject was connected to the ceiling with a safety harness to prevent falls. Bottom: Treadmill walking gait sequence over one cycle. From left to right: Heel strike, mid-stance, toe-off, and mid-swing.

5.5. **Results**

Results from the benchtop tests are illustrated in Figure 5.9. The 98% rise and fall times for the translation actuator were 0.057 ± 0.000 s (mean ± 1SD) each, with overshoot of 3.8% and 4.3%, respectively. Rise and fall times for plantarflexion torque were 0.191 ± 0.001 s and 0.179 ± 0.001 s, with overshoot of 2.2% and 0.0%, respectively. Note that dorsiflexion torque cannot be measured as the system is designed, making a true measurement of plantarflexion torque overshoot below zero infeasible. Translation force and plantarflexion torque control amplitude fell below -3dB for a bandwidth of 15.0 Hz and 7.2 Hz, respectively. The phase margin falls below 45° at 19.5 and 11.3 Hz for translation force and flexion torque, respectively. The control bandwidth for both actuators is gain-limited.

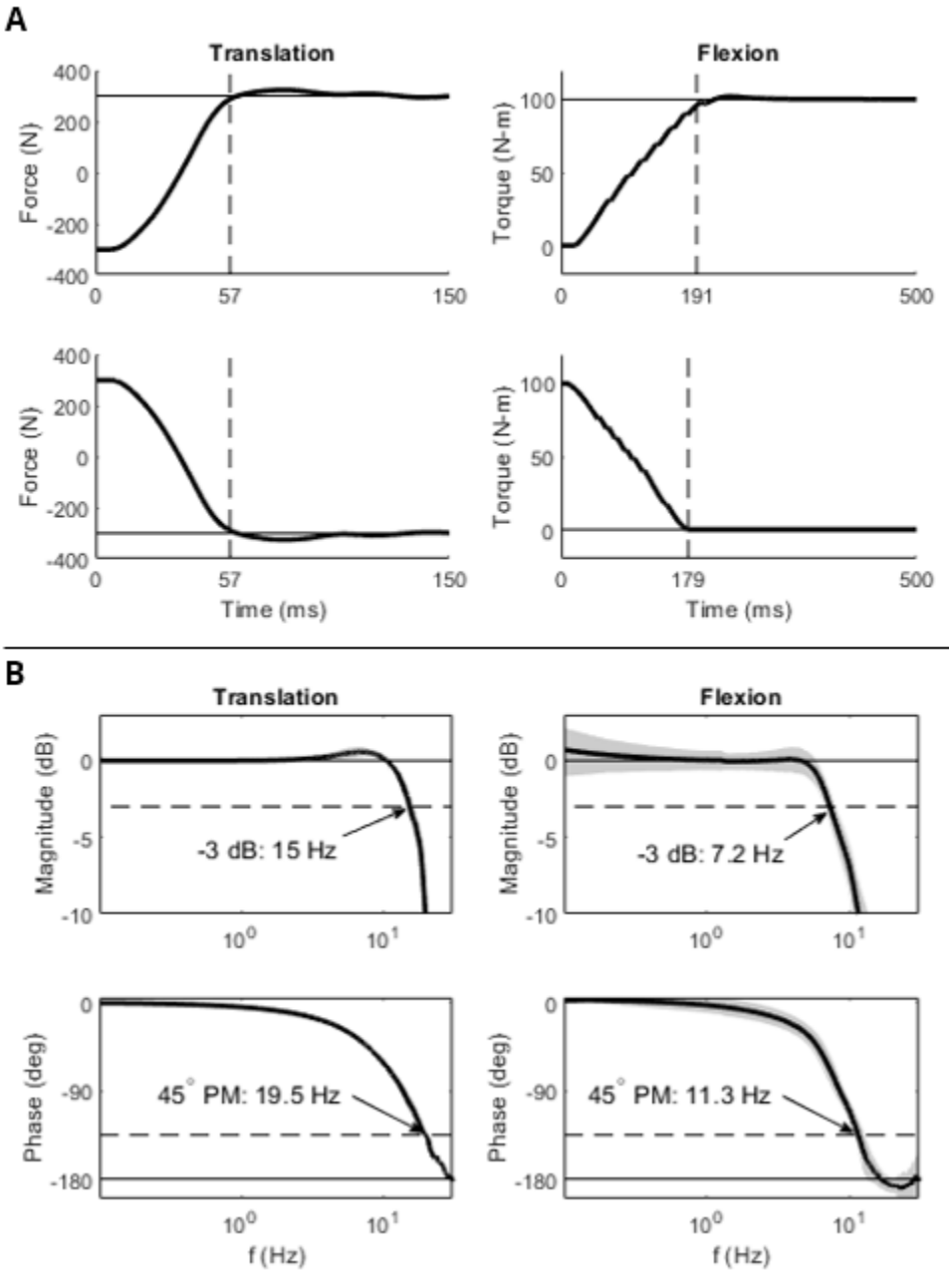

Figure 5.9. Closed loop force and torque controller (a) step responses and (b) frequency responses. Rise and fall times for the translation actuator are both 0.057 s, and range from 0.179 to 0.191 s for the flexion actuator. Bandwidth was limited by the gain margin for both actuators, at 15.0 Hz in translation and 7.2 Hz in flexion. Shaded bounds represent ±1SD in all plots.

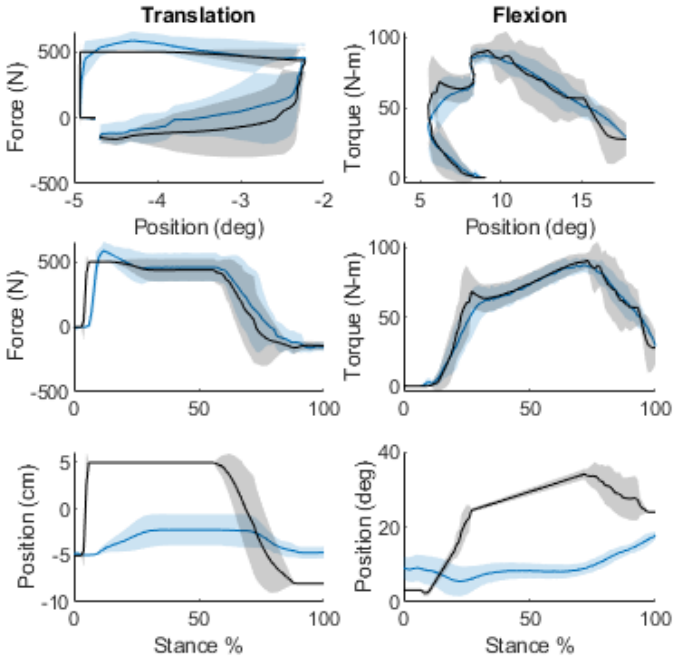

Figure 5.10. Actual and desired prosthesis dynamics during walking for walking at 0.9 m/s. The difference between actual prosthesis position and the virtual setpoint defines the commanded loads. Shaded bounds represent ±1SD in all plots.

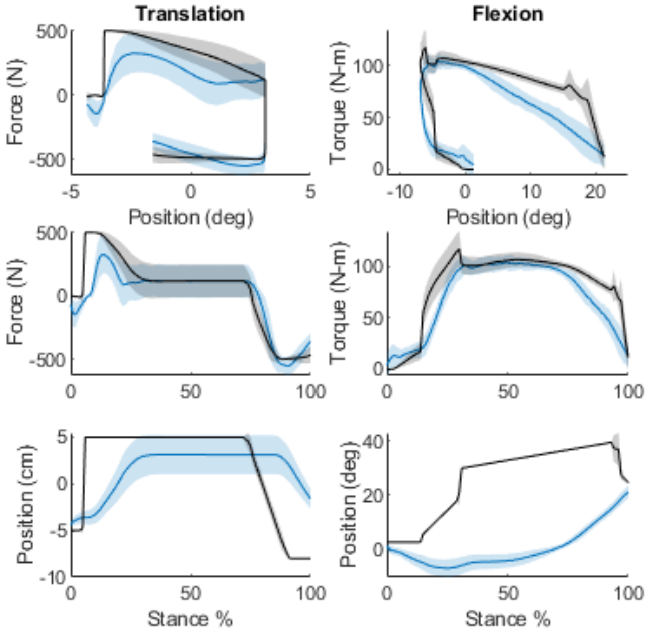

Figure 5.11. Actual and desired prosthesis dynamics during walking for walking at 1.1 m/s. The difference between actual prosthesis position and the virtual setpoint defines the commanded loads.

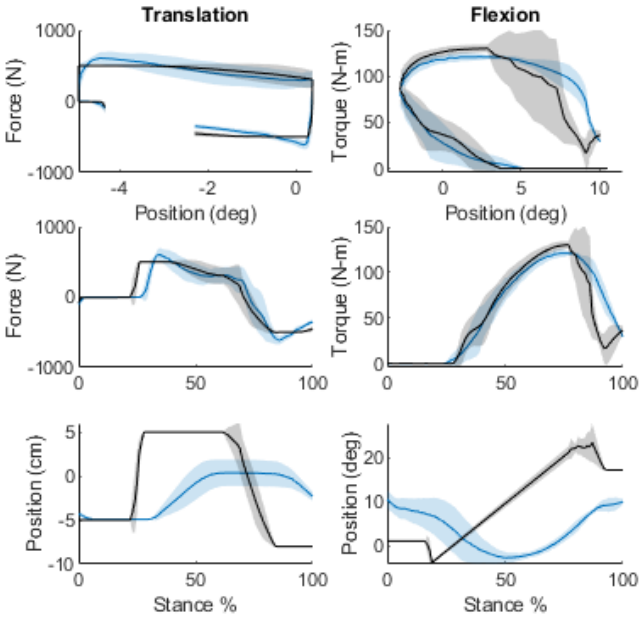

Figure 5.12. Actual and desired prosthesis dynamics during walking for walking at 1.3 m/s. The difference between actual prosthesis position and the virtual setpoint defines the commanded loads.

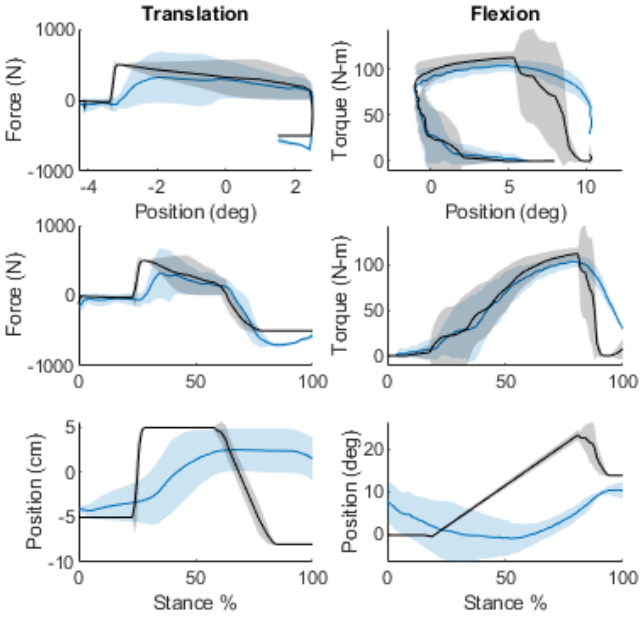

Figure 5.13. Actual and desired prosthesis dynamics during walking for walking at 1.5 m/s. The difference between actual prosthesis position and the virtual setpoint defines the commanded loads.

During walking trials, the subject walked at the selected speeds using the adapters without incident. Due to the artificially extended leg length, the subject used shorter strides than their preferred stride length to avoid the trailing foot falling off the back of the treadmill, leading to a more flat-footed gait than normal. Otherwise, top-level walking control performed as designed, recognizing heel-strike and proceeding through impedance control trajectories as illustrated in Figure 5.10s – 5.13. Force and torque tracking average RMS errors reached a maximum of 159 N and 21.3 N-m, respectively. The largest errors were recorded during the fastest walking speed and the lowest errors were recorded during the slowest walking speed. Translation force was repeatedly saturated during these trials across walking speeds, with values in excess of 500 N recorded in both directions. Maximum torque was recorded during the 1.3 m/s trial at 121.1 ± 3.5 N-m. Average RMS tracking errors are reported for each walking speed in Table 5.3.

Table 5.3. Walking trial load tracking errors

Walking speed (m/s)	**0.9**	**1.1**	**1.3**	**1.5**
RMSE - Translation	**93**	**135**	**119**	**159**
RMSE - % Max force	**15.8%**	**24.4%**	**19.5%**	**22.6%**
RMSE - Flexion	**4.6 N-m**	**18.1 N-m**	**16.3 N-m**	**21.3 N-m**
RMSE -% Max torque	**5.3%**	**17.4%**	**13.4%**	**20.5%**

5.6. **Discussion**

The presented control scheme translates key results of optimal control simulations into real prosthesis behavior. The impedance control parameter matching method is capable of distilling simulated prosthesis forces and motions into a self-contained, responsive physical model which interfaces between the user and their environment. This capability has been demonstrated through walking trials on the prototype simulation test platform. The optimized impedance control trajectories are reliably and repeatably reproduced as controller targets at the beginning of each step, with slight

step-to-step variations accounted for by user variation in step timing. The impedance controller has been demonstrated to accurately track desired torques corresponding to changing stiffness and setpoint parameters across four different walking control modalities.

However, as revealed by both the benchtop and walking tests, the control performance is mostly limited by the actuation and sensing capabilities rather than the control method itself. The primary source for load tracking error during walking was lag between the actual and desired trajectory. Load sensing hysteresis may be a factor in this control lag, considering that it primarily occurs for plantarflexion torque as it sharply falls at the end of stance. However, closed-loop torque control bandwidth and step response time determine the ability of the device to quickly respond to changing load demands, such as the rapid changes in target torque at the beginning and end of stance. In comparison with other powered ankle devices, the 1-DoF emulator device achieved 17 Hz closed loop bandwidth with a large offboard motor [9], and the Empower prototype achieved 9.4 Hz with its linear actuator mounted directly to the artificial foot [198] (versus the 7.6 Hz plantarflexion torque bandwidth achieved with this device). Despite this, the torque bandwidth still exceeds estimates of the biological ankle plantarflexion torque bandwidth [199]. Additionally, the magnitude of the plantarflexion loads are large enough that motor saturation is a relevant factor, considering that plantarflexion torque is approximately 85% of ideal at the maximum plantarflexion angle. Perhaps unsurprisingly, torque tracking was far more consistent for the 0.9 m/s trial, in which load magnitude and rate of change was lower.

Translation closed loop bandwidth is more than double and its step response speed is more than triple the corresponding plantarflexion values, which is expected given the design decisions made in the previous chapter. It is important to consider the large hysteresis associated with the translation force measurement, but since these tests are determined by the speed of increasing load in each direction, hysteresis should not significantly impact the results. These parameters are nearly

on par with the emulator project and exceed the performance of the Empower prototype. However, this fast response is primarily because the actuator is designed for relatively low loads as indicated by the optimal control simulations. As a result, the translation control was occasionally overpowered despite motor saturation through the force of the subject's weight and inertia alone. In fact, both degrees of freedom are very easily backdriven while wearing the adapters and the motors are inactive. The boot adapters increase the leverage the wearer exerts on the device, adding 30.5 cm of height to the subject. However, even under standard use conditions, simulated translation loads are generally not sufficient to overpower the user. Considering that one of the primary objectives is to minimize user effort, and the other is to minimize peak socket loads, the inability to "fight" the user is likely not a true design limitation. The translation degree of freedom provides some assist to help propel and align the user for minimum socket loading which can be overridden if the user resists that motion. The preliminary walking trials indicate some inconsistency in the user's response to these forces, achieving full range of motion at some speeds and a substantially reduced range at others, suggesting that a training period may be necessary to acclimate to the unconventional motion and exploit the benefits it offers.

Future refinements on this control approach should focus on improved continuity between phase transitions and step-to-step consistency. Future optimizations of the impedance control parameters should be constrained to enforce continuous changes in output loads between phases. Additionally, optimal impedance parameters may vary based on the user height and mass, indicating that ranges of these factors may also be necessary in simulations for deriving average controller parameters. Methods being developed by other groups should be investigated and implemented where appropriate, such as automatically adjusting an offset to the the torque controller output to counter changing elasticity and friction conditions in the cable transmission system [197]. Additionally, the current method of changing phase based on estimated progression through stance may prove

inflexible to users with different preferred walking patterns. Changes in the inertial signals or load measurements instead of time-based events to signal phase transitions during stance may be more robust to inter-user variation.

Additionally, it is recommended to add a brake to the translation actuator which engages in response to the motors being disabled as a failsafe. The current emergency stop functionality of cutting power to the motors is not sufficient to ensure safety to the wearer due to the high backdrivability of the device, which is very unstable to walk on when the motors are disengaged.

5.7. **Conclusion**

Simulations of theoretically optimal dynamic behavior for a prosthesis has been translated into an impedance control scheme for a functioning prototype. Preliminary walking trials were performed with an able-bodied subject on a treadmill, demonstrating separate optimal control patterns for four different walking speeds. Walking trials have revealed key insights into the function and behavior of anatomical and non-anatomical axes of motion. It is recommended to allow future subjects a training period to acclimate to an additional, non-anatomical joint added to their interface to the ground, and to adjust device failsafes to ensure passive stability should the operation of the device be interrupted.

CHAPTER 6

SUMMARY, DISCUSSION, AND FUTURE DIRECTIONS

The primary objective of the work presented in this dissertation was to develop a functional framework and toolset for biomechanical simulation-guided lower limb prosthesis design. This objective is motivated by the idea that stripping away assumptions about conventional prosthesis form and function is a necessary step to better meet the needs of prosthesis users. In this work, this is accomplished by simulating the full bio-mechatronic system of a person walking with an artificial limb capable of generating whatever loads and motions are required, and optimizing this system for targeted user outcome objectives. The optimized behavior of this generalized prosthesis model is used as the basis to generate design specifications for hardware capable of reproducing the same behavior. The prototype design presented is capable of reproducing a range of simulated behaviors, and is designed to be adaptable to future simulations with different constraints and design objectives, with the objective of serving as a test platform to validate that simulated improvements in user outcomes are also observed experimentally.

The presented work fits into the context of a larger design framework. The development of an effective simulation-based prosthesis design method not only requires validation of the simulation results, but also the refinement of the simulation itself based on feedback from the validation experiments. This work fills a gap in this design loop to provide experimental feedback to the simulation process. A key limitation of the presented work is that this feedback step was not performed. The prototype is capable of recreating more typical revolute prosthesis behavior by locking the translation axis at the neutral position and adjusting the walking controller to follow a biomimetic plantarflexion torque profile. Experimentally measuring the simulated outcome measures with the prototype device with human subjects who regularly use a below-knee prosthesis and using

the resulting findings to refine the optimization objectives and simulation assumptions are essential next steps in this research.

Aside from investigations of socket loading and metabolic effort, there is a broad range of useful studies that are now possible with the development of the prototype. Objective function values such as joint contact loading, biological joint moments, metrics of walking stability such as projected base of support, or three-dimensional considerations like out-of-plane destabilizing loads could be considered in future optimizations. Parametric variation of these objectives would result in a range of prosthesis control targets which can be tested experimentally. Comparing a systematic variation of simulated outcome measures against actual outcomes may aid in adjusting objective function weights to more accurately capture the neural process that leads to actual prosthesis-augmented gait patterns.

Additionally, the importance of user feedback in future studies should not be ignored. It has been shown that the theoretical optimal prosthesis output is very often not the output setting preferred by the actual wearers. No quantitative biomechanical measure can provide a more accurate assessment of how well a device is satisfying the needs of the wearer than the opinion of the wearer themself. Surveying user preference for different prosthesis behaviors corresponding to different objective function weights may help determine the correct weights and terms to include for simulating control strategies for specific tasks. Further refinement with individual subjects may allow for the development of optimal subject-specific designs based on modifications to a general design that performs well for a statistical sample, at least for certain categories of users (activity level, suspension type, etc.). Human-in-the-loop experiments should also be considered, in which the user is given direct control over the amount which each optimization objective is reflected in the device behavior to gain further insights about what factors take priority during certain gait tasks for self-selected gait patterns.

This work also leaves open the possibility for alternative test platform designs. With further refinement of the existing design, a 3-DoF sagittal plane test platform may be possible. As simulations move into three dimensions, additional test platforms which can accommodate the loads and motions outside of the saggital plane will also be necessary. The effect of the added mass of the actuator pack should be investigated so as to develop specific size and weight limits for these designs, as it seems likely that the 2-DoF actuator pack presented in this work may have been able to accommodate larger motors with further refinement of the actuator configuration and structure design.

While a complete loop of the design framework developed in this dissertation was not performed, the tools required to execute this design method have been successfully developed and demonstrated. The work represents an outcomes-focused design philosophy which seeks to challenge conventional assumptions about the proper form and function of artificial limbs. The opportunities to explore this philosophy with the tools developed here are wide-ranging.

REFERENCES

[1] A. D. Kuo and J. M. Donelan, "Dynamic Principles of Gait and Their Clinical Implications," *Phys. Ther.*, vol. 90, no. 2, pp. 157–174, 2010.

[2] P. G. Adamczyk and A. D. Kuo, "Mechanisms of Gait Asymmetry Due to Push-Off Deficiency in Unilateral Amputees," *IEEE Trans. Neural Syst. Rehabil. Eng.*, vol. 23, no. 5, pp. 776–785, 2015.

[3] A. D. Segal *et al.*, "The effects of a controlled energy storage and return prototype prosthetic foot on transtibial amputee ambulation," *Hum. Mov. Sci.*, vol. 31, no. 4, pp. 918–931, 2012.

[4] H. M. Herr and A. M. Grabowski, "Bionic ankle-foot prosthesis normalizes walking gait for persons with leg amputation," *Proc. R. Soc. B Biol. Sci.*, vol. 279, no. 1728, pp. 457–464, 2012.

[5] F. Sup, H. A. Varol, J. Mitchell, T. J. Withrow, and M. Goldfarb, "Preliminary evaluations of a self-contained anthropomorphic transfemoral prosthesis," *IEEE/ASME Trans. Mechatronics*, vol. 14, no. 6, pp. 667–676, 2009.

[6] P. Cherelle *et al.*, "The Ankle Mimicking Prosthetic Foot 3—Locking mechanisms, actuator design, control and experiments with an amputee," *Rob. Auton. Syst.*, vol. 91, pp. 327–336, 2017.

[7] M. K. Shepherd and E. J. Rouse, "The VSPA Foot A Quasi-Passive Ankle-Foot," *IEEE Trans. Neural Syst. Rehabil. Eng.*, vol. 25, no. 12, pp. 2375–2386, 2017.

[8] M. Cempini, L. J. Hargrove, and T. Lenzi, "Design, Development, and Bench-top Testing of a Powered Polycentric Ankle Prosthesis," in *Proc. IEEE/RSJ International Conference on Intelligent Robots and Systems (IROS)*, 2017, pp. 1064–1069.

[9] J. M. Caputo and S. H. Collins, "A Universal Ankle–Foot Prosthesis Emulator for Human Locomotion Experiments," *J. Biomech. Eng.*, vol. 136, no. 3, p. 035002, 2014.

[10] R. E. Quesada, J. M. Caputo, and S. H. Collins, "Increasing ankle push-off work with a powered prosthesis does not necessarily reduce metabolic rate for transtibial amputees," *J. Biomech.*, vol. 49, no. 14, pp. 3452–3459, 2016.

[11] E. Russell Esposito and J. M. Wilken, "Biomechanical risk factors for knee osteoarthritis when using passive and powered ankle-foot prostheses," *Clin. Biomech.*, vol. 29, no. 10, pp. 1186–1192, 2014.

[12] A. M. Grabowski and S. D'Andrea, "Effects of a powered ankle-foot prosthesis on kinetic loading of the unaffected leg during level-ground walking," *J. Neuroeng. Rehabil.*, vol. 10, no. 49, 2013.

[13] M. Ackermann and A. J. van den Bogert, "Optimality principles for model-based prediction of human gait," *J. Biomech.*, vol. 43, no. 6, pp. 1055–1060, 2010.

[14] F. C. Anderson and M. G. Pandy, "Dynamic optimization of human walking," *J. Biomech. Eng.*, vol. 123, no. 5, pp. 381–390, 2001.

[15] T. W. Dorn, J. M. Wang, J. L. Hicks, and S. L. Delp, "Predictive simulation generates human adaptations during loaded and inclined walking," *PLoS One*, vol. 10, no. 4, pp. 1–16, 2015.

[16] B. R. Umberger, Brian R. Umberger, and B. R. Umberger, "Stance and swing phase costs in human walking.," *J. R. Soc. Interface*, vol. 7, no. 50, pp. 1329–40, 2010.

[17] L. Ren, R. K. Jones, and D. Howard, “Predictive modelling of human walking over a complete gait cycle,” *J. Biomech.*, vol. 40, no. 7, pp. 1567–1574, 2007.

[18] E. Russell Esposito, R. H. Miller, E. R. Esposito, and R. H. Miller, “Maintenance of muscle strength retains a normal metabolic cost in simulated walking after transtibial limb loss,” *PLoS One*, vol. 13, no. 1, p. e0191310, 2018.

[19] M. L. Handford and M. Srinivasan, “Robotic lower limb prosthesis design through simultaneous computer optimizations of human and prosthesis costs,” *Sci. Rep.*, vol. 6, p. 19983, 2016.

[20] A. D. Koelewijn and A. J. van den Bogert, “Joint contact forces can be reduced by improving joint moment symmetry in below-knee amputee gait simulations,” *Gait Posture*, vol. 49, pp. 219–225, 2016.

[21] M. A. Price, S. Member, P. Beckerle, and F. C. Sup, “Design Optimization in Lower Limb Prostheses : A Review,” vol. 27, no. 8, pp. 1574–1588, 2019.

[22] K. Ziegler-Graham, E. J. MacKenzie, P. L. Ephraim, T. G. Travison, and R. Brookmeyer, “Estimating the Prevalence of Limb Loss in the United States: 2005 to 2050,” *Arch. Phys. Med. Rehabil.*, vol. 89, no. 3, pp. 422–429, 2008.

[23] R. Gailey, “Review of secondary physical conditions associated with lower-limb amputation and long-term prosthesis use,” *J. Rehabil. Res. Dev.*, vol. 45, no. 1, pp. 15–30, 2008.

[24] D. C. Morgenroth *et al.*, “The effect of prosthetic foot push-off on mechanical loading associated with knee osteoarthritis in lower extremity amputees,” *Gait Posture*, vol. 34, no. 4, pp. 502–507, 2011.

[25] A. M. Simon *et al.*, “Configuring a powered knee and ankle prosthesis for transfemoral amputees within five specific ambulation modes,” *PLoS One*, vol. 9, no. 6, 2014.

[26] S. Au, M. Berniker, and H. Herr, “Powered ankle-foot prosthesis to assist level-ground and stair-descent gaits,” *Neural Networks*, vol. 21, no. 4, pp. 654–666, 2008.

[27] F. Sup, H. A. Varol, and M. Goldfarb, “Upslope walking with a powered knee and ankle prosthesis: Initial results with an amputee subject,” *IEEE Trans. Neural Syst. Rehabil. Eng.*, vol. 19, no. 1, pp. 71–78, 2011.

[28] L. Fradet, M. Alimusaj, F. Braatz, and S. I. Wolf, “Biomechanical analysis of ramp ambulation of transtibial amputees with an adaptive ankle foot system,” *Gait Posture*, vol. 32, no. 2, pp. 191–198, 2010.

[29] M. Alimusaj, L. Fradet, F. Braatz, H. J. Gerner, and S. I. Wolf, “Kinematics and kinetics with an adaptive ankle foot system during stair ambulation of transtibial amputees,” *Gait Posture*, vol. 30, no. 3, pp. 356–363, 2009.

[30] E. M. Ficanha, M. Rastgaar, and K. R. Kaufman, “A two-axis cable-driven ankle-foot mechanism,” *Robot. Biomimetics*, vol. 1, no. 1, pp. 1–13, 2014.

[31] C. Pew and G. K. Klute, “Pilot testing of a variable stiffness transverse plane adapter for lower limb amputees,” *Gait Posture*, vol. 51, pp. 104–108, 2017.

[32] F. Stuhlenmiller, J. Schuy, P. Beckerle, and S. Rinderknecht, “A user-specific human-machine interaction strategy for a prosthetic shank adapter,” *Curr. Dir. Biomed. Eng.*, vol. 3, no. 2, pp. 493–496, 2017.

[33] E. J. Wolf, V. Q. Everding, A. A. Linberg, J. M. Czerniecki, and C. J. M. Gambel, “Comparison of the Power Knee and C-Leg during step-up and sit-to-stand tasks,” *Gait Posture*, vol. 38, no. 3, pp. 397–402, 2013.

[34] A. M. Simon, N. P. Fey, K. A. Ingraham, S. B. Finucane, E. G. Halsne, and L. J. Hargrove, “Improved Weight-Bearing Symmetry for Transfemoral Amputees during Standing Up and Sitting Down with a Powered Knee-Ankle Prosthesis,” *Arch. Phys. Med. Rehabil.*, vol. 97, no. 7, pp. 1100–1106, 2016.

[35] A. H. Shultz, B. E. Lawson, and M. Goldfarb, “Running with a powered knee and ankle prosthesis,” *IEEE Trans. Neural Syst. Rehabil. Eng.*, vol. 23, no. 3, pp. 403–412, 2015.

[36] P. Beckerle, O. Christ, T. Schürmann, J. Vogt, O. von Stryk, and S. Rinderknecht, “A human–machine-centered design method for (powered) lower limb prosthetics,” *Rob. Auton. Syst.*, vol. 95, pp. 1–12, 2017.

[37] M. J. Major and N. P. Fey, “Considering passive mechanical properties and patient user motor performance in lower limb prosthesis design optimization to enhance rehabilitation outcomes,” *Phys. Ther. Rev.*, vol. 22, no. July, pp. 1–15, 2017.

[38] E. Russell Esposito, K. M. Rodriguez, C. A. Ràbago, and J. M. Wilken, “Does unilateral transtibial amputation lead to greater metabolic demand during walking?,” *J. Rehabil. Res. Dev.*, vol. 51, no. 8, pp. 1287–1296, 2014.

[39] D. C. Norvell, J. M. Czerniecki, G. E. Reiber, C. Maynard, J. A. Pecoraro, and N. S. Weiss, “The prevalence of knee pain and symptomatic knee osteoarthritis among veteran traumatic amputees and nonamputees,” *Arch. Phys. Med. Rehabil.*, vol. 86, no. 3, pp. 487–493, 2005.

[40] J. Kulkarni, W. J. Gaine, J. G. Buckley, J. J. Rankine, and J. Adams, “Chronic low back pain in traumatic lower limb amputees,” *Clin. Rehabil.*, vol. 19, no. 1, pp. 81–86, 2005.

[41] B. J. Fregly and F. E. Zajac, “A State-Space Analysis of Mechanical Energy Generation, Absorption, and Transfer During Pedaling,” *J. Biomech.*, vol. 29, no. 1, pp. 81–90, 1996.

[42] R. R. Neptune, S. A. Kautz, and F. E. Zajac, “Contributions of the individual ankle plantar flexors to support, forward progression and swing initiation during walking,” *J. Biomech.*, vol. 34, no. 11, pp. 1387–1398, 2001.

[43] F. E. Zajac, “Understanding muscle coordination of the human leg with dynamical simulations,” *J. Biomech.*, vol. 35, no. 8, pp. 1011–1018, 2002.

[44] C. Hubley-kozey, K. Deluzio, and M. Dunbar, “Muscle co-activation patterns during walking in those with severe knee osteoarthritis,” *Clin. Biomech.*, vol. 23, no. 1, pp. 71–80, 2008.

[45] A. K. LaPrè *et al.*, “A Robotic Ankle Prosthesis with Dynamic Alignment,” *J. Med. Device.*, vol. 10, no. c, pp. 025001-1–9, 2016.

[46] A. F. Mak, M. Zhang, and D. A. Boone, “State-of-the-art research in lower-limb prosthetic biomechanics-socket interface: a review.,” *J. Rehabil. Res. Dev.*, vol. 38, no. 2, pp. 161–174, 2001.

[47] V. Noll, N. Eschner, C. Schumacher, P. Beckerle, and S. Rinderknecht, “A physically-motivated model describing the dynamic interactions between residual limb and socket in lower limb prostheses,” *Curr. Dir. Biomed. Eng.*, vol. 3, no. 1, pp. 15–18, 2017.

[48] A. K. LaPrè, M. A. Price, R. D. Wedge, B. R. Umberger, and F. C. Sup, “Approach for gait analysis in persons with limb loss including residuum and prosthesis socket dynamics,” *Int. j. numer. method. biomed. eng.*, vol. 34, no. 4, p. e2936, 2017.

[49] L. Paterno *et al.*, “Sockets for limb prostheses: A review of existing technologies and open challenges,” *IEEE Trans. Biomed. Eng.*, vol. 65, no. 9, pp. 1996–2010, 2018.

[50] K. Hagberg and R. Brånemark, “One hundred patients treated with osseointegrated transfemoral amputation prostheses—Rehabilitation perspective,” *J. Rehabil. Res. Dev.*, vol. 46, no. 3, pp. 331–344, 2009.

[51] D. A. Winter, “Biomechanics of below-knee amputee gait,” *J. Biomech.*, vol. 21, no. 5, pp. 361–367, 1988.

[52] L. Nolan and A. Lees, “The functional demands on the intact limb during walking for active trans-femoral and trans-tibial amputees,” *Prosthet. Orthot. Int.*, vol. 24, no. 2, pp. 117–125, 2000.

[53] D. A. Winter and S. E. Sienko, “Biomechanics of Below-Knee Amputee Gait,” *J. Biomech.*, vol. 21, no. 5, pp. 361–367, 1988.

[54] R. J. Zmitrewicz, R. R. Neptune, and K. Sasaki, “Mechanical energetic contributions from individual muscles and elastic prosthetic feet during symmetric unilateral transtibial amputee walking: A theoretical study,” *J. Biomech.*, vol. 40, no. 8, pp. 1824–1831, 2007.

[55] M. J. Hsu, D. H. Nielsen, S. J. Lin-Chan, and D. Shurr, “The effects of prosthetic foot design on physiologic measurements, self-selected walking velocity, and physical activity in people with transtibial amputation,” *Arch. Phys. Med. Rehabil.*, vol. 87, no. 1, pp. 123–129, 2006.

[56] J. F. Lehmann, R. Price, R. Okumura, K. Questad, B. J. De Lateur, and A. Négretot, “Mass and mass distribution of below-knee prostheses: Effect on gait efficacy and self-selected walking speed,” *Arch. Phys. Med. Rehabil.*, vol. 79, no. 2, pp. 162–168, 1998.

[57] P. Cherelle, V. Grosu, A. Matthys, B. Vanderborght, and D. Lefeber, “Design and validation of the ankle mimicking prosthetic (AMP-) Foot 2.0,” *IEEE Trans. Neural Syst. Rehabil. Eng.*, vol. 22, no. 1, pp. 138–148, 2014.

[58] A. H. Shultz, B. E. Lawson, and M. Goldfarb, “Variable Cadence Walking and Ground Adaptive Standing with a Powered Ankle Prosthesis,” *IEEE Trans. Neural Syst. Rehabil. Eng.*, vol. 24, no. 4, pp. 495–505, 2016.

[59] C. E. Clauser, J. T. McConville, and J. W. Young, “Weight, Volume, and Center of Mass of Segments of the Human Body,” Wright-Patterson Air Force Base, Ohio, 1969.

[60] O. Christ *et al.*, “User-centered prosthetic development: Comprehension of amputees’ needs,” *Biomed. Eng. / Biomed. Tech.*, vol. 57, no. SI-1 Track-R, pp. 1098–1101, 2012.

[61] P. A. Struyf, C. M. van Heugten, M. W. Hitters, and R. J. Smeets, “The Prevalence of Osteoarthritis of the Intact Hip and Knee Among Traumatic Leg Amputees,” *Arch. Phys. Med. Rehabil.*, vol. 90, no. 3, pp. 440–446, 2009.

[62] E. Yaşar *et al.*, “Epidemiologic data of trauma-related lower limb amputees: A single center 10-year experience,” *Injury*, vol. 48, no. 2, pp. 349–352, 2017.

[63] H. E. Meulenbelt, J. H. Geertzen, M. F. Jonkman, and P. U. Dijkstra, “Determinants of Skin Problems of the Stump in Lower-Limb Amputees,” *Arch. Phys. Med. Rehabil.*, vol. 90, no. 1, pp. 74–81, 2009.

[64] A. Mündermann, C. O. Dyrby, and T. P. Andriacchi, “Secondary gait changes in patients with medial compartment knee osteoarthritis: Increased load at the ankle, knee, and hip during walking,” *Arthritis Rheum.*, vol. 52, no. 9, pp. 2835–2844, 2005.

[65] “C-Leg,” *ottobock*. [Online]. Available: https://professionals.ottobockus.com/Prosthetics/Lower-Limb-Prosthetics/Knees--Microprocessor/C-Leg/c/1203.

[66] “OP4 Knee,” *Össur*. [Online]. Available: https://www.ossur.com/prosthetic-solutions/products/dynamic-solutions/op4-knee.

[67] “Rheo Knee,” *Össur*. [Online]. Available: https://www.ossur.com/prosthetic-solutions/products/dynamic-solutions/rheo-knee.

[68] “Total Knee 1900,” *Össur*. [Online]. Available: https://www.ossur.com/prosthetic-solutions/products/balance-solutions/total-knee-1900.

[69] M. P. Greene, “Four Bar Linkage Knee Analysis,” *J. Prosthetics Orthot.*, vol. 37, no. 1, pp. 15–24, 1983.

[70] “Computer controlled knees,” *ottobock*. [Online]. Available: http://www.ottobockus.com/prosthetics/info-for-new-amputees/prosthetics-101/computer-controlled-knees/.

[71] “Endolite Orion3,” *Endolite USA*. [Online]. Available: http://www.endolite.com/products/orion3.

[72] D. Berry, “Microprocessor prosthetic knees,” *Phys. Med. Rehabil. Clin. N. Am.*, vol. 17, no. 1, pp. 91–113, 2006.

[73] H. Stinus, “Biomechanics and evaluation of the microprocessor-controlled C-Leg exoprosthesis knee joint,” *Z Orthop Ihre Grenzgeb*, vol. 138, no. 3, pp. 278–282, 2000.

[74] A. H. Hansen and E. A. Nickel, “Development of a Bimodal Ankle-Foot Prosthesis for Walking and Standing/Swaying,” *J. Med. Device.*, vol. 7, no. 3, p. 035001, 2013.

[75] C. H. Soo and J. M. Donelan, “Mechanics and energetics of step-to-step transitions isolated from human walking,” *J. Exp. Biol.*, vol. 213, no. 24, pp. 4265–4271, 2010.

[76] A. H. Hansen, D. S. Childress, S. C. Miff, S. A. Gard, and K. P. Mesplay, “The human ankle during walking: Implications for design of biomimetic ankle prostheses,” *J. Biomech.*, vol. 37, no. 10, pp. 1467–1474, 2004.

[77] D. A. Winter, “Energy generation and absorption at the ankle and knee during fast, natural, and slow cadences,” *Clin. Orthop. Relat. Res.*, no. 175, pp. 147–54, 1983.

[78] R. J. Zmitrewicz, R. R. Neptune, J. G. Walden, W. E. Rogers, and G. W. Bosker, “The Effect of Foot and Ankle Prosthetic Components on Braking and Propulsive Impulses During Transtibial Amputee Gait,” *Arch. Phys. Med. Rehabil.*, vol. 87, no. 10, pp. 1334–1339, 2006.

[79] M. Windrich, M. Grimmer, O. Christ, S. Rinderknecht, and P. Beckerle, “Active lower limb prosthetics: a systematic review of design issues and solutions,” *Biomed. Eng. Online*, vol. 15, no. S3, p. 140, 2016.

[80] S. H. Collins and A. D. Kuo, “Recycling energy to restore impaired ankle function during human walking,” *PLoS One*, vol. 5, no. 2, 2010.

[81] A. M. Grabowski, J. Rifkin, and R. Kram, “K3 Promoter™ Prosthetic Foot Reduces the Metabolic Cost of Walking for Unilateral Transtibial Amputees,” *JPO J. Prosthetics Orthot.*, vol. 22, no. 2, pp. 113–120, 2010.

[82] M. Grimmer, M. Eslamy, and A. Seyfarth, “Energetic and Peak Power Advantages of Series Elastic Actuators in an Actuated Prosthetic Leg for Walking and Running,” *Actuators*, vol. 3, no. 1, pp. 1–19, 2014.

[83] J. K. Hitt, T. G. Sugar, M. Holgate, and R. Bellman, “An Active Foot-Ankle Prosthesis With Biomechanical Energy Regeneration,” *J. Med. Device.*, vol. 4, no. 1, p. 011003, 2010.

[84] J. W. Michael, “Energy storing feet: A clinical comparison,” *Clin. Prosthetics Orthot.*, vol. 11, no. 3, pp. 154–168, 1987.

[85] D. G. Barth, L. Schumacher, and S. S. Thomas, “Gait Analysis and Energy Cost of Below-Knee Amputees Wearing Six Different Prosthetic Feet,” *J. Prosthetics Orthot.*, vol. 4, no. 2, pp. 63–75, 1992.

[86] “Vari-Flex,” *Össur*. [Online]. Available: https://www.ossur.com/prosthetic-solutions/products/dynamic-solutions/vari-flex.

[87] “SACH Foot with Titanium Pyramid,” *Ohio Willow Wood*. [Online]. Available: https://www.willowwoodco.com/products-services/feet/low-activity/sach-foot-with-titanium-pyramid/.

[88] L. Nolan, “Carbon fibre prostheses and running in amputees: A review,” *Foot Ankle Surg.*, vol. 14, no. 3, pp. 125–129, 2008.

[89] J. D. Lee, L. M. Mooney, and E. J. Rouse, “Design and characterization of a quasi-passive pneumatic foot-ankle prosthesis,” *IEEE Trans. Neural Syst. Rehabil. Eng.*, vol. 25, no. 7, pp. 823–831, 2017.

[90] M. K. Shepherd and E. J. Rouse, “The VSPA foot: A quasi-passive ankle-foot prosthesis with continuously variable stiffness,” *IEEE Trans. Neural Syst. Rehabil. Eng.*, vol. 25, no. 12, pp. 2375–2386, 2017.

[91] “Proprio Foot,” *Össur*, 2018. [Online]. Available: https://www.ossur.com/prosthetic-solutions/products/dynamic-solutions/proprio-foot. [Accessed: 25-Jan-2018].

[92] “Elan,” *Endolite*. [Online]. Available: https://www.endolite.com/products/elan.

[93] M. Grimmer, M. Eslamy, S. Gliech, and A. Seyfarth, “A comparison of parallel- and series elastic elements in an actuator for mimicking human ankle joint in walking and running,” in *Proc. IEEE International Conference on Robotics and Automation (ICRA)*, 2012, pp. 2463–2470.

[94] G. A. Pratt and M. M. Williamson, “Series elastic actuators,” in *Proc. IEEE/RSJ International Conference on Intelligent Robots and Systems (IROS)*, 1995, pp. 399–406.

[95] P. Beckerle, “Practical relevance of faults, diagnosis methods, and tolerance measures in elastically actuated robots,” *Control Eng. Pract.*, vol. 50, pp. 95–100, 2016.

[96] E. J. Rouse, L. M. Mooney, and H. M. Herr, “Clutchable series-elastic actuator: Implications for prosthetic knee design,” *Int. J. Rob. Res.*, vol. 33, no. 13, pp. 1611–1625, 2014.

[97] J. Geeroms, L. Flynn, R. Jimenez-Fabian, B. Vanderborght, and D. Lefeber, “Ankle-Knee prosthesis with powered ankle and energy transfer for CYBERLEGs α-prototype,” in *Proc. IEEE International Conference on Rehabilitation Robotics (ICORR)*, 2013.

[98] H. Bateni and S. J. Olney, “Kinematic and Kinetic Variations of Below-Knee Amputee Gait,” *Prosthet. Orthotic Sci.*, vol. 14, no. 1, pp. 2–10, 2002.

[99] R. Versluys *et al.*, “A pneumatically powered below-knee prosthesis: Design specifications and first experiments with an amputee,” in *Proc. IEEE/RAS-EMBS International Conference on Biomedical Robotics and Biomechatronics (BioRob)*, 2008, pp. 372–377.

[100] M. F. Eilenberg, H. Geyer, and H. Herr, “Eilenberg_2010_TNSRE - Control of a Powered Ankle-Foot Prosthesis Based on a Neuromuscular Model - Geyer - Herr,” *IEEE Trans. Neural Syst. Rehabil. Eng.*, vol. 18, no. c, pp. 164–173, 2009.

[101] A. H. Shultz, J. E. Mitchell, D. Truex, B. E. Lawson, and M. Goldfarb, “Preliminary Evaluation of a Walking Controller for a Powered Ankle Prosthesis,” in *Proc. IEEE International Conference on Robotics and Automation (ICRA)*, 2013, pp. 4823–4828.

[102] B. J. Bergelin and P. A. Voglewede, “Design of an Active Ankle-Foot Prosthesis Utilizing a Four-Bar Mechanism,” *J. Mech. Des.*, vol. 134, no. 6, p. 061004, 2012.

[103] “Empower,” *ottobock*. [Online]. Available: https://www.ottobockus.com/prosthetics/lower-limb-prosthetics/solution-overview/empower-ankle/.

[104] M. Grimmer *et al.*, “A powered prosthetic ankle joint for walking and running,” *Biomed. Eng. Online*, vol. 15, no. 3, pp. 37–52, 2016.

[105] D. A. Winter, *Biomechanics and Motor Control of Human Movement*, 4th ed. Hoboken, NJ: John Wiley & Sons, 2009.

[106] R. Riener, M. Rabuffetti, and C. Frigo, “Stair ascent and descent at different inclinations,” *Gait Posture*, vol. 15, no. 1, pp. 32–44, 2002.

[107] R. Jacobs, M. F. Bobbert, and G. J. van Ingen Schenau, “Mechanical Output From Individual Muscles During Explosive Leg Extensions: the Role of Biarticular Muscles,” *J. Biomech.*, vol. 29, no. 4, pp. 513–523, 1996.

[108] E. C. Martinez-Villalpando, J. Weber, G. Elliott, and H. Herr, “Design of an agonist-antagonist active knee prosthesis,” in *Proc. IEEE/RAS-EMBS International Conference on Biomedical Robotics and Biomechatronics (BioRob)*, 2008, pp. 529–534.

[109] H. Vallery, R. Burgkart, C. Hartmann, J. Mitternacht, R. Riener, and M. Buss, “Complementary limb motion estimation for the control of active knee prostheses,” *Biomed. Tech.*, vol. 56, no. 1, pp. 45–51, 2011.

[110] A. O. Kapti and M. S. Yucenur, “Design and control of an active artificial knee joint,” *Mech. Mach. Theory*, vol. 41, no. 12, pp. 1477–1485, 2006.

[111] C. D. Hoover, G. D. Fulk, and K. B. Fite, “The Design and Initial Experimental Validation of an Active Myoelectric Transfemoral Prosthesis,” *J. Med. Device.*, vol. 6, no. 1, p. 011005, 2012.

[112] G. Waycaster, S.-K. Wu, and X. Shen, “Design and Control of a Pneumatic Artificial Muscle Actuated Above-Knee Prosthesis,” *J. Med. Device.*, vol. 5, no. 3, p. 031003, 2011.

[113] “Power Knee,” *Össur*, 2018. [Online]. Available: https://www.ossur.com/prosthetic-solutions/products/dynamic-solutions/power-knee. [Accessed: 29-Jan-2018].

[114] S. H. Collins, M. Kim, T. T. Chen, T. T. Chen, and S. H. Collins, “An ankle-foot prosthesis emulator with control of plantarflexion and inversion-eversion torque,” *IEEE Trans. Robot.*, vol. 34, no. 5, pp. 1183–1194, 2018.

[115] J. T. Panzenbeck and G. K. Klute, “A powered inverting and everting prosthetic foot for balance assistance in lower limb amputees,” *J. Prosthetics Orthot.*, vol. 24, no. 4, pp. 175–180, 2012.

[116] E. M. Ficanha, M. Rastgaar, and K. R. Kaufman, “Control of a 2-DOF powered ankle-foot mechanism,” in *Proc. IEEE International Conference on Robotics and Automation (ICRA)*, 2015, pp. 6439–6444.

[117] “College Park - Trustep,” *College Park*, 2017. [Online]. Available: https://www.college-park.com/lower-limb/prosthetic-feet/trustep. [Accessed: 24-Jan-2018].

[118] "ReFlex Rotate," *Össur*, 2018. [Online]. Available: https://www.ossur.com/prosthetic-solutions/products/dynamic-solutions/re-flex-rotate. [Accessed: 24-Jan-2018].

[119] A. G. Hatfield and J. D. Morrison, "Polyurethane gel liner usage in the Oxford prosthetic service," *Prosthet. Orthot. Int.*, vol. 25, no. 1, pp. 41–46, 2001.

[120] E. Boutwell, R. Stine, A. Hansen, K. Tucker, and S. Gard, "Effect of prosthetic gel liner thickness on gait biomechanics and pressure distribution within the transtibial socket," *J. Rehabil. Res. Dev.*, vol. 49, no. 2, pp. 227–240, 2012.

[121] J. T. Kahle, J. J. Orriola, W. Johnston, and M. J. Highsmith, "The Effects of Vacuum-Assisted Suspension on Residual Limb Physiology, Wound Healing, and Function: a Systematic Review," *Technol. Innov.*, vol. 15, no. 4, pp. 333–341, 2014.

[122] "ReFlex Shock," *Össur*, 2018. [Online]. Available: https://www.ossur.com/prosthetic-solutions/products/dynamic-solutions/re-flex-shock. [Accessed: 24-Jan-2018].

[123] A. K. Laprè, R. D. Wedge, B. R. Umberger, and F. C. Sup, "Preliminary study of a robotic foot-ankle prosthesis with active alignment," in *Proc. IEEE International Conference on Rehabilitation Robotics (ICORR)*, 2017, pp. 1299–1304.

[124] G. Papaioannou, C. Mitrogiannis, G. Nianios, and G. Fiedler, "Assessment of internal and external prosthesis kinematics during strenuous activities using dynamic roentgen stereophotogrammetric analysis," *J. Prosthetics Orthot.*, vol. 22, no. 2, pp. 91–105, 2010.

[125] C. R. Bocobo, J. M. Castellote, D. MacKinnon, and A. Gabrielle-Bergman, "Videofluoroscopic evaluation of prosthetic fit and residual limbs following transtibial amputation," *J. Rehabil. Res. Dev.*, vol. 35, no. 1, pp. 6–13, 1998.

[126] J. E. Sanders, A. Karchin, J. R. Fergason, and E. A. Sorenson, "A noncontact sensor for measurement of distal residual-limb position during walking," *J. Rehabil. Res. Dev.*, vol. 43, no. 4, p. 509, 2006.

[127] V. Noll, S. Rinderknecht, and P. Beckerle, "Systematic experimental assessment of a 2D-motion sensor to detect relative movement between residual limb and prosthetic socket," *Sensors*, vol. 18, no. 7, p. 2170, 2018.

[128] B. J. Fregly, F. E. Zajac, and P. Alto, "a State-Space Analysis of Mechanical Generation , Absorption , and Transfer Pedaling Energy," *J. Biomech.*, vol. 29, no. 1, pp. 81–90, 1996.

[129] B. R. Umberger, S. Augsburger, J. A. Resig, D. Oeffinger, R. Shapiro, and C. Tylkowski, "Generation, absorption, and transfer of mechanical energy during walking in children," *Med. Eng. Phys.*, vol. 35, no. 5, pp. 644–651, 2013.

[130] G. Chen, "Induced acceleration contributions to locomotion dynamics are not physically well defined," *Gait Posture*, vol. 23, no. 1, pp. 37–44, 2006.

[131] R. D. Crowninshield and R. A. Brand, "The predcition of forces in joint structures: distribution of intersegmental resultants," *Exerc. Sport Sci. Rev.*, vol. 9, p. 159181, 1981.

[132] A. Erdemir, S. McLean, W. Herzog, and A. J. van den Bogert, "Model-based estimation of muscle forces exerted during movements," *Clin. Biomech.*, vol. 22, no. 2, pp. 131–154, 2007.

[133] R. H. Miller, B. R. Umberger, J. Hamill, and G. E. Caldwell, "Evaluation of the minimum energy hypothesis

and other potential optimality criteria for human running," *Proc. R. Soc. B Biol. Sci.*, vol. 279, no. 1733, pp. 1498–1505, 2012.

[134] N. P. Fey, G. K. Klute, and R. R. Neptune, "The influence of energy storage and return foot stiffness on walking mechanics and muscle activity in below-knee amputees," *Clin. Biomech.*, vol. 26, no. 10, pp. 1025–1032, 2011.

[135] J. D. Ventura, G. K. Klute, and R. R. Neptune, "The effect of prosthetic ankle energy storage and return properties on muscle activity in below-knee amputee walking," *Gait Posture*, vol. 33, no. 2, pp. 220–226, 2011.

[136] N. P. Fey, G. K. Klute, and R. R. Neptune, "Optimization of prosthetic foot stiffness to reduce metabolic cost and intact knee loading during below-knee amputee walking: a theoretical study.," *J. Biomech. Eng.*, vol. 134, no. 11, p. 111005, 2012.

[137] N. P. Fey, G. K. Klute, and R. R. Neptune, "Altering prosthetic foot stiffness influences foot and muscle function during below-knee amputee walking: A modeling and simulation analysis," *J. Biomech.*, vol. 46, no. 4, pp. 637–644, 2013.

[138] P. Malcolm, R. E. Quesada, J. M. Caputo, and S. H. Collins, "The influence of push-off timing in a robotic ankle-foot prosthesis on the energetics and mechanics of walking," *J. Neuroeng. Rehabil.*, vol. 12, no. 1, p. 21, 2015.

[139] S. I. Wolf, M. Alimusaj, L. Fradet, J. Siegel, and F. Braatz, "Pressure characteristics at the stump/socket interface in transtibial amputees using an adaptive prosthetic foot," *Clin. Biomech.*, vol. 24, no. 10, pp. 860–865, 2009.

[140] J. L. Johansson, D. M. Sherrill, P. O. Riley, P. Bonato, and H. Herr, "A clinical comparison of variable-damping and mechanically passive prosthetic knee devices," *Am. J. Phys. Med. Rehabil.*, vol. 84, no. 8, pp. 563–575, 2005.

[141] E. Boutwell, R. Stine, and S. Gard, "Impact testing of the residual limb: system response to changes in prosthetic stiffness," *J. Rehabil. Res. Dev.*, vol. 53, no. 3, pp. 369–378, 2016.

[142] E. Boutwell, R. Stine, and S. Gard, "Shock absorption during transtibial amputee gait: Does longitudinal prosthetic stiffness play a role?," *Prosthet. Orthot. Int.*, vol. 41, no. 2, pp. 178–185, 2017.

[143] C. Pew and G. K. Klute, "Design of Lower Limb Prosthesis Transverse Plane Adaptor With Variable Stiffness," *J. Med. Device.*, vol. 9, no. 3, p. 035001, 2015.

[144] K. M. Ingraham, N. P. Fey, A. M. Simon, and L. J. Hargrove, "Assessing the relative contributions of active ankle and knee assistance to the walking mechanics of transfemoral amputees using a powered prosthesis," *PLoS One*, vol. 11, no. 1, pp. 1–19, 2016.

[145] E. C. Baars, E. Schrier, P. U. Dijkstra, and J. H. B. Geertzen, "Prosthesis satisfaction in lower limb amputees: A systematic review of associated factors and questionnaires," *Medicine (Baltimore).*, vol. 97, no. 39, p. e12296, 2018.

[146] P. G. Adamczyk, M. Roland, and M. E. Hahn, "Sensitivity of biomechanical outcomes to independent variations of hindfoot and forefoot stiffness in foot prostheses," *Hum. Mov. Sci.*, vol. 54, pp. 154–171, 2017.

[147] A. D. Kuo, "The six determinants of gait and the inverted pendulum analogy: A dynamic walking

perspective," *Hum. Mov. Sci.*, vol. 26, no. 4, pp. 617–656, 2007.

[148] P. G. Adamczyk and A. D. Kuo, "Redirection of center-of-mass velocity during the step-to-step transition of human walking," *J. Exp. Biol.*, vol. 212, no. 16, pp. 2668–2678, 2009.

[149] K. E. Zelik, T. W. P. Huang, P. G. Adamczyk, and A. D. Kuo, "The role of series ankle elasticity in bipedal walking," *J. Theor. Biol.*, vol. 346, pp. 75–85, 2014.

[150] R. J. Full and D. E. Koditschek, "Templates and anchors: neuromechanical hypotheses of legged locomotion on land.," *J. Exp. Biol.*, vol. 202, pp. 3325–3332, 1999.

[151] H. Geyer, A. Seyfarth, and R. Blickhan, "Compliant leg behaviour explains basic dynamics of walking and running," *Proc. R. Soc. B Biol. Sci.*, vol. 273, no. 1603, pp. 2861–2867, 2006.

[152] R. M. Alexander, "Optimum walking techniques for quadrupeds and bipeds," *J. Zool.*, vol. 192, no. 1, pp. 97–117, 1980.

[153] M. Srinivasan, "Fifteen observations on the structure of energy-minimizing gaits in many simple biped models," *J. R. Soc. Interface*, vol. 8, no. 54, pp. 74–98, 2011.

[154] A. E. Minetti and R. M. N. Alexander, "A theory of metabolic costs for bipedal gaits," *J. Theor. Biol.*, vol. 186, no. 4, pp. 467–476, 1997.

[155] A. Seth, M. Sherman, J. A. Reinbolt, and S. L. Delp, "OpenSim: A musculoskeletal modeling and simulation framework for in silico investigations and exchange," *Procedia IUTAM*, vol. 2, pp. 212–232, 2011.

[156] M. A. Sherman, A. Seth, and S. L. Delp, "Simbody: Multibody dynamics for biomedical research," *Procedia IUTAM*, vol. 2, pp. 241–261, 2011.

[157] A. Seth *et al.*, "OpenSim: Simulating musculoskeletal dynamics and neuromuscular control to study human and animal movement," *PLOS Comput. Biol.*, vol. 14, no. 7, p. e1006223, 2018.

[158] J. Sushko, C. Honeycutt, and K. B. Reed, "Prosthesis design based on an asymmetric passive dynamic walker," in *Proc. IEEE/RAS-EMBS International Conference on Biomedical Robotics and Biomechatronics (BioRob)*, 2012, pp. 1116–1121.

[159] W. C. Flowers and W. C., "Use of an amputee-computer interactive facility in above-knee prosthesis research," in *Proceedings of the 1974 annual conference on - ACM 74*, 1974, pp. 335–339.

[160] P. Beckerle *et al.*, "Design and control of a robot for the assessment of psychological factors in prosthetic development," in *Proc. IEEE International Conference on Systems, Man and Cybernetics (SMC)*, 2012, pp. 1485–1490.

[161] J. Zhang *et al.*, "Human-in-the-loop optimization of exoskeleton assistance during walking," *Science (80-.).*, vol. 356, no. 6344, pp. 1280–1284, 2017.

[162] P. Högberg, "How do stride length and stride frequency influece the energy-output during running?," *Eur. J. Appl. Physiol. Occup. Ther.*, vol. 14, no. 6, pp. 437–441, 1952.

[163] H. J. Ralston, "Energetics of Human Walking," in *Neural Control of Locomotion*, Boston, MA: Springer, 1976, pp. 77–98.

[164] M. Y. Zarrugh and C. W. Radcliffe, "Predicting metabolic cost of level walking," *Eur. J. Appl. Physiol. Occup.*

Ther., vol. 38, no. 3, pp. 215–223, 1978.

[165] M. L. Handford and M. Srinivasan, "Energy-optimal human walking with feedback-controlled robotic prostheses: a computational study," *IEEE Trans. Neural Syst. Rehabil. Eng.*, vol. 26, no. 9, pp. 1773–1782, 2018.

[166] P. Beckerle, J. Wojtusch, A. Seyfarth, O. Von Stryk, and S. Rinderknecht, "Analyzing and considering inertial effects in powered lower limb prosthetic design," *IEEE Int. Conf. Rehabil. Robot.*, vol. 2015-Septe, pp. 325–330, 2015.

[167] J. Wojtusch, "Uncertainty and Sensitivity in Human Motion Dynamics Simulations," 2017.

[168] S. Futamure, V. Bonnet, R. Dumas, and G. Venture, "A sensitivity analysis method for the body segment inertial parameters based on ground reaction and joint moment regressor matrices," *J. Biomech.*, vol. 64, pp. 85–92, 2017.

[169] R. Dumas and J. Wojtusch, *Estimation of the Body Segment Inertial Parameters for the Rigid Body Biomechanical Models Used in Motion Analysis*. 2017.

[170] L. F. Lee and B. R. Umberger, "Generating optimal control simulations of musculoskeletal movement using OpenSim and MATLAB," *PeerJ*, vol. 4, p. e1638, 2016.

[171] M. A. Price, B. R. Umberger, and F. C. Sup IV, "Dynamic Optimization of Gait with a Generalized Lower-Limb Prosthesis Model," in *Proc. IEEE International Conference on Rehabilitation Robotics (ICORR)*, 2019, pp. 734–739.

[172] M. L. Handford and M. Srinivasan, "Energy-optimal human walking with feedback-controlled robotic prostheses: A computational study," *IEEE Trans. Neural Syst. Rehabil. Eng.*, vol. 26, no. 9, pp. 1773–1782, 2018.

[173] M. Millard, T. Uchida, A. Seth, and S. L. Delp, "Flexing Computational Muscle: Modeling and Simulation of Musculotendon Dynamics," *J. Biomech. Eng.*, vol. 135, no. 2, p. 021005, 2013.

[174] I. H. Chen, K. N. Kuo, and T. P. Andriacchi, "The influence of walking speed on mechanical joint power during gait," *Gait Posture*, vol. 6, no. 3, pp. 171–176, 1997.

[175] J. Rasmussen, M. Damsgaard, and M. Voigt, "Muscle recruitment by the min/max criterion - A comparative numerical study," *J. Biomech.*, vol. 34, no. 3, pp. 409–415, 2001.

[176] V. Q. Nguyen *et al.*, "Bi-level optimization for cost function determination in predictive simulation of human gait," *IEEE Trans. Neural Syst. Rehabil. Eng.*, vol. 27, no. 7, pp. 1426–1435, 2019.

[177] A. J. Van Den Bogert, D. Blana, and D. Heinrich, "Implicit methods for efficient musculoskeletal simulation and optimal control," *Procedia IUTAM*, vol. 2, pp. 297–316, 2011.

[178] S. Porsa, Y.-C. Lin, and M. G. Pandy, "Direct Methods for Predicting Movement Biomechanics Based Upon Optimal Control Theory with Implementation in OpenSim," *Ann. Biomed. Eng.*, vol. 44, no. 8, pp. 2542–2557, 2016.

[179] A. Wächter and L. Biegler, "On the implementation of an interior-point filter line-search algorithm for large-scale nonlinear programming," *Math. Program.*, vol. 106, no. 1, pp. 25–57, 2005.

[180] S. K. Au, J. Weber, and H. Herr, "Powered ankle-foot prosthesis improves walking metabolic economy,"

IEEE Trans. Robot., vol. 25, no. 1, pp. 51–66, 2009.

[181] L. Torburn, J. Perry, E. Ayyappa, and S. L. Shanfield, "Below-knee amputee gait with dynamic elastic response prosthetic feet: A pilot study," *J. Rehabil. Res. Dev.*, vol. 27, no. 4, pp. 369–384, 1990.

[182] S. Porsa, Y. C. Lin, and M. G. Pandy, "Direct Methods for Predicting Movement Biomechanics Based Upon Optimal Control Theory with Implementation in OpenSim," *Ann. Biomed. Eng.*, vol. 44, no. 8, pp. 2542–2557, 2016.

[183] A. Wächter and L. T. Biegler, *On the Implementation of a Primal-Dual Interior Point Filter Line Search Algorithm for Large-Scale Nonlinear Programming*, vol. 106, no. 1. 2006.

[184] "Empower - Technical Specification," *ottobock*. [Online]. Available: https://shop.ottobock.us/Prosthetics/Lower-Limb-Prosthetics/Feet---Microprocessor/1A1-1-Empower/p/1A1-1. [Accessed: 03-Feb-2020].

[185] M. Cempini, L. J. Hargrove, and T. Lenzi, "Design, Development, and Bench-top Testing of a Powered Polycentric Ankle Prosthesis," *IEEE/RSJ Int. Conf. Intell. Robot. Syst.*, pp. 1–6, 2017.

[186] V. L. Chiu, A. S. Voloshina, and S. H. Collins, "An Ankle-Foot Prosthesis Emulator Capable of Modulating Center of Pressure," *IEEE Trans. Biomed. Eng.*, vol. 9294, no. c, pp. 1–11, 2019.

[187] E. M. Ficanha, G. A. Ribeiro, H. Dallali, and M. Rastgaar, "Design and Preliminary Evaluation of a Two DOFs Cable-Driven Ankle–Foot Prosthesis with Active Dorsiflexion–Plantarflexion and Inversion–Eversion," *Front. Bioeng. Biotechnol.*, vol. 4, no. May, 2016.

[188] M. A. Price and F. C. Sup, "RaspberryPIC GoPack." [Online]. Available: http://www.ecs.umass.edu/gopack/. [Accessed: 11-Feb-2020].

[189] Maxon, "Maxon Selection Guide," 2020.

[190] C. J. Walsh, K. Pasch, and H. Herr, "An autonomous, underactuated exoskeleton for load-carrying augmentation," in *IEEE International Conference on Intelligent Robots and Systems*, 2006, pp. 1410–1415.

[191] M. Goršič *et al.*, "Online phase detection using wearable sensors for walking with a robotic prosthesis," *Sensors*, vol. 14, no. 2, pp. 2776–2794, 2014.

[192] D. Quintero, D. J. Villarreal, D. J. Lambert, S. Kapp, and R. D. Gregg, "Continuous-Phase Control of a Powered Knee-Ankle Prosthesis: Amputee Experiments Across Speeds and Inclines," *IEEE Trans. Robot.*, vol. 34, no. 3, pp. 686–701, 2018.

[193] Y. Ding, I. Galiana, C. Siviy, F. A. Panizzolo, and C. Walsh, "IMU-based iterative control for hip extension assistance with a soft exosuit," in *IEEE International Conference on Robotics and Automation*, 2016, pp. 3501–3508.

[194] K. Seo *et al.*, "RNN-based on-line continuous gait phase estimation from shank-mounted imus to control ankle exoskeletons," in *IEEE International Conference on Rehabilitation Robotics*, 2019, pp. 809–815.

[195] N. Hogan and S. P. Buerger, "Impedance and Interaction Control," in *Robotics and Automation Handbook*, T. R. Kurfess, Ed. Taylor & Francis, 2005, pp. 19-1-19–24.

[196] G. A. Pratt, P. Willisson, C. Bolton, and A. Hoftnan, "Late motor processing in low-impedance robots: Impedance control of series-elastic actuators," in *Proc. American Control Conference*, 2004, pp. 3245–3251.

[197] J. Zhang, C. C. Cheah, and S. H. Collins, “Chapter 5 - Torque control in legged locomotion,” in *Bioinspired Legged Locomotion*, M. Sharbafi and A. Seyfarth, Eds. Elsevier, 2017, pp. 347–400.

[198] S. K. Au, J. Weber, and H. Herr, “Biomechanical design of a powered ankle-foot prosthesis,” *2007 IEEE 10th Int. Conf. Rehabil. Robot. ICORR’07*, vol. 00, no. c, pp. 298–303, 2007.

[199] P. Bawa and R. B. Stein, “Frequency Response of Human Soleus Muscle,” *J. Neruophysiology*, vol. 39, no. 4, pp. 788–793, 1976.